



Cleveland State University  
EngagedScholarship@CSU

---

ETD Archive


---

Winter 1-2020

## Characterization of the Immune Response To Anti-mullerian Hormone

Justin M. Johnson  
*Cleveland State University*

Follow this and additional works at: <https://engagedscholarship.csuohio.edu/etdarchive>

 Part of the [Biology Commons](#)

[How does access to this work benefit you? Let us know!](#)

---

### Recommended Citation

Johnson, Justin M., "Characterization of the Immune Response To Anti-mullerian Hormone" (2020). *ETD Archive*. 1271.

<https://engagedscholarship.csuohio.edu/etdarchive/1271>

This Thesis is brought to you for free and open access by EngagedScholarship@CSU. It has been accepted for inclusion in ETD Archive by an authorized administrator of EngagedScholarship@CSU. For more information, please contact [library.es@csuohio.edu](mailto:library.es@csuohio.edu).

CHARACTERIZATION OF THE IMMUNE RESPONSE TO ANTI-MÜLLERIAN  
HORMONE

JUSTIN M. JOHNSON

Bachelor of Science in Biology

University of Akron

December 1994

Submitted in partial fulfillment of requirements for the degree

DOCTOR OF PHILOSOPHY IN REGULATORY BIOLOGY

WITH SPECIALIZATION IN CELLULAR AND MOLECULAR MEDICINE

at the

CLEVELAND STATE UNIVERSITY

December 2020

© Copyright 2020 Justin M. Johnson

We hereby approve this dissertation

For

Justin M. Johnson

Candidate for the Doctor of Regulatory Biology degree

with specialization in Cellular and Molecular Medicine

for the Department of

Biological, Geological, and Environmental Sciences

And

CLEVELAND STATE UNIVERSITY'S

College of Graduate Studies by

Date: \_\_\_\_\_

Dr. Vincent K. Tuohy, Department of Inflammation and Immunity, Cleveland Clinic  
Major Advisor

Date: \_\_\_\_\_

Dr. Anton Komar, Department of BGES, Cleveland State University  
Advisory Committee Member

Date: \_\_\_\_\_

Dr. Xiaoxia Li, Department of Inflammation and Immunity, Cleveland Clinic  
Advisory Committee Member

Date: \_\_\_\_\_

Dr. William Baldwin, Department of Inflammation and Immunity, Cleveland Clinic  
Advisory Committee Member

Date: \_\_\_\_\_

Dr. Barsanjit Mazumder, Department of BGES, Cleveland State University  
Internal Examiner

Date: \_\_\_\_\_

Dr. Anna Valujskikh, Department of Inflammation and Immunity, Cleveland Clinic  
External Examiner

## **DEDICATION**

To Miss Mencl, who taught me how to put on my jacket all by myself.  
And to my Mom, for believing me when I pretended that I couldn't.

To Mr. Taylor, who put the idea of "Doc" in my head.  
And to Dr. Tuohy who made it happen.

To my colleagues who encouraged me.  
And to my committee that inspired me.

To my family and friends who motivated me to push on.  
And to my students who knew that I could do it.

You are all my teachers.

## ACKNOWLEDGMENTS

Let me start by stating the obvious: earning a Ph.D. is hard work—just as it should be. But for all of the countless hours that the graduate student spends in the laboratory and at the computer, buried in books and journal articles, there are countless more hours spent by those who live with, work with, and support that student. First and foremost, my family has made incredible sacrifices to make this accomplishment possible. We'll always remember holidays punctuated by my frequent and untimely visits to the lab. Beautiful weekends given up for studying. Vacation opportunities missed. And most of all, those daily work and school stresses that inevitably spill over into home life. You all survived the chronic neuroses of a doctoral student for much longer than any of us had ever anticipated. And you did it with grace and unwavering strength. For this I will always be grateful to Valerie, Aidan, and Paige.

Of course, we all agree that this extraordinary journey was well worth the challenges, and it would not have been possible without the constant support and inspiration from my supervisor and mentor, Dr. Vincent Tuohy. He gave me my first opportunity to intern in a professional research laboratory while I was still a young undergraduate student. The mission that he entrusted me with that fateful summer was to manually synthesize a peptide to create a disease in a mouse model. And after months of work and anticipation, when I saw the first signs of the telltale phenotype, I was hooked. Dr. Tuohy has since provided me with 25 years of continuous full-time employment, and from the very first day, he motivated me to further my education. It didn't seem likely that I could balance the responsibilities of a job, a family, and graduate school all at once. A Master's degree seemed improbable, and a Ph.D. was certainly impossible. But with

the encouragement of Dr. Tuohy and my advisory committee, Dr. Anton Komar, Dr. Xiaoxia Li, and Dr. William Baldwin, I made the most important decision of my career and I went for it. There are no words to express how much I appreciate the wisdom, guidance, and inspiration that I received from the first committee meeting all the way through the dissertation defense and beyond. In addition, I would like to extend that heartfelt thanks to Dr. Barsanjit Mazumder and Dr. Anna Valujskikh who joined the committee for the defense, as well as to all of the members of my candidacy examination committee, including Dr. Trine Jorgensen, Dr. Neetu Gupta, Dr. Roman Kondratov, and Dr. Dennis Stuehr. For the innumerable time and effort that all of these professors selflessly volunteered, I will always be grateful.

Furthermore, I would like to recognize all of the advice and technical assistance that I received from my colleagues. There are numerous members of the Tuohy Lab, past and present, who helped make all of this work possible. Dr. Suparna Mazumder shared helpful feedback and insights that helped propel this project to completion. Heather, Bryan, Nisha, Valerie, Patrick, Lauren, and Holly were always there to lend a hand. I also relied heavily on the technical expertise and wisdom of a great many members of the Lerner Research Institute's Core Services—Cathy, Sage, Eric, Joe, Jena, Diane, Carmel, and Dr. Judy Drazba to name a few. And Nina Dvorina from Dr. Baldwin's lab deserves special recognition for teaching me everything I know about histology.

And finally, the occasional diversion from science proved to be a vital means of preserving sanity during this difficult journey. I enjoyed the philosophical discussions and poetry readings with the late Jim Lang, as well as reveling with fellow students and co-workers at social events, and most of all, making music with Brittany, Jim, Patrick,

Courtney, Janet, Bryan, Shane, and everyone else that I had the pleasure of sharing the Lerner Commons stage with over the years. I believe that science and art are symbiotic, and I find it a great privilege to indulge those dual passions with so many colleagues and friends. Most importantly, I was inspired by how many fellow students successfully balanced science with art, careers with families, and achieved advanced degrees while meeting multiple challenges head-on.

Earning a Ph.D. is indeed hard work, and it is not just the labor of the student that earns the degree. It takes a village. And too often the hardships were greater on those who supported me along the way. But somehow we all made it. And I am thrilled to share the joys of success with everyone who helped me to achieve it. This one's for all of you. Cheers!



CHARACTERIZATION OF THE IMMUNE RESPONSE  
TO ANTI-MÜLLERIAN HORMONE

JUSTIN M. JOHNSON

**ABSTRACT**

Anti-Müllerian hormone (AMH) has been known since the mid-twentieth century as the substance secreted by the testes of the male fetus that is responsible for directing the proper development of the male reproductive organs from the primordial structures that would otherwise become the uterus and fallopian tubes. However, despite its long-known significance in male development, only recently has its importance in the adult female become evident. AMH is now considered to be not only a clinical indicator of the finite ovarian egg supply, but a vital regulator thereof throughout the reproductive life of the female. Dysfunctions in AMH regulation may lead to infertility that underlies conditions such as primary ovarian insufficiency (POI) and polycystic ovarian syndrome (PCOS). Moreover, mounting clinical and experimental evidence suggests that many such cases may be the result of autoimmunity to AMH. To test this hypothesis, an animal model of AMH autoimmunity was developed by immunization of C57BL/6J female mice with recombinant AMH protein. These mice developed a typical autoimmune profile with a robust antigen-specific type-1/type-17 immune response with high frequencies of CD4<sup>+</sup> T cells that transiently infiltrated ovarian tissues as well as long-lasting high titers of IgG<sub>1</sub> and IgG<sub>2b</sub> in the serum. Most importantly, the mice exhibited a unique and previously unreported phenotype in which their reproductive lifespan was extended. Mice immunized with AMH in complete Freund's adjuvant (CFA) remained fertile at ten months of age at a time when control mice immunized with CFA alone exhibited a

natural decline in fertility due to reproductive senescence. AMH-immunized mice had more litters, greater numbers of pups per litter, and conserved more active follicles than controls at ten months. This effect correlated with a significant lengthening of the estrous cycle, resulting in fewer cycles over time which did not reduce the probability of conception or the health and viability of the offspring, but rather extended the fertile lifespan of the mice. This novel model of experimental autoimmune oophoritis (EAO) helps advance the knowledge of the physiologic role of AMH in the female, and may aid in understanding and managing human health conditions such as menopause and infertility.

# TABLE OF CONTENTS

	Page
ABSTRACT .....	viii
LIST OF TABLES .....	xiv
LIST OF FIGURES .....	xv
LIST OF ABBREVIATIONS .....	xviii
CHAPTER	
I. BACKGROUND AND INTRODUCTION	
Anti-Müllerian Hormone	
Introduction .....	1
AMH Expression and Activation .....	2
AMH Signaling Pathway .....	4
AMH Physiology	
AMH as a Hormone .....	8
Sexual Dimorphism and Role in Males .....	8
Role in the Female .....	10
The Hypothalamic-Pituitary-Ovarian Axis and Ovarian Cycle .....	10
The Menstrual Cycle .....	12
The Estrous Cycle .....	17
AMH in Reproductive Senescence and Menopause .....	18
AMH Dysfunction and Disease	
AMH Dysfunction in Development .....	21

Primary Ovarian Insufficiency (POI).....	22
Polycystic Ovary Syndrome (PCOS).....	24
AMH in Endometriosis.....	25
AMH and Cancer .....	25
AMH Autoimmunity	
General Features of Autoimmunity .....	26
Organ-Specific Autoimmunity.....	29
Animal Models of Autoimmunity.....	29
Autoimmunity in Ovarian Dysfunction .....	30
Animal Models of Ovarian Autoimmunity.....	32

## II. MATERIALS AND METHODS

Cloning of the mAMH Gene.....	37
Construction of the rmAMH Expression Vector .....	38
Screening of Expression Clones .....	39
Determination of Protein Solubility.....	40
Expression of Recombinant AMH.....	41
Affinity Purification of Recombinant mAMH.....	41
HPLC Purification of Recombinant mAMH .....	43
Refolding of Recombinant mAMH .....	45
Quantification of Recombinant Proteins.....	46
Mice and Immunization .....	46
T Cell Proliferation Assays.....	47
Responses by CD4 <sup>+</sup> and CD8 <sup>+</sup> T Cell Subpopulations .....	48

FACS Analysis of Enriched CD4+ and CD8+ T cells.....	49
Cytokine ELISA Assays .....	49
Cytokine ELISpot Assays.....	50
qRT-PCR Analysis.....	51
Immunohistochemistry .....	55
Serum Autoantibody Isotyping.....	56
Serum Hormone ELISAs .....	57
Fertility Assessments .....	58
Follicle Quantification and Ovary Measurements .....	59
Estrous Cycle Staging.....	61
Passive Transfer of Autoimmunity .....	63
Statistical Analyses .....	64

### III. RESULTS

Immunization with AMH Elicits a Robust Antigen-Specific T Cell Response .....	65
AMH-reactive T Cells are Primarily of the CD4+ Phenotype.....	66
AMH Immunization Elicits a Type-1/Type-17 Cytokine Profile .....	69
ELISpot Analysis of Type-1/Type-17 T Cell Frequencies.....	71
qRT-PCR Analysis Reveals Expression of Type-1/Type-17 Inflammatory Genes .....	72
Immunohistochemistry Shows Mild Transient T cell Infiltration of Ovarian Tissues .....	75

AMH Immunization Produces Long-Lasting High Titers of Antigen-Specific Autoantibodies .....	76
Immunization with AMH Extends Fertility .....	78
Immunization with AMH Conserves Ovarian Follicles .....	83
Immunization with AMH Significantly Lengthens the Estrous Cycle .....	90
<b>IV. DISCUSSION</b>	
Evaluating the Immune Response and Phenotype of AMH Autoimmunity .....	96
Possible Mechanisms of AMH Autoimmunity-Mediated Fertility Extension.....	99
Insights Gained into the Natural Functions of AMH.....	105
Insights on Menopause and Aging.....	109
Novel Clinical Applications for AMH.....	113
<b>V. REFERENCES.....</b>	<b>119</b>
<b>VI. APPENDIX.....</b>	<b>138</b>

## LIST OF TABLES

Table	Page
2.1 Primers for Cloning the mAMH Gene.....	38
2.2 Primers for qRT-PCR Analysis of Gene Expression.....	54
3.1 Proportion of Fertile Females In Each Mating Round.....	83
4.1 Comparison of Phenotypes in Animal Models of Infertility and Human Disease.....	110

## LIST OF FIGURES

Figure	Page
1.1 AMH Cleavage and Biologically Active Complex .....	4
1.2 AMH Receptor Signaling .....	6
1.3 Serum AMH Levels in Men and Women .....	9
1.4 The Hypothalamic-Pituitary-Ovarian Axis.....	11
1.5 The Menstrual Cycle.....	14
1.6 AMH and the Ovarian Cycle .....	17
1.7 Lifetime Decline in Serum AMH Levels in Women .....	19
1.8 Serum AMH Levels in PCOS and POF .....	23
2.1 SDS-PAGE of Recombinant mAMH .....	42
2.2 Western Blot of Recombinant mAMH .....	43
2.3 HPLC Profile of Recombinant mAMH .....	45
2.4 Fertility Assessment Mating Scheme.....	59
2.5 Follicle Quantification Scheme.....	60
2.6 Estrous Cycle Staging Scheme .....	62
3.1 T Cell Proliferation Response to AMH .....	66
3.2 Flow Cytometry Analysis of Enriched CD4+ and CD8+ T Cells .....	68
3.3 Proliferation Assays .....	69
3.4 Cytokine ELISA Profile of AMH-Specific T Cells .....	70
3.5 Cytokine ELISpot Profile of AMH-Specific T Cells.....	72
3.6 qRT-PCR Inflammatory Marker Profile of Ovarian Tissue .....	74
3.7 CD3+ T Cell Infiltration of Ovarian Tissue.....	75



3.8	Serum AMH Autoantibody Titers at 8 Weeks.....	77
3.9	Long-term Serum AMH Autoantibody Titers .....	78
3.10	Mean Numbers of Pups Per Litter .....	80
3.11	Mean Weights of Litters and Birth Weights of Pups.....	81
3.12	Percentage of Mice Producing Litters.....	82
3.13	Ovary Weight and Size Decline with Age.....	84
3.14	AMH Immunized Mice Have More Active Follicles at 10 Months.....	85
3.15	AMH Immunized Mice Have Greater Total Numbers at 10 Months.....	86
3.16	Follicle Differences by Subtype at 10 Months .....	87
3.17	AMH Immunized Mice Express Greater Levels of the AMH Gene at 10 Months .....	89
3.18	AMH Immunization Disrupts the Estrous Cycle.....	91
3.19	AMH Immunization Results in Fewer Estrous Cycles.....	92
3.20	AMH Immunization Lengthens the Estrous Cycle.....	93
3.21	Mean Estrous Phase Length.....	94
4.1	Proposed Mechanism for AMH Autoantibody-Mediated Fertility Extension.....	104
S1	Complement Activity is Absent as Evidenced by Negative C4d Staining in Ovarian Tissues .....	139
S2	Serum AMH Levels at 10 Months.....	140
S3	Serum FSH Levels at 8 Weeks and 10 Months .....	141
S4	Total Estrous Cycle Lengths in Passive Transfer to Naive Hosts .....	142

S5	Follicular Phase Lengths in Passive Transfer to Naive Hosts .....	143
S6	Luteal Phase Lengths in Passive Transfer to Naive Hosts.....	144

## LIST OF ABBREVIATIONS

ABTS	2,2'-azino-bis(3-ethylbenzothiazoline-6-sulphonic acid)
ADCC	antibody-dependent cellular cytotoxicity
AIRE	autoimmune regulator
ALK	activin receptor-like kinase
AMH	anti-Müllerian hormone
AMH-C	anti-Müllerian hormone, C-terminal fragment
AMHR2	anti-Müllerian hormone receptor type 2
AMHR2-ED	anti-Müllerian hormone receptor type 2, extracellular domain
AMHRI	anti-Müllerian hormone receptor type 1
AMHRII	anti-Müllerian hormone receptor type 2
ANM	age at natural menopause
AO	autoimmune oophoritis
amp	ampicillin
APECED	autoimmune polyendocrinopathy-candidiasis-ectodermal dystrophy
APS	autoimmune polyendocrine syndromes
BCIP/NBT	5-bromo-4-chloro-3-indolyl-phosphate/nitro blue tetrazolium
bp	base pairs
BSA	bovine serum albumin
cDNA	complementary DNA
C4d	complement component 4d
CFA	complete Freund's adjuvant

CL	corpus luteum/corpora lutea
CNS	central nervous system
cpm	counts per minute
DAB	3,3'-diaminobenzidine
DDD	double-distilled deionized
DEPC	diethyl pyrocarbonate
DMEM	Dulbecco's modified Eagle's medium
EAE	experimental autoimmune encephalomyelitis
EAO	experimental autoimmune oophoritis
ECL	electrochemiluminescence
ELISA	enzyme-linked immunosorbent assay
ELISpot	enzyme-linked immunospot
EOC	epithelial ovarian carcinoma
FACS	fluorescence-activated cell sorting
FBS	fetal bovine serum
FITC	fluorescein isothiocyanate
FSH	follicle stimulating hormone
FSH-R	follicle stimulating hormone receptor
GCT	granulosa cell tumor
GnRH	gonadotropin releasing hormone
H&E	hematoxylin and eosin
HEPES	4-(2-hydroxyethyl)-1-piperazineethanesulfonic acid
HPLC	high performance liquid chromatography

HRP	horseradish peroxidase
IACUC	institutional animal care and use committee
IFN $\gamma$	interferon gamma
IHC	immunohistochemistry
IL-1 $\beta$	interleukin 1 beta
IL-2	interleukin 2
IL-4	interleukin 4
IL-5	interleukin 5
IL-10	interleukin 10
IL-17	interleukin 17
<i>i.p.</i>	intraperitoneal
IPEX	immunodysregulation, polyendocrinopathy, enteropathy, X-linked
IPTG	isopropyl $\beta$ -D-1-thiogalactopyranoside
<i>i.v.</i>	intravenous
IVF	<i>in vitro</i> fertilization
kDa	kilodaltons
LAL	limulus amoebocyte lysate
LB	lysogeny broth
LH	luteinizing hormone
LHCGR	luteinizing hormone/choriogonadotropin receptor
LNC	lymph node cells
MACS	magnetic-activated cell sorting

mAMH	mouse anti-Müllerian hormone
MBP	myelin basic protein
MHC	major histocompatibility complex
MIF	Müllerian-inhibiting factor
MIS	Müllerian-inhibiting substance
MISRII	Müllerian-inhibiting substance receptor type 2
MISIIR	Müllerian-inhibiting substance receptor type 2
MOG	myelin oligodendrocyte glycoprotein
MS	multiple sclerosis
MTS	(3-(4,5-dimethylthiazol-2-yl)-5-(3-carboxymethoxyphenyl)-2-(4-sulfophenyl)-2H-tetrazolium)
MWCO	molecular weight cutoff
NCBI	National Center for Biotechnology Information
Ni-NTA	nickel nitrotriacetic acid
NTx	neonatal thymectomy
OD	optical density
OVA	ovalbumin
PBS	phosphate-buffered saline
PCR	polymerase chain reaction
PDX	patient-derived xenograft
PE	phycoerythrin
PerCP	peridinin chlorophyll
PLP	proteolipid protein

PMDS	persistent Müllerian duct syndrome
POF	premature ovarian failure
POI	primary ovarian insufficiency
PVDF	polyvinylidene fluoride
qRT-PCR	quantitative real-time polymerase chain reaction
RBC	red blood cell
SFU	spot-forming units
rmAMH	recombinant mouse anti-Müllerian hormone
rm $\beta$ -cas	recombinant mouse $\beta$ -casein
RT-PCR	reverse transcription polymerase chain reaction
Sav-AP	streptavidin-alkaline phosphatase
<i>s.c.</i>	subcutaneous
SDS-PAGE	sodium dodecyl sulfate polyacrylamide gel electrophoresis
SI	stimulation index
SLE	systemic lupus erythematosus
SMAD	small mothers against decapentaplegic
SNPs	single-nucleotide polymorphisms
T1DM	diabetes mellitus type 1
TBS	Tris-buffered saline
TGF $\beta$	transforming growth factor-beta
T <sub>H</sub>	T helper cell
TMB	3,3',5,5'-tetramethylbenzidine
T <sub>reg</sub>	regulatory T cell

VEGF-A	Vascular endothelial growth factor A
ZP3	zona pellucida sperm-binding protein 3



# CHAPTER I

## BACKGROUND AND INTRODUCTION

### ANTI-MÜLLERIAN HORMONE

#### Introduction

Anti-Müllerian hormone (AMH), also known as Müllerian-inhibiting substance (MIS) or Müllerian-inhibiting factor (MIF)<sup>1</sup>, is a homodimeric glycoprotein of the transforming growth factor beta (TGF $\beta$ ) superfamily that is present in all vertebrates and has important but disparate effects in both males and females. It was first described by the French physician Alfred Jost (Jost, 1947) as the critical factor secreted by the testes during male fetal development that caused regression of the Müllerian ducts—primordial structures named for discoverer Johannes Peter Müller—which would otherwise develop into the fallopian tubes, uterus, and upper vagina in the female (Roly, et al., 2018). In a series of elegant experiments in rabbits using a pioneering intrauterine castration technique (Jost, 1947; Jost, 1953), Jost showed that the effect of AMH, secreted by the

---

<sup>1</sup> Other nomenclature variations exist, but AMH, MIS, and MIF appear most often in scientific literature. AMH is the most universally recognized designation and was preferred by its discoverer (Josso, et al., 1993); therefore it is the canonical term used in this document.

Sertoli cells of the testes, was independent of testosterone, which is secreted by the Leydig cells. Whereas testosterone could promote further development of the male urogenital structures, it could not itself cause Müllerian duct regression. Jost reasoned that this effect must be caused by some yet undiscovered hormone that he putatively termed "Müllerian inhibitor" (Josso, 1991).

While it was widely known for many decades thereafter for its eponymous role in male fetal development, only recently has AMH become appreciated for its function in the sexually mature female as an important regulator of the ovarian cycle. Contemporary research is primarily aimed at elucidating this regulatory mechanism, and at establishing a clinical role for AMH—as a biomarker of fertility and ovarian pathology; as a possible underlying cause of ovarian diseases that impair fertility, such as primary ovarian insufficiency (POI) and polycystic ovary syndrome (PCOS); and as a potential treatment for these and other diseases of the ovary. Mounting evidence suggests that autoimmunity to ovarian proteins may play a role in many cases of infertility (Tuohy & Altuntas, 2007; Sen, et al., 2014), and yet autoimmunity to AMH remains unexplored. Thus, the current study characterizes the immunologic response to AMH and describes a novel phenotype that may have important clinical implications.

### **AMH Expression and Activation**

In humans, the AMH gene is located on chromosome 19 and is under the control of a unique promoter (Josso, et al., 1993). It is expressed primarily in the ovaries and testes as a primary transcript containing 5 exons that is spliced into an 1883 bp mRNA (Cate, et al., 1986). The mature mRNA is subsequently translated to a 560 amino acid

59.2 kDa protein that contains two glycosylation sites, as well as four disulfide bonds that stabilize the two chains of the mature homodimer (Josso, et al., 1993). Prior to secretion, the signal peptide (residues 1-18) is cleaved. Once secreted, AMH must undergo a proteolytic cleavage to become biologically active, in a manner similar to its close relative TGF $\beta$ . The 140 kDa mature homodimer is cleaved between R451 and S452 by proteases in the gonadal environment resulting in a 110 kDa N-terminal proregion and a 25 kDa C-terminal active region (Pepinsky, et al., 1988). The C-terminal fragment by itself is capable of biologic activity, whereas full-length AMH or the N-terminal proregion alone are not (di Clemente, et al., 2010). Interestingly, it has been observed that after cleavage, both regions remain non-covalently associated (Figure 1.1), and this complex exhibits greater biologic activity than the C-terminal region alone (Wilson, et al., 1993). AMH is highly conserved across mammalian species in terms of structure and function; not surprisingly, the receptor-binding C-terminal domain is the most conserved region, with human, bovine, mouse, and rat AMH-C-terminal domains sharing  $\geq 90\%$  homology (Josso, et al., 1993).

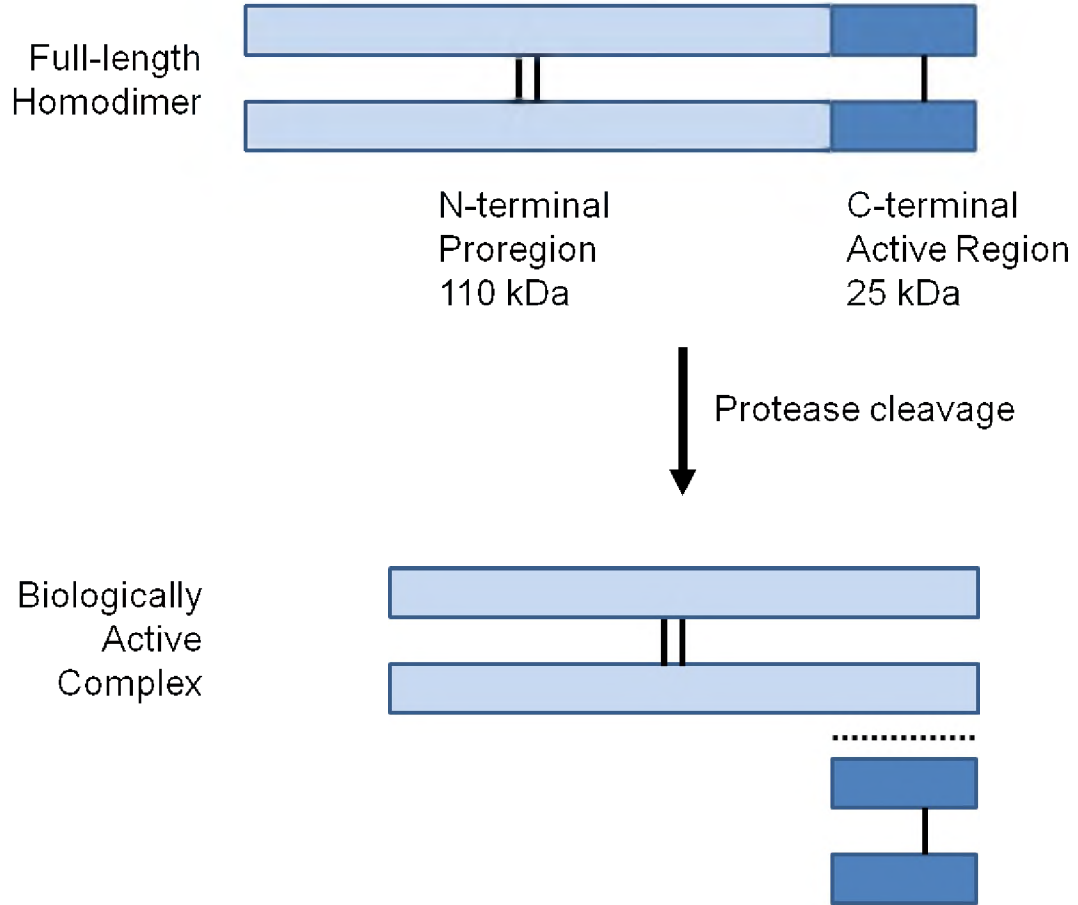


**Figure 1.1 AMH Cleavage and Biologically Active Complex.** AMH is secreted as an inactive 140 kDa disulfide-linked (solid black lines) homodimer that must be cleaved by proteases in the ovarian microenvironment to become biologically active. The resulting 110 kDa proregion and 25 kDa active region homodimer fragments remain non-covalently associated (dotted black line) to induce maximal signaling through the AMHR2 receptor. Diagram adapted from (Dewailly, et al., 2014).

### AMH Signaling Pathway

As a member of the TGF $\beta$  superfamily, AMH shares the canonical signaling pathway that is common to the group: a ligand-binding type 2 receptor, an associated type 1 receptor, and a cytoplasmic small mothers against decapentaplegic (SMAD) cascade that activates transcription in the nucleus. AMH is known to have only one

native receptor, anti-Müllerian hormone receptor type 2 (AMHR2)<sup>2</sup> and three known type 1 activin receptor-like kinase (ALK) receptors: ALK2, ALK3, and ALK6. Unlike its ligand AMH, which was first characterized in the early 1970s and subsequently isolated and purified in 1984, the hunt for the AMH receptor proved to be a much more confounding and difficult undertaking (Josso, et al., 1993). AMHR2 was finally identified in 1994 as a novel transmembrane serine/threonine kinase receptor associated with the Müllerian ducts (Baarends, et al., 1994). Subsequent work showed that in adult women, AMHR2 is a 62.7 kDa transmembrane protein, with a 127 amino acid extracellular domain, a 26 amino acid helical transmembrane domain, and a 403 amino acid cytoplasmic domain (Uhlen, et al., 2015). In humans, the AMHR2 gene is located on chromosome 12 and encodes an 11-exon transcript (Mishina, et al., 1997) with multiple splice variants of unclear function (Faure, et al., 1996). Like AMH, AMHR2 is highly conserved across mammalian species, especially in the ligand-binding region of exon 2 (Mishina, et al., 1997). Upon binding of biologically-active AMH, AMHR2 forms a non-covalent complex with a transmembrane anti-Müllerian hormone receptor type 1 (AMHR1; also AMHRI), causing the cytoplasmic domain of AMHR1 to become phosphorylated. This in turn activates a signaling cascade through the SMAD 1/5/8 pathway (Figure 1.2). SMAD 1/5/8 then associates with SMAD 4, and the entire complex translocates to the nucleus to activate the transcription of target genes (Josso, et al., 2001).

---

<sup>2</sup> Also abbreviated AMHR2 or referred to as Müllerian inhibiting substance receptor type 2 (MISR2, MISR2, or MISR2). The abbreviation AMHR followed by arabic numerals is currently the preferred format for AMH type 1 and type 2 receptors and are used as the standard throughout this document.

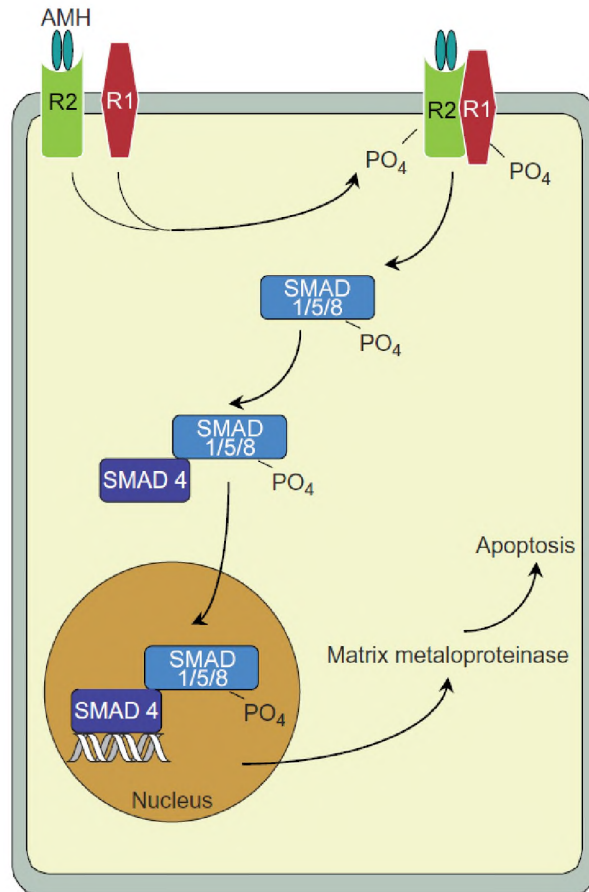


**Figure 1.2 AMH Receptor Signaling.** AMH binds to the AMHR2 receptor, which then complexes with AMHR1 triggering a SMAD 1/5/8 cascade. This SMAD 1/5/8 complex joins with SMAD 4 and translocates to the nucleus to initiate expression of pro-apoptotic genes. Reproduced with modification from (Goodman, 2009).

While the classical action of AMH—vis-à-vis the regression of the Müllerian ducts in fetal male development—is well-defined, AMH appears to have additional roles in the mature reproductive system. These include subtle and poorly understood regulatory effects on spermatogenesis and the ovarian cycle (Durlinger, et al., 1999; Fujisawa, et al., 2002). What is common among the seemingly disparate effects of AMH is the ability to promote growth arrest and cell elimination. Not surprisingly, then, AMH has been shown to regulate many pathways of cell cycle arrest and apoptosis (Seifer &

Merhi, 2014; Rehman, et al., 2017; Anttonen, et al., 2011). As expected, AMHR2 is expressed most abundantly in its canonical target reproductive tissues such as the Müllerian ducts, testes, and ovaries. However, substantial expression of AMHR2 has also been demonstrated in the adrenal gland, and minor expression has been shown in the spleen, pancreas, and skeletal muscle (Uhlen, et al., 2015). Interestingly, AMHR2 in non-reproductive tissues is expressed as a truncated isoform which lacks the extracellular domain encoded by exons 1-3 of the mRNA transcript; and for reasons that remain unclear, this extracellular domain is "*retired*" with age in the ovaries of post-menopausal women and in comparably-aged mice, as its expression significantly diminishes independently of the rest of the molecule (Mazumder, et al., 2017). It is also important to note that AMH and AMHR2 expression patterns vary by species; for example, mRNA encoding AMHR2 is broadly expressed in mouse and pig brain structures, but virtually absent in the adult human brain (Uhlen, et al., 2015). Like its receptor, AMH expression is predictably high in testes and ovaries, but it has been shown to be expressed in non-reproductive tissues as well, most notably in the brain. Conversely to AMHR2, expression of AMH in the brain of humans is substantial, yet expression in the brains of mice and pigs is virtually undetectable (Uhlen, et al., 2015). The actions and physiologic relevance of AMH on organs outside of the reproductive system and remain speculative, but the presence of the receptor in such diverse tissues suggests additional cryptic actions of the AMH/AMHR2 pathway (McLennan & Pankhurst, 2015).

## **AMH PHYSIOLOGY**

### **AMH as a Hormone**

Physiologically, AMH is a hormone with autocrine/paracrine effects; as such it is not a true endocrine hormone and is occasionally referred to as a cytokine. It typically exerts its effects locally in the gonadal microenvironment, acting on the secreting cell as well as nearby cells. Paradoxically, it is readily detectable in the serum, reinforcing the notion that it may have cryptic effects elsewhere in the body (McLennan & Pankhurst, 2015).

### **Sexual Dimorphism and Role in Males**

AMH has sexually dimorphic expression patterns and disparate effects in males and females. It is primarily expressed by the Sertoli cells of the testes and by the granulosa cells of the ovaries; these cells have similar roles, as they both serve to secrete hormones and regulatory factors to support and nurture developing sperm and ova, respectively (Carre & Greenfield, 2016). However, the temporal expression pattern of AMH is critically different between the sexes. As previously discussed, the canonical role for AMH in the male fetus is to cause regression of the Müllerian ducts, which would by default become female reproductive structures. Therefore, AMH measured in serum is predictably highest in males during fetal development, remaining high until puberty, and finally dropping to low but stable levels (Figure 1.3). In stark contrast, the expression pattern in females is virtually the opposite, with no detectable serum AMH *in utero*, gradually increasing amounts from birth through puberty, and reaching highest



levels in early adulthood. In further contrast to males, after peaking in females, AMH begins a steady lifelong decline to complete absence after menopause. These patterns and the role(s) of AMH in both sexes after birth are still somewhat unclear. In mature males, it is believed that AMH helps to regulate spermatogenesis (Rehman, et al., 2017). In addition, there is growing evidence that AMH may exert masculinizing properties on neurons, contributing both in the womb and in early childhood to the innate male behavioral bias (Wang, et al., 2009).

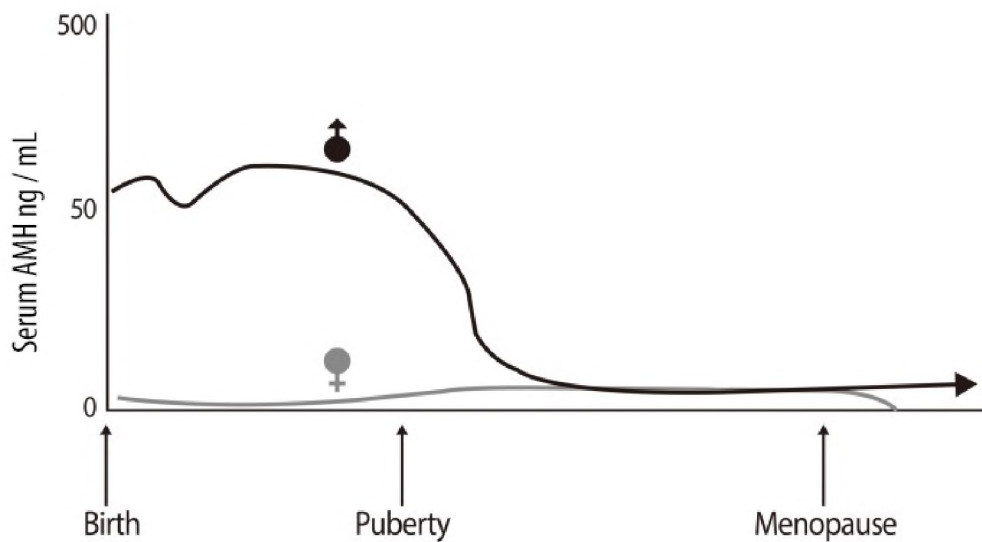


**Figure 1.3 Serum AMH Levels in Men and Women.** AMH presents an extremely sexually dimorphic and age-related expression pattern. In men (♂), AMH is highest before and after birth, then drops precipitously during puberty to low but stable levels. In women (♀), AMH is absent during fetal development but is detectable after birth, rising significantly during puberty to a peak in the mid-twenties. After peaking, women exhibit a steady lifelong decline to absence after menopause. Reproduced with modification from (Kim, et al., 2014).

## **Role in the Female**

While the pioneering work of Alfred Jost in the middle of the twentieth century paved the way to understanding the role of AMH during male fetal development, it was not recognized that the hormone had any relevance in females until three decades later, when it was unexpectedly discovered to be produced by the ovaries of hens (Hutson, et al., 1981). Subsequent research showed that AMH expression in sexually mature females was common to many mammalian species, including humans. Thus began the era of intense interest in elucidating the function of AMH in the ovary, with early speculation that it may play a regulatory role in the ovarian cycle (Josso, et al., 1993).

## **The Hypothalamic-Pituitary-Ovarian Axis and Ovarian Cycle**

The ovarian cycle is a critical physiologic process that underlies female fertility, ensuring the proper regulation and timing of ovulation. As endocrine glands, the ovaries are under the master control of the pituitary, which is itself directed by the hypothalamus. The elegant coordination among these three elements is known as the hypothalamic-pituitary-ovarian axis (Figure 1.4). At the seat of control is the hypothalamus, a small structure located below the cerebrum in front of the brain stem. It is aptly classified as a “neuroendocrine” organ, as it forms a vital link between the nervous and endocrine systems (Plant, 2015). It essentially functions as a master clock, rhythmically secreting gonadotropin releasing hormone (GnRH), which acts on the adjacent pituitary gland to stimulate secretion of follicle stimulating hormone (FSH) and luteinizing hormone (LH). These latter two hormones are collectively responsible for promoting follicle recruitment, maturation, and ovulation, and thus are the primary

drivers of the ovarian cycle. Although the pituitary provides central control, the ovaries themselves contribute to setting the tempo of the cycle by secreting critical hormones—such as estrogen, progesterone, activin, and inhibin—that provide positive and negative feedback to the pituitary. In addition, there are many important autocrine/paracrine factors that act within the ovary itself to "fine tune" the ovarian cycle locally without any direct feedback on the pituitary. Evidence has mounted over the past two decades that AMH is one such regulatory factor (Durlinger, et al., 1999; Durlinger, et al., 2001; Weenen, et al., 2004; Seifer & Merhi, 2014).

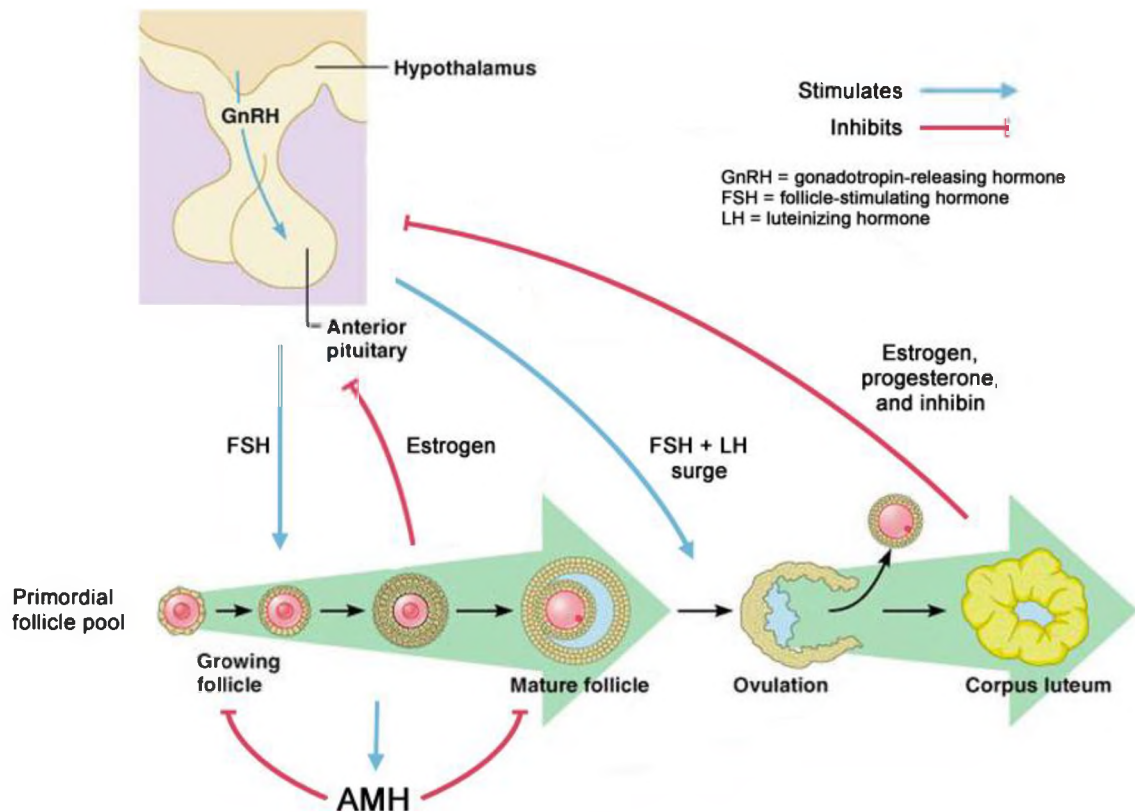


**Figure 1.4 The Hypothalamic-Pituitary-Ovarian Axis.** The hypothalamus acts through GnRH as a master regulator of the pituitary gland. The pituitary imposes central control over the ovarian cycle by secreting FSH and LH. The ovary provides feedback to the pituitary through secretion of estrogen, progesterone and inhibin. AMH acts at a local level within the ovary by limiting the number of follicles entering and exiting the developing pool for each cycle. Reproduced with modification from (Gilbert & Barresi, 2016).

## **The Menstrual Cycle**

In humans and higher primates, the ovarian cycle forms the foundation of the menstrual cycle, which encompasses all of the cyclical physiologic changes associated with the reproductive system. The menstrual cycle ensures proper coordination between the ovaries and uterus to maximize the potential for fertilization and successful gestation. Females are born with a finite quantity of oocytes (the primordial ova or eggs) and this supply cannot be replenished (Zuckerman, 1951)<sup>3</sup>. Therefore, careful regulation of ovulation is critical in balancing a steady supply of ova for fertilization while maintaining the ovarian reserve across a wide span of childbearing years. On average, a single ovum is released every 28 days beginning at menarche, the onset of menstruation during puberty, and lasting until menopause. This pattern results in a lifelong total of about 400 ovulations from the approximately 300,000 oocytes present at puberty (Seifer & Merhi, 2014; Walker & Herndon, 2008).

A single cycle begins with menses, the flow blood and endometrial tissue that is expelled from the uterus in the absence of a pregnancy (Figure 1.5). This phase is triggered by nadir levels of estrogen and progesterone, and typically lasts 5 days. It is immediately followed by the follicular phase, which lasts 10 days on average and is characterized by the development of a cohort of primary ovarian follicles as candidates for ovulation (Clement & Monniaux, 2013). Each primary follicle originates from the germinal epithelium of the ovary and initially consists of a sole oocyte surrounded by a single layer of granulosa cells. The granulosa cells provide a nurturing environment for the developing oocytes by supplying nutrients and growth factors (El-Hayek & Clarke,

---

<sup>3</sup> This long-standing dogma of female fertility has been scientifically challenged (Johnson, et al., 2004), but the concept of post-natal renewal of the ovarian supply by germline stem cells remains controversial (Kerr, et al., 2012).

2016). The growth and development of primary follicles during the follicular phase is driven primarily by FSH secretion by the pituitary. During this time, follicles gradually increase in size by adding multiple layers of granulosa cells and an external shell of estrogen precursor-secreting theca cells (Magoffin, 2005) around the core to become secondary follicles. This process continues until some of the follicles in the cohort expand dramatically and develop fluid-filled cavities called antra. These antral follicles continue to grow until one or more of them become very large mature or “Graafian” follicles—the finalists for ovulation. These larger follicles begin to secrete high levels of estrogen, which provides negative feedback to the pituitary, causing downregulation of FSH production. While it is still unclear precisely how the dominant follicle is selected, evidence suggests that one of the mature follicles becomes less dependent on FSH for growth, and thus quickly outgrows its competitors (Hawkins & Matzuk, 2008). Those follicles that are not selected for ovulation will be eliminated through atresia, an apoptosis-driven process of involution and reabsorption. The sharp rise in estrogen (which is inhibitory throughout the rest of the cycle, but is stimulatory in this context) secreted by the dominant follicle prompts the pituitary to simultaneously release sharp spikes of FSH and LH, triggering ovulation. During this process, the dominant follicle docks with the ovarian epithelium and ruptures, releasing its ovum into the peritoneal cavity.

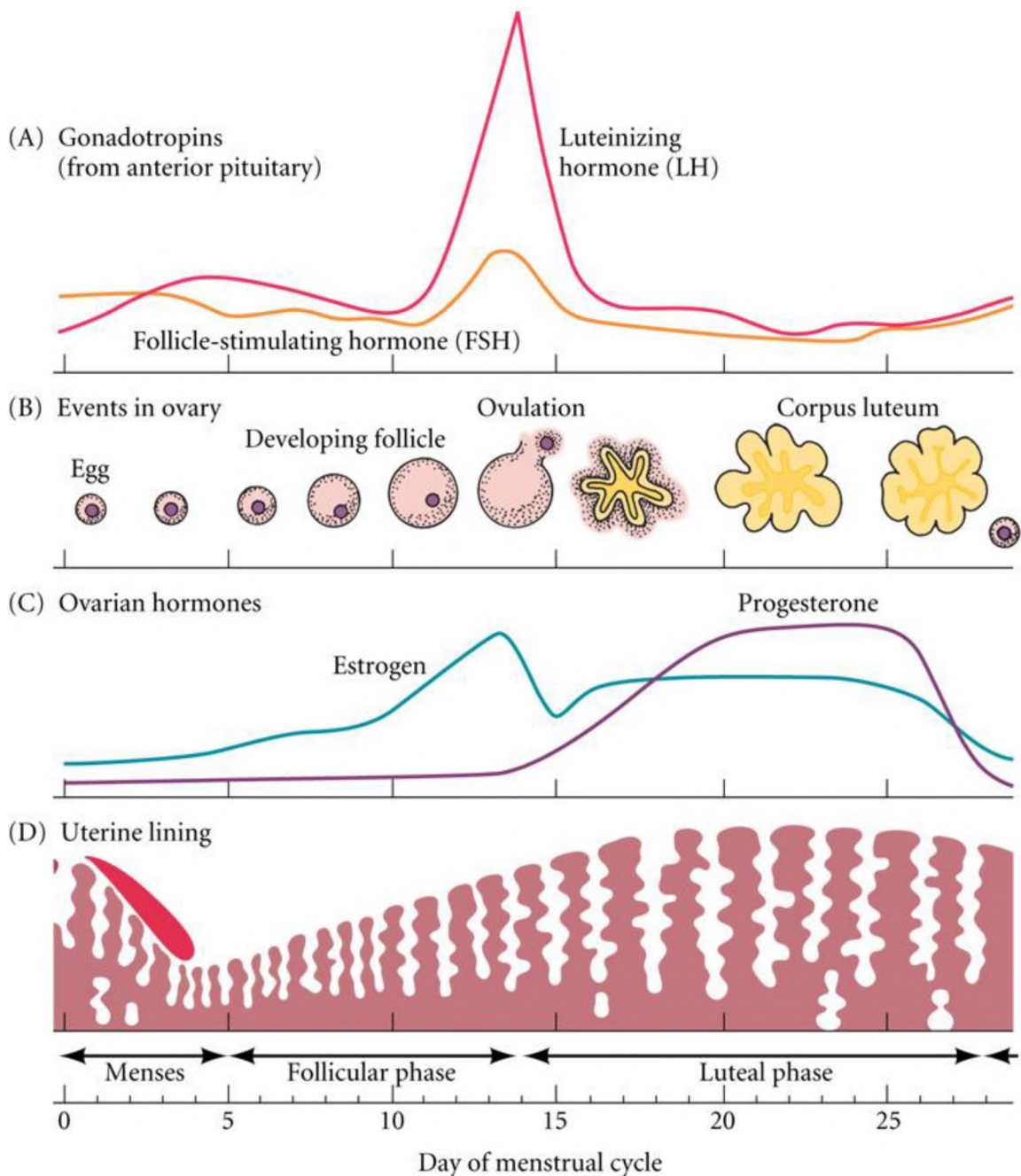


**Figure 1.5 The Menstrual Cycle.** The actions of the pituitary, ovaries, and uterus are precisely coordinated in each cycle by a complex interplay of hormones and organ physiology. (A) Pituitary gonadotropins FSH and LH exert master control over follicle development and ovulation. (B) Follicles respond to pituitary signals to develop, ovulate, and become corpora lutea. (C) Follicles provide feedback to the pituitary by secreting the hormones estrogen and progesterone. (D) The uterus responds to hormonal signals to prepare for pregnancy by a thickening of the endometrium; this lining is shed each cycle in the absence of implantation of the blastocyst. One complete cycle lasts on average 28 days. Reproduced from (Gilbert & Barresi, 2016).

Ovulation is the watershed event in the cycle; it separates the follicular phase from the subsequent luteal phase. Whereas the follicular phase is characterized by follicular development culminating in release of a dominant ovum, the goal of the luteal phase is to anticipate and prepare the uterus for pregnancy. It is characterized by a dramatic rise in progesterone concurrent with high estrogen levels. These hormonal signals cause the lining of the uterus to thicken and become highly vascular to support implantation and growth of the fertilized ovum. The increase in estrogen also suppresses production of FSH by the pituitary, ensuring that no additional follicles will mature during this phase. Interestingly, the source of these luteal phase hormones is the remnants of the dominant follicle in the ovary. In the absence of an ovum, the follicle morphs into the corpus luteum, a distinctive yellowish-colored temporary endocrine organ. It continues to secrete progesterone, as well as estrogen and inhibin, for approximately two weeks. If during that time pregnancy occurs, then the menstrual cycle is suspended; otherwise, menses will ensue and the cycle will begin again. It is important to note that the human menstrual cycle is highly variable between individuals and also among cycles in the same individual, especially near the beginning and end of the reproductive lifespan (Mihm, et al., 2011). While 28 days is presented as a standard human menstrual cycle, normal cycles may actually range from 24-35 days (Bakos, et al., 1994).

Although control of the cycle is dominated by FSH, LH, estrogen, and progesterone, other minor hormones dynamically influence the process. Activin and inhibin are two hormones produced by the ovary that apply additional positive and negative feedback, respectively, on the FSH production by the pituitary. Together, these

hormones help maintain homeostatic levels of FSH. In addition, AMH exerts a local influence on follicle maturation in a more subtle way. While AMH has no direct effect on FSH secretion, it is believed that it opposes the action of FSH on follicles both at the initial recruitment stage and at the maturation stage (Figure 1.6). Thus, AMH may act analogously to the escapement wheel of a clock, a critical timing gear that is momentarily inhibited on alternating sides with each swing of the pendulum. In a similar manner, AMH likely limits both the entry and exit of follicles from the developing cohort in each cycle. It has been demonstrated in an AMH *null* (-/-) mouse model that AMH is not absolutely necessary in females for fertility. While males of this genotype have predictably dysmorphic reproductive systems and are hence infertile, females are fertile and able to deliver healthy litters. However, long-term studies in this model have shown that these females exhaust their supply of oocytes early and become infertile significantly sooner than wild type controls (Durlinger, et al., 1999). Thus, AMH may play a subtle yet critical role as a gatekeeper of the precious finite oocyte supply over the fertile lifespan of the host.



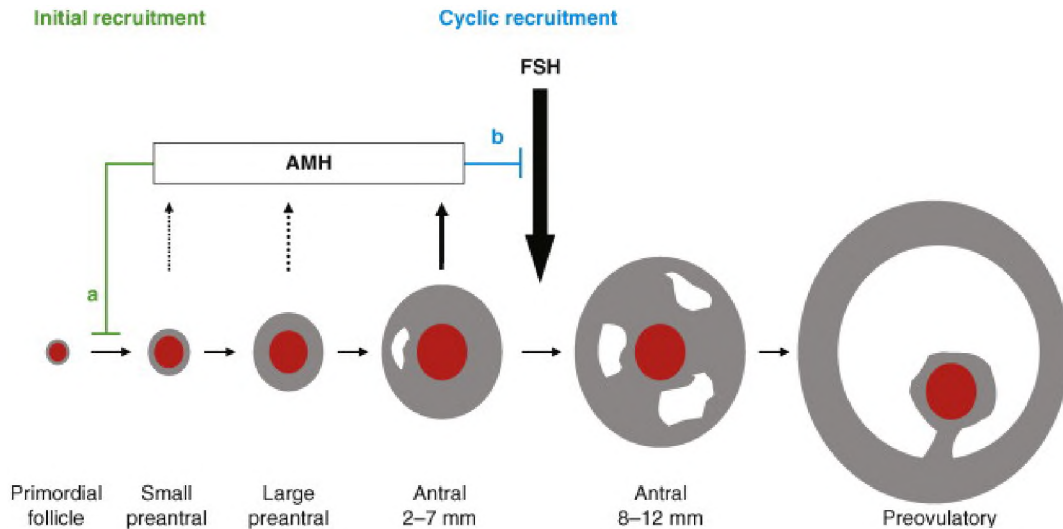


**Figure 1.6 AMH and the Ovarian Cycle.** AMH is produced by the granulosa cells of small and large preantral and early antral follicles, and it exhibits inhibitory effects in two distinct modes. It acts in an autocrine/paracrine fashion to limit entry of primordial follicles into the developing pool (initial recruitment at *a*), and opposes the action of FSH to limit recruitment of preovulatory follicles (cyclic recruitment at *b*). Reproduced from (Broekmans, et al., 2008).

### The Estrous Cycle

The menstrual cycle is unique to humans and higher primates; most mammals undergo an analogous yet distinct process called the estrous cycle. While the two processes share the same goal and are topologically and hormonally similar, there are several important differences between the two. Firstly, in the estrous cycle, there is no menses phase. Rather than being shed, the intrauterine lining is simply reabsorbed. Although many mammals outwardly shed blood when they are sexually receptive or “in heat,” this is not related to menstrual blood, and in fact is associated with ovulation in the opposite part of the cycle. Secondly, because menses is effectively skipped, estrous consists entirely of two phases in common with the menstrual cycle: follicular and luteal. These are physiologically equivalent to their counterparts in the menstrual cycle, but are

further divided into two stages each. Early follicular phase is termed *proestrus*, and the latter portion including ovulation is *estrus* (distinct from estrous). Post-ovulation begins the luteal phase, which is subdivided into *metestrus* and *diestrus*. Each of these four stages is readily identified by vaginal smear; the relative abundance and shape of shed epithelial cells and leukocytes is a distinguishing trait (Cora, et al., 2015). Lastly, females with estrous cycles are sexually receptive only during the estrus phase, when fertility is greatest. This behavior has an obvious reproductive advantage, and is believed to hold true of most primates with menstrual cycles—with the notable exception of human females, who are potentially receptive at any point in their cycles (Motta-Mena & Puts, 2017).

The mouse (*Mus musculus*) exhibits a typical estrous cycle, lasting on average 4-5 days, spending approximately one day in each of the four stages. In contrast to humans who rarely birth more than one offspring at a time, mice typically give birth to litters of between 1-10 pups depending on the strain, and the number of eggs released at ovulation is believed to be roughly equivalent to litter size (The Staff of The Jackson Laboratory, 1966).

### **AMH in Reproductive Senescence and Menopause**

As previously mentioned, AMH has sexually dimorphic expression patterns, extending into advanced age. In adult males, AMH drops to very low but sustained levels; in reproductive-age females, it peaks early and declines steadily until menopause, when it permanently drops to undetectable levels. Unlike most other reproductive hormones, AMH is known to be expressed at relatively steady levels throughout the

entire ovarian cycle (La Marca, et al., 2010). However, since it is secreted by granulosa cells, its expression is directly proportional to the ovarian reserve, *i.e.*, the total number of remaining follicles in both ovaries. As this number steadily declines, so does the level of AMH (Figure 1.7). Because of this correlation, serum AMH levels have become a widely accepted clinical marker of ovarian reserve (Kevenaar, et al., 2006; Broer, et al., 2014). Evidence suggests that it may even be useful in predicting the age at menopause (Tehrani, et al., 2011; Kruszynska & Slowinska-Srzednicka, 2017).

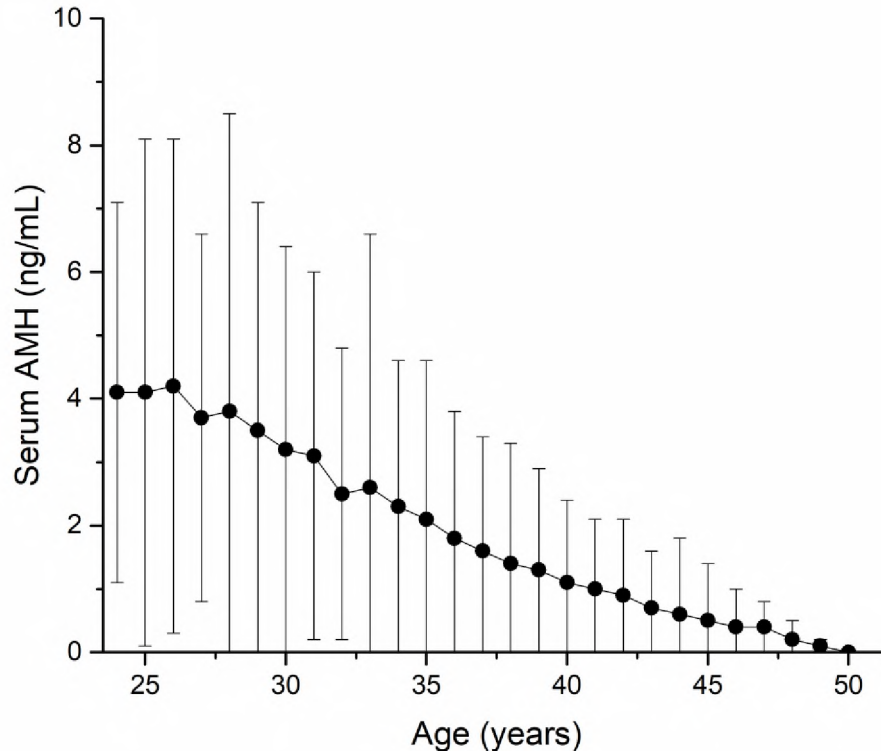


**Figure 1.7 Lifetime Decline in Serum AMH Levels in Women.** Serum AMH levels were clinically assessed in women aged 24-50 in a multi-center retrospective study with data from more than 17,000 patients. The mean values (black circles) dropped steadily with age across the entire range of the study. The average AMH serum concentration declined 0.2 ng/mL/year from ages 24-35, then tapered to 0.1 ng/mL/year from ages 36-50. At 50, an age typically at or near menopause, the mean dropped to zero. Error bars represent  $\pm$ SD. Replotted from (Seifer, et al., 2011).

Menopause represents the time in a woman's life after her final menstrual period, and it is clinically defined retrospectively as the cessation of spontaneous menstruation for one year (Takahashi & Johnson, 2015). Among industrialized nations, the median age of menopause ranges from 50-52 years, with early symptoms typically beginning with the transitional phase of *perimenopause* around age 47; however, ethnicity and lifestyle factors may affect age of onset (Gold, 2011). Menopause is a natural process associated with aging and senescence, and signifies the end of a woman's reproductive lifespan. It is believed that the underlying cause is the complete exhaustion of the ovarian reserve, resulting in cessation of the ovarian cycle. This condition in turn leads to a precipitous drop in estrogen, progesterone, and inhibin production. Without the negative feedback imposed by these hormones on the pituitary, FSH levels maintain a steady high state. The depletion of the ovarian reserve causes AMH to permanently drop to undetectable levels (Bertone-Johnson, et al., 2018). These major hormonal shifts are hallmarks of menopause and underlie substantial physiological and psychological changes. While menopause is not a disease state, it may bring about serious health issues, such as pronounced bone density loss (osteoporosis) and increased risk of cardiovascular disease. Other symptoms can negatively affect quality of life, such as hot flashes, night sweats, vaginal dryness, migraines, decreased libido, and depression (Skaznik-Wikiel, et al., 2015). While many women embrace this life change that brings liberation from menstruation and pregnancy, others may seek hormone therapy to alleviate unpleasant side effects (Thacker, 2009). Many others lament the inability to conceive, particularly when menopause is premature due to natural variation or pathological factors. In this context, AMH may be useful not only as a gauge of ovarian

reserve, but also as a predictor of *in vitro* fertilization (IVF) success for women who struggle to conceive as they approach the age of menopause (La Marca, et al., 2010).

## **AMH DYSFUNCTION AND DISEASE**

### **AMH Dysfunction in Development**

Early clues to the existence and function of AMH came from observations in cases of its dysfunction. When AMH signaling is weak or absent in the male fetus, the Müllerian ducts fail to regress, resulting in a condition known as persistent Müllerian duct syndrome (PMDS). Males with PMDS typically exhibit a normal male phenotype and external genitalia. However, one or both testes may be undescended (cryptorchidism), often accompanied by inguinal hernia. Female reproductive structures, such as the uterus and fallopian tubes, are present and often require surgical removal. Surprisingly, many males with PMDS are fertile, or can become so with medical intervention. PMDS may be caused by defects in either AMH or AMHR2 expression (Josso, et al., 2005), which suggests that no alternative ligand, receptor, or pathway exists that can compensate these deficiencies.

Conversely, problems can also arise in female fetal development when AMH is expressed inappropriately; this disorder causes regression of the Müllerian ducts typical of the male phenotype, causing infertility. A similar condition known as freemartinism in cows may be the earliest recorded observation of AMH dysfunction. Freemartin calves are females from a male/female pair of twins that share a placenta; AMH secretion from the male passes to the female, causing improper Müllerian duct regression and infertility

(Munsterberg & Lovell-Badge, 1991). AMH *null* (-/-) male mice serve as an excellent model for PMDS. Conversely, a transgenic mouse model has been developed in which AMH is overexpressed shortly after birth. This type of postnatal overexpression of AMH results in impaired fertility in females (McLennan, et al., 2017). Taken together, these naturally-occurring defects and their respective mouse models have provided invaluable understanding of the function of the AMH/AMHR2 signaling pathway.

### **Primary Ovarian Insufficiency (POI)**

Primary ovarian insufficiency (POI), also known as premature ovarian failure (POF)<sup>4</sup>, is an abnormal condition in which the ovaries cease to function before the age of 40. POI results in symptoms characteristic of menopause—amenorrhea (failure to menstruate), anovulation (failure to ovulate), early depletion of the ovarian reserve, and hormonal changes including decreased estrogen and elevated FSH (Kovanci & Schutt, 2015). As in menopause, serum AMH levels (Figure 1.8) are generally low or undetectable (Meduri, et al., 2007). However, it is important to note that POI is a pathological condition and not simply premature menopause (Kalantaridou & Nelson, 2000). POI is estimated to affect 1-3% of women under 40 (Kovanci & Schutt, 2015). Known causes include genetic disorders, infections, environmental toxins, chemotherapy, radiation, surgery, and autoimmunity (Ebrahimi & Asbagh, 2001). In most cases, however, the specific etiology cannot be determined. It is presently unclear whether the drop in AMH production is simply a useful clinical marker, or whether AMH

---

<sup>4</sup> Primary ovarian insufficiency (POI) was proposed to replace premature ovarian failure (POF) as it better describes the condition in scientific terms and is less stigmatizing to patients (Welt, 2008); it is therefore the preferred term in this document.

dysregulation may in fact play a mechanistic role in the pathology of the disorder (Meduri, et al., 2007).

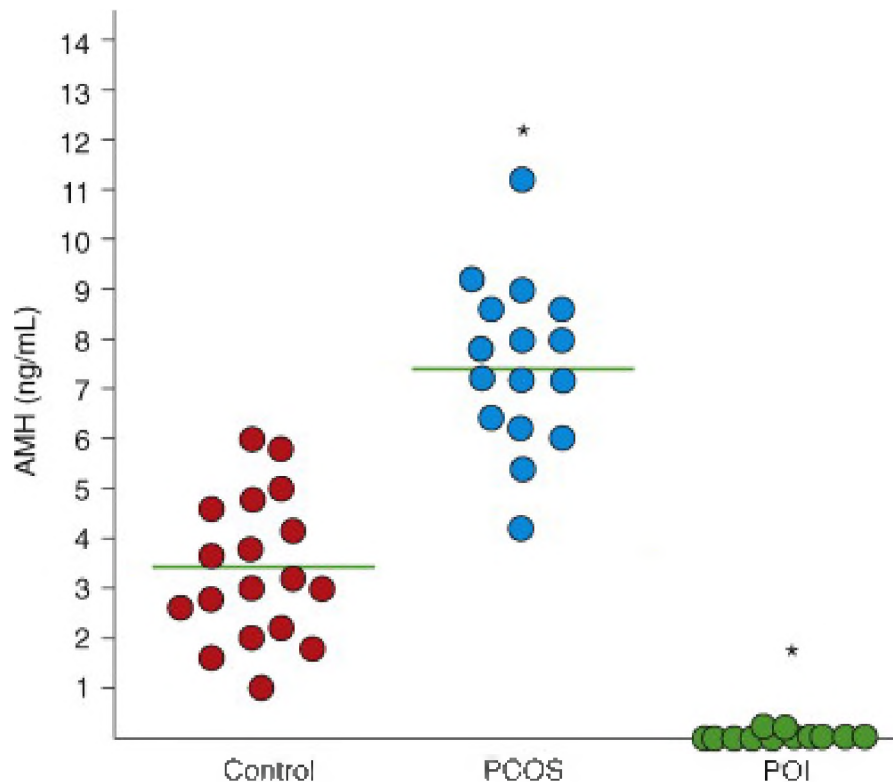


**Figure 1.8** Serum AMH Levels in PCOS and POI. Serum levels of AMH as measured by ELISA are dramatically elevated over normal controls in patients with PCOS and extremely low or undetectable in patients with POI ( $P < 0.05$ ). Reproduced with modification from (La Marca, et al., 2006).

Current treatment options for POI are limited, and often egg donation is the only solution. However, in some patients, small numbers of residual dormant follicles remain, and recent studies have shown that *in vitro* activation of these primordial follicles is possible and may lead to novel infertility treatments (Kawamura, et al., 2016).

## **Polycystic Ovary Syndrome (PCOS)**

Polycystic ovary syndrome (PCOS) is a disorder in which an abnormal excess of antral follicles, also termed "cysts", accumulate in the ovaries. It is the most common female reproductive disorder, affecting up to 10% of all women (Broekmans & Fauser, 2006). In addition to the excess of ovarian cysts, distinguishing symptoms of PCOS include irregularity or absence of menses, as well as aberrant elevation of male sex hormones which can cause hirsutism, acne, and hair loss. PCOS is often accompanied by metabolic abnormalities such as insulin resistance, metabolic syndrome, and obesity (Moran, et al., 2015).

In stark contrast to POI, serum AMH levels in PCOS are abnormally high (Figure 1.8). Typically, the concentration is two to three times greater than normal, which is proportional to the increased numbers of follicles present (Weenen, et al., 2004). Serum AMH levels are therefore useful in the clinical diagnosis of PCOS (Sathyapalan, et al., 2017). More importantly, AMH dysregulation may be directly involved in the pathology of the disease (Dewailly, et al., 2014). Evidence suggests that initially, inadequate AMH secretion by primary follicles is responsible for over-recruitment of follicles into the developing pool, and subsequent overproduction of AMH by mature follicles may block ovulation by nullifying the effects of FSH (Qi, et al., 2016). This suggests a possible biphasic mechanism by which a surplus of follicles becomes indefinitely "stuck" in the ovaries, and also implies a potential route for treatment.



### **AMH in Endometriosis**

Endometriosis is a common gynecological disease in which endometrial tissue grows ectopically outside the uterus. This condition can cause severe pelvic and back pain, abnormal menstruation, and fertility problems. Although it affects approximately 5% of women, the etiology is still unknown (Vercellini, et al., 2014). However, it has recently been shown that endometrial tissue normally expresses AMH and AMHR2, and that this circuit may act in a paracrine fashion to regulate endometrial growth (Wang, et al., 2009). It has been suggested that a defect in signaling may underlie the disease pathogenesis, and that exogenous AMH therapy can potentially serve as a treatment by enhancing cell cycle arrest and apoptosis of the aberrant tissue (Signorile, et al., 2014).

### **AMH and Cancer**

In addition to its established diagnostic role in POI and PCOS, AMH may also prove to be a valuable clinical marker of ovarian cancer. While ovarian tumors of granulosa cell origin are relatively uncommon, accounting for only 3% to 5% of all ovarian neoplasms, serum AMH levels have been shown to be greatly elevated in patients with progressive granulosa cell tumors (GCTs), which then return to normal range upon remission (Rey, et al., 1996). It has also been demonstrated that serum AMH levels directly correlate with aggregate tumor mass (Chang, et al., 2009). These associations make AMH not only useful in detection, but also for evaluating the efficacy of ongoing treatment.

In addition to its clinical diagnostic value, AMH has shown promise *per se* as a cancer treatment. Since the biologic function of AMH is to induce cell growth arrest and

apoptosis, it may be intrinsically therapeutic for any tumor expressing AMHR2. This receptor has been detected in GCTs, epithelial ovarian carcinomas (EOCs), breast cancer, prostate cancer, and even ocular melanoma (Kim, et al., 2014). Conversely, AMH expression has been shown to be significantly decreased or absent in GCTs larger than 10 cm (Anttonen, et al., 2005). The putative downregulation of AMH suggests a mechanism by which tumors may escape growth regulation, and also presents a strategy to overcome it. Treatment of human GCT lines *in vitro* with recombinant AMH has demonstrated its ability to eliminate tumor cells by apoptosis (Anttonen, et al., 2011). Furthermore, a potential clinical application of AMH as a cancer therapy has been successfully tested in a patient-derived xenograft (PDX) model, in which the growth of chemoresistant EOCs were effectively inhibited (Pepin, et al., 2015).

As an alternative approach to exploit the AMH signaling pathway to inhibit tumors, the AMH receptor may be targeted immunologically. Successful inhibition of EOCs in mice has been achieved by active immunization with the cytoplasmic domain of AMHR2 (Sakalar, et al., 2015) as well as with passive transfer of antibodies to the extracellular domain of AMHR2 (Mazumder, et al., 2017). Taken together, these strategies represent a new horizon in treatment of gynecologic and other malignancies.

## **AMH AUTOIMMUNITY**

### **General Features of Autoimmunity**

Autoimmunity is defined as an inappropriate sustained immune response against the host. The immune system has long been described as having the broad capability of

distinguishing "self" from "non-self," with its primary function focused on detection and eradication of non-self elements such as pathogens and foreign materials that pose imminent threats to survival and well-being (Burnet, et al., 1941). However, more recent views indicate that the primary role of the immune system is to recognize “danger” signaled by pathogens through pattern recognition molecules (Matzinger, 1994). In any event, it has long been recognized that the immense power of the immune system could potentially be misdirected against the host itself and cause great harm, and that the immune system must naturally exercise restraint against such an attack. This concept was named "horror autotoxicus" by the pioneering immunologist Paul Ehrlich, and it formed the foundation of the modern view of immunologic tolerance (Punt, et al., 2019).

While tolerance is actively established and maintained at multiple levels in healthy individuals, it can often fail. An unrestrained autoimmune attack may result in acute or chronic conditions with serious damage to tissues and harmful physiologic consequences. For example, in multiple sclerosis (MS), a T cell-mediated autoimmune attack against the myelin sheath of motor neuron axons causes limb weakness and paralysis (Constantinescu, et al., 2011). A humoral response can also mediate autoimmune disease, as in the case of myasthenia gravis (MG), a disorder in which antibodies recognize acetylcholine receptors at neuromuscular junctions thereby blocking normal transmission of signals, causing progressive muscle weakening, and eventually destroying the junctions themselves (Gilhus, 2016). However, autoimmunity is rarely mediated by a single arm of the immune system. The complex interplay among antigen-presenting cells, T cells, and B cells creates a web of co-dependence in which no component acts alone. For example, although MS is primarily T cell-mediated,

autoantibodies have been shown to play a significant role in the pathogenesis of the disease (Kapadia & Dmytriw, 2020).

In all autoimmune diseases, tolerance has failed at some level; when tolerance fails at a grand level, rampant autoimmunity often results. In the syndrome known as IPEX (immunodysregulation, polyendocrinopathy, enteropathy, X-linked), a major component in the active maintenance of immunologic tolerance—regulatory T cells ( $T_{regs}$ )—are severely impaired. This defect can lead to wide ranging consequences, including skin and intestinal disorders, anemia, diabetes, and thyroiditis (Husebye, et al., 2018).

To date, over 80 autoimmune diseases have been identified, affecting as much as 8% of the human population (Punt, et al., 2019). Although the etiologies of many of these conditions have been elucidated, the specific causes and underlying mechanisms for the majority are still poorly understood. Furthermore, there are many other diseases not traditionally considered autoimmune in which autoimmunity is now understood to play a role, such as in atherosclerosis (Schoenfeld, et al., 2005). Still more diseases of unknown etiology exist in which autoimmunity may be the cause in at least a subset of patients, such as in hearing loss (Solares, et al., 2003), infertility (Tuohy & Altuntas, 2007), and heart failure (Jane-wit, et al., 2007). These latter cases are of particular interest to researchers and clinicians as they represent potentially unrecognized pathologies and present pathways for novel therapeutic interventions.

## **Organ-Specific Autoimmunity**

Autoimmunity may target a single organ, an entire organ system, or multiple systems throughout the host. In diabetes mellitus type 1 (T1DM), the attack is focused entirely on the pancreas, and it is directed specifically at the insulin producing beta cells within the organ (Katsarou, et al., 2017). Multiple sclerosis extensively afflicts the central nervous system (CNS), causing lesions in the optic nerves, spinal cord, and brain (Constantinescu, et al., 2011). Systemic lupus erythematosus (SLE) causes widespread damage across diverse organs such as the skin, lungs, kidneys, and joints (Rekvig & Van der Vlag, 2014). The range of sites affected can often be attributed to a single target that is broadly distributed, such as myelin in MS, or DNA in SLE. In general, organ-specific autoimmunity lends itself well to scientific research, as the causes and effects are focused and animal models are readily available or relatively straightforward to develop.

## **Animal Models of Autoimmunity**

The most beneficial tool in autoimmunity research is the animal model of human disease. With an animal as a surrogate, a researcher can explore pathogenic mechanisms and test novel treatments in a way that would not be possible in human patients. While no research animal is a perfect reflection of the human anatomy and physiology, the results of animal studies can be extrapolated to significant extent in the human.

The earliest and best-studied model of autoimmune disease is experimental autoimmune encephalomyelitis (EAE), which closely mimics human MS. It was first developed in the 1930s by Rivers and Schwentker, who elicited ataxia and lesions of the CNS myelin in rhesus monkeys after repeated intramuscular injections of rabbit brain

extracts (Rivers & Schwentker, 1935). This method was further refined over time by substituting crude brain extracts with specific proteins or peptides derived from CNS myelin, such as proteolipid protein (PLP), myelin basic protein (MBP), or myelin oligodendrocyte glycoprotein (MOG). The immunogenicity of these antigens is increased by combining them in an emulsion with complete Freund's adjuvant (CFA), a mixture of paraffin oil and dead *Mycobacterium tuberculosis* extract (Constantinescu, et al., 2011). This method is sufficient to break intrinsic immunologic tolerance and cause a chronic and debilitating autoimmune disease in mice. It also serves as a paradigm for creating new mouse models of organ-specific autoimmune disease, whereby an investigator identifies a suitable organ-specific protein, generates the recombinant protein or synthetic peptide of an appropriate region of the protein, and immunizes the animal and evaluates the disease phenotype. Since the development of the EAE model nearly a century ago, this paradigm has been used to develop scores of models for autoimmune diseases of nearly every type. However, many further human disorders—both known and undiscovered—still await the development of appropriate animal models.

### **Autoimmunity in Ovarian Dysfunction**

Ovarian autoimmunity represents a potentially under-recognized pathology (Sen, et al., 2014). It is estimated that infertility (clinically defined as failure to conceive after 12 consecutive months of regular intercourse) affects approximately 11% of women of childbearing age (Luborsky, et al., 2011). Female infertility may result from anovulation, endocrine irregularities, mechanical causes, or idiopathic (unexplained) reasons (Carp, et al., 2012). Often overlooked is the possibility that autoimmunity may underlie infertility

in any of these four broad categories. This fact may be especially relevant in idiopathic cases, which comprise as many as 20% of all female infertility diagnoses (Deroux, et al., 2017). More intriguingly, autoimmunity may also represent the root cause in at least a cohort of patients with classically characterized disease. Of the approximately 8% of the human population living with autoimmune disease, for reasons that remain unresolved, women are more likely than men to be afflicted by a factor of approximately 3:1 (Smith & Germolec, 1999). This disproportionality gives additional impetus to investigate the role of autoimmunity in female infertility.

The prospect of autoimmunity as a cause of human infertility was first explored in the early 1960s. It was recognized that patients with known autoimmune endocrine diseases involving the thyroid or adrenal glands, or autoimmune polyendocrine syndromes (APS), often presented with POI (Moncayo & Moncayo, 1992), and that general immunosuppression in such cases could often restore ovarian function (Coulam, et al., 1981). Endocrine autoimmunity, particularly of the thyroid, has also been strongly associated with the development of PCOS (Novais, et al., 2015; Mobeen, et al., 2016). As a hormone-responsive organ, it is obvious how dysfunction of the ovary can result secondarily to systemic hormone irregularities caused by organ-specific autoimmunity in another endocrine gland. However, it has also been shown that infertility is often a component in many diverse autoimmune diseases, such as myasthenia gravis, SLE, rheumatoid arthritis, MS, Sjögren syndrome, T1DM, and vitiligo (Moncayo & Moncayo, 1992; Carp, et al., 2012; Silva, et al., 2014; Sen, et al., 2014). In all of these examples, the ovary is indirectly or non-specifically disrupted by factors such as hormonal changes, the failure of other organs, overall poor health, or antibodies to ubiquitous targets, such as

DNA and phospholipids. In the case of thyroid autoimmunity, it has been demonstrated that autoreactive antibodies specific for thyroid hormones that are present in the serum and ovarian follicular fluid are associated with reduced fertility (Monteleone, et al., 2011). However, the ovary itself may be the primary target of an organ-specific inflammatory autoimmune attack; this condition is known as autoimmune oophoritis (AO), and it typically results in POI. It is currently estimated that AO accounts for 5% of all POI cases (La Marca, et al., 2010).

Clinical AO is characterized by autoantibodies to the steroid-producing cells of the ovary and/or T cell infiltration of ovarian tissues. The cells targeted may include the follicular theca cells, granulosa cells, or the oocyte itself, as well as the corpus luteum. Antibodies to specific antigens that have been identified include steroidogenic enzymes, FSH and LH receptors, and the zona pellucida (Silva, et al., 2014). Autoimmune oophoritis may be diagnosed by the presence of ovarian autoantibodies in serum and/or mononuclear inflammatory cell infiltration detected by biopsy (Gao, et al., 2017). These observations have compelled the development of animal models of human infertility as well as having suggested possible ovarian-specific self-proteins as immune targets for creating them.

### **Animal Models of Ovarian Autoimmunity**

The ovary presents an appealing target for autoimmunity research. Unlike the male testis, which is considered an "immunologically privileged" organ that restricts entry of cells of the immune system, the ovary is readily accessible and well-vascularized (Warren, et al., 2014). As in other historical autoimmunity models, the earliest attempts



at developing ovarian autoimmunity involved immunizing animals with crude homogenate derived from the target organ. This strategy first proved successful in a pioneering study in which rats were immunized with crude bovine ovarian homogenate in a CFA emulsion (Jankovic, et al., 1973). The rats developed oophoritis with lymphocytic infiltration 14 days after immunization, as well as ovarian-specific serum antibodies at 28 days. Thus, having the hallmarks of AO, this was the first useful experimental model for studying human AO, and provided the earliest example of *experimental autoimmune oophoritis* (EAO).

An early alternative approach to inducing EAO did not involve immunization with an antigen, but rather initiated the disease by neonatal thymectomy (NTx). It had been well-established that removal of the thymus in mice in a critical window 2-4 days after birth could induce multi-organ autoimmunity, such as thyroiditis, gastritis, and oophoritis (Kojima & Prehn, 1981), in a manner similar to human APS. Taguchi & colleagues further characterized this model by establishing that 3-day-old thymectomized mice produce oocyte autoantibodies (Taguchi, et al., 1980) and further demonstrated that this oophoritis could be passively transferred into normal syngeneic recipients using enriched T cells alone (Taguchi & Nishizuka, 1980), thus reinforcing the dual roles of cellular and humoral immunity in the pathogenesis of AO. Additional studies in the model revealed an acute lymphocytic infiltration, rapid loss of oocytes, ovarian atrophy, autoantibodies to several ovarian components including ooplasm, zona pellucida (sperm binding region), and steroid producing cells (Miyake, et al., 1988), leading the authors to propose it as a model for human POI. Notably, in addition to these similarities to the clinical condition, the mice also exhibited irregular estrous cycles analogous to the

irregular menstrual periods (oligomenorrhea) that are often a symptom of human POI (Shestakova, et al., 2016).

Studies into the mechanisms of NTx-induced autoimmunity have revealed that the primary cause is the depletion of T<sub>reg</sub> cells that would otherwise restrain any pathogenic autoreactive T cells that had already escaped thymic deletion (Asano, et al., 1996). Similarly, a thymic defect in which the autoimmune regulator (AIRE) gene is deleted has been shown in a mouse model to cause ovarian T cell infiltration, early follicle depletion, and infertility (Jasti, et al., 2012). AIRE is known to activate organ-specific proteins not natively expressed in the thymus, and its function is critical to eliminating tissue-specific autoreactive T cells from the repertoire through a negative selection process (Passos, et al., 2018). AIRE-deficient mice also exhibit a range of polyglandular autoimmunity that mirrors human APS. Not surprisingly, defects in AIRE are also responsible for causing APS type-1, also known as autoimmune polyendocrinopathy-candidiasis-ectodermal dystrophy or APECED (Aaltonen, et al., 1997).

More recently, as many of the specific targets of ovarian autoimmunity have been speculated or identified, the original autoantigen-induced model of EAO has been revisited and further refined by replacing crude ovarian homogenate with defined ovarian proteins and peptides. For example, after the discovery of autoantibodies to the oocyte zona pellucida in human and pig sera (Shivers & Dunbar, 1977), another group showed that immunization of mice with synthetic peptides derived from the sequence of zona pellucida sperm-binding protein 3 (ZP3) produced classic EAO with substantial follicular T cell infiltration and high ZP3-specific antibody titers in the serum (Rhim, et al., 1992). As in the NTx model of autoimmunity, adoptive transfer of activated T cells alone from

mice immunized with ZP3 peptide can produce EAO in naive recipients (Hoek, et al., 1997).

Building upon the ovarian self-antigen induction strategy, Altuntas and colleagues developed a novel model of EAO with an intriguing biphasic phenotype (Altuntas, et al., 2006). Immunization with a peptide derived from mouse inhibin- $\alpha$  yielded classic symptoms of POI: ovarian T cell infiltrates, high titers of circulating ovarian-specific antibodies, increased levels of serum FSH, and irregular estrous cycles with a prolonged luteal phase. Surprisingly, however, these mice exhibited an early enhancement of ovulation with gross ovarian hypertrophy and numbers of active follicles significantly higher than controls at four weeks after immunization. This finding was supported by an enhanced fertility as measured by an increased production of pups when mated with normal males 7-9 weeks after immunization with peptide. In stark contrast, when evaluated at 43-45 weeks, inhibin- $\alpha$  immunized mice showed a sharp decline in fertility as evidenced by abnormally low litter sizes and ovarian atrophy. Unlike previous models, EAO could not be passively transferred using purified antigen-specific T cells, but rather B cells or serum alone from immunized mice were capable of producing the phenotype in naive recipients. Thus, it was speculated and subsequently demonstrated that the observed pathology in inhibin- $\alpha$  induced ovarian autoimmunity is mediated by autoantibody neutralization of the biologic activity of inhibin- $\alpha$ . With the negative feedback on pituitary production of FSH alleviated, increased production of FSH leads to superovulation and transient increased fertility; the eventual outcome of this elevated output is a premature depletion of the ovarian reserve, resulting in the classic POI observed at the later time point. This curious biphasic phenotype led the authors to

speculate that perhaps superovulation might be a clinically silent and previously unknown component of the early phase of human POI where women are unknowingly highly fertile.

As underscored by the aforementioned study, there is much still unknown about ovarian autoimmunity. Given the broad spectrum of human ovarian disease and the relatively few animal models available for scientific study, the development of additional models is necessary. EAO has only been achieved using a handful of defined antigens, and scores of ovary-specific proteins are still untested using this paradigm. Among these proteins, AMH stands out not only because of its potential as an ovarian-specific self-protein, but also because its natural function and its relationship to ovarian disease is still poorly understood. For these reasons, the consequences of autoimmunity against AMH was chosen as the focus of the studies presented here.

## CHAPTER II

### MATERIALS AND METHODS

#### **Cloning of the mAMH Gene**

Fresh ovaries were removed from normal healthy 8-week-old euthanized female SWXJ mice (The Jackson Laboratory, Bar Harbor, ME). The tissues were dissected and the RNA was extracted using an RNeasy kit (Qiagen, Valencia, CA). Complementary DNA (cDNA) was generated from total RNA using a RETROscript<sup>®</sup> first strand synthesis kit (Ambion, Austin, TX) with random decamers. The mAMH gene was amplified by reverse transcription polymerase chain reaction (RT-PCR) using Platinum *pfx* DNA polymerase (Invitrogen, Carlsbad, CA) and custom gene-specific primers (Table 2.1) for 25 cycles with an annealing temperature of 65°C. The PCR product was electrophoresed and a 1668 bp fragment was excised and cloned into a TOPO Zero Blunt vector (Invitrogen) and transformed into DH5 $\alpha$  chemically competent *E. coli* (Invitrogen). TOPO clones were miniprepmed with a QIAprep spin miniprep kit (Qiagen) and analyzed by restriction digests with *EcoRI* to show presence of the insert and with *SmaI* (Roche Diagnostics, Indianapolis, IN) to show orientation of the insert. A

candidate clone was selected and sequenced to confirm the identity of the gene (NCBI reference sequence NM\_007445.3) and no mutations were observed.

Target	Primer	Sequence (5' - 3')	Amplicon Length (bp)
mAMH	Forward	ATGCAGGGGCCACACCTCTCTCCACT	1668
	Reverse	TCACCGGCAGCCGCACTCGG	

**Table 2.1 Primers for Cloning the mAMH Gene.** RNA was extracted from fresh mouse ovarian tissue, and 25 cycles of RT-PCR was performed on cDNA using gene-specific primers. The full-length 1668 bp gene was amplified and isolated by gel electrophoresis.

### **Construction of the rmAMH Expression Vector**

The verified mAMH clone was maxiprepmed with a Plasmid Maxi kit (Qiagen) and the insert was excised from the TOPO vector with *EcoRI* and the expression vector pQE81L (Qiagen) was cut at its multiple cloning site with *BamHI* and *HindIII*. Both the insert and the vector were blunted by filling overhangs using T4 DNA polymerase (Roche). The insert and vector were joined using a Rapid Ligation Kit (Roche) and transformed into XLI-Blue supercompetent *E. coli* (Stratagene, La Jolla, CA). Clones were miniprepmed and analyzed by *SmaI* and *BamHI* digestion to show presence and orientation of the insert, and four candidate clones were chosen from those that had the insert in the correct orientation. The construct was designed such that rmAMH would be expressed as an N-terminal 6xHis-tagged fusion protein. DNA sequencing confirmed the presence of the mAMH gene in the correct orientation and in the same reading frame as the 6xHis tag.

### **Screening of Expression Clones**

Four candidate clones were screened for protein expression by small scale culture followed by sodium dodecyl sulfate polyacrylamide gel electrophoresis (SDS-PAGE) and western blot analysis. Starter cultures of each clone in 10 mL of lysogeny broth (LB) medium with 100 µg/mL ampicillin (amp) were growth overnight at 37°C in a shaker incubator. After 16 hours, 100 µL of each starter culture was used to inoculate a fresh 10 mL culture of LB/amp and incubated until the optical density at 600 nm (OD<sub>600</sub>) reached 0.5 (mid-log phase). At this point, expression was induced by adding isopropyl β-D-1-thiogalactopyranoside (IPTG) to a final concentration of 1 mM. The cultures were then incubated for an additional 4 hours to allow protein expression. Culture samples were taken both pre- and post-induction. Cells were pelleted by centrifugation and resuspended in SDS-PAGE buffer and electrophoresed on a 15% Tris-HCl polyacrylamide gel in a mini gel system (Bio-Rad, Hercules, CA) at 200 V for 45 minutes. The gel was stained with 0.05% Coomassie Brilliant Blue R-250 (Bio-Rad). A second gel was run with the same samples under identical conditions for a western blot. The gel was transferred to polyvinylidene fluoride (PVDF) membrane (Bio-Rad) in the mini gel system overnight at 30 V. The membrane was blocked with proprietary blocking agent (Qiagen) and stained with a horseradish peroxidase (HRP)-labeled 6xHis antibody at 1:10,000 dilution for one hour at room temperature with gentle agitation. The blot was washed with Tris-buffered saline (TBS)-tween solution and detection was performed with electrochemiluminescent (ECL) reagents (Amersham, Piscataway, NJ) and exposure to Hyblot CL autoradiography film (Denville Scientific, Holliston, MA). The Coomassie-stained gel revealed a prominent band in the range of the predicted

product size (62 kDa) in three of the four clones and only in the IPTG-induced lane from each pair of samples. Western blot analysis confirmed that this band stained positively for the 6xHis tag in all three samples. The identity of this protein as AMH was subsequently confirmed by western blot using a primary polyclonal rabbit IgG specific for a sequence near C-terminus of AMH (Abcam, Cambridge, MA) followed by detection with an HRP-labeled mouse anti-rabbit IgG secondary antibody (Southern Biotech, Birmingham, AL). One clone, designated AMHEX-3, was selected for use in all subsequent work based on the robustness of expression.

### **Determination of Recombinant Protein Solubility**

To determine whether to purify rmAMH from AMHEX-3 under native or denaturing conditions, the product solubility was assessed. A small scale (50 mL) culture was grown and induced with IPTG as described previously. The cells were pelleted by centrifugation 4 hours post-induction. The pellet was resuspended in lysis buffer (50 mM  $\text{NaH}_2\text{PO}_4$ , 300 mM NaCl, 10 mM imidazole) and lysed by freezing in dry ice/ethanol and thawing in cold water. The pellet was then sonicated on ice using six cycles of 10 seconds on/10 seconds off at 300 W with a sonicator fitted with a microtip probe (Fisher Scientific, Waltham, MA). Lysate was centrifuged at 10,000 x *g* for 25 minutes at 4°C. Supernatant containing the soluble fraction was collected. The remaining insoluble fraction was resuspended in lysis buffer and collected. Samples of each fraction were mixed with SDS-PAGE buffer and run on a 10% Tris-HCl gel under denaturing conditions and stained with Coomassie blue. The rmAMH band appeared in the insoluble fraction.



### **Expression of Recombinant mAMH**

Recombinant mAMH was prepared from batch cultures and purified under denaturing conditions. 500 mL LB/amp cultures were inoculated with 10 mL of LB/amp overnight starter cultures and grown at 37°C in a shaker incubator until an OD<sub>600</sub> of 0.5 was reached. Protein expression was then induced with IPTG at a final concentration of 1 mM. Cultures were then grown an additional 4.5 hours. Cells were pelleted by centrifugation at 6,000 x g and frozen at -20°C for further processing.

### **Affinity Purification of Recombinant mAMH**

Frozen cell pellets from 500 mL batch cultures were thawed on ice and resuspended in 7.5 mL of denaturing lysis buffer (100 mM NaH<sub>2</sub>PO<sub>4</sub>, 10 mM Tris, 6 M guanidine HCl, pH 8.0), split into two 250 mL centrifuge bottles and stirred at room temperature for one hour. The centrifuge bottles were spun at 10,000 x g for 25 minutes at 4°C to remove the insoluble debris from the lysate. The cleared lysate was then transferred to 15 ml tubes and 350 µL of a suspension of nickel nitrotriacetic acid (Ni-NTA) agarose (Qiagen) was added to each. The tubes were agitated slowly on an orbital shaker at room temperature for one hour. The mixtures from both tubes was combined and loaded on a poly-prep chromatography column (Bio-Rad) and the liquid phase was allowed to flow through by gravity. The column was then washed twice with 4 mL aliquots of wash buffer (100 mM NaH<sub>2</sub>PO<sub>4</sub>, 10 mM Tris, 8 M urea, pH 6.3). Elution was first attempted by lowering the pH of the wash buffer to 5.9, which did not result in significant recovery of AMH. The pH was then lowered to 4.5, which resulted in successful elution of AMH from the column. For quality control purposes, samples were

taken at each step of purification and run on denaturing SDS-PAGE gels and either stained with Coomassie blue (Figure 2.1) or subjected to western blot (Figure 2.2) analysis as described previously.

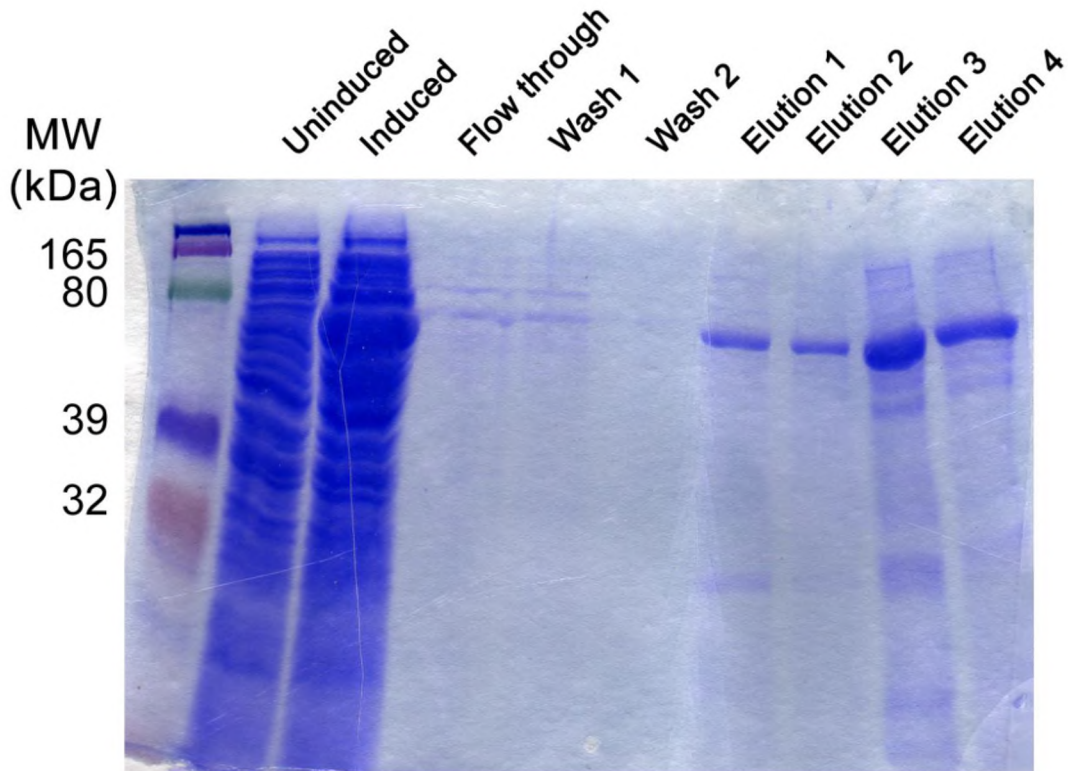


**Figure 2.1 SDS-PAGE of Recombinant mAMH.** Denaturing SDS-PAGE was performed on samples from Ni-NTA purification of rmAMH. Samples were run on a 15% Tris gel at 200 V for 45 minutes, then the gel was stained with Coomassie blue. Kaleidoscope prestained marker was used to estimate molecular weight (MW). Samples were taken pre-IPTG induction (uninduced) and at culture harvest (induced). Samples from the column flow through and washes were collected (flow through; washes 1-2) and from protein elution at pH 4.5 (elutions 1-4). Maximum protein was observed in elution 3. All eluted proteins ran at the expected MW of 62 kDa for rmAMH.

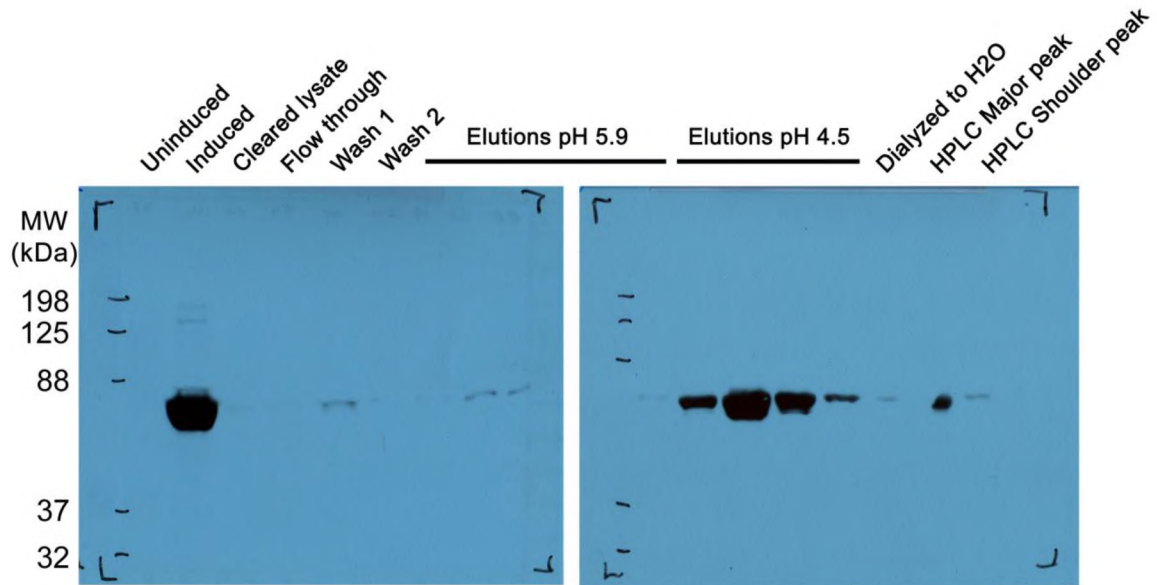


**Figure 2.2 Western Blot of Recombinant mAMH.** Denaturing SDS-PAGE was performed on samples from Ni-NTA purification of rmAMH. Samples were run on 15% Tris gels at 200 V for 45 minutes, then the gel was transferred to polyvinylidene fluoride (PVDF) membrane and stained with HRP-labeled AMH antibody and exposed to electrochemiluminescence (ECL) reagents and captured on autoradiography film. Kaleidoscope prestained marker was used to estimate molecular weight, and the ladder positions were marked manually on the film (MW). Samples were taken pre-IPTG induction (uninduced) and at culture harvest (induced). Samples from the cleared lysate, column flow through, and washes were collected (cleared lysate; flow through; washes 1-2). Column elutions with buffer at pH 5.9 (elutions pH 5.9, four lanes) and at pH 4.5 (elutions pH 4.5, four lanes) were collected. Elutions at pH 4.5 were pooled and dialyzed to water, then run on high performance liquid chromatography (HPLC) where the major peak and shoulder were collected (final three lanes). The blot shows positive identification of the recombinant protein as AMH. Greatest AMH detection occurred in the induced sample, the elutions at pH 4.5, and the HPLC major peak. Detection in the sample from AMH dialyzed to water was low due to the sample being highly dilute. All AMH samples ran at the expected MW of 62 kDa.

### HPLC Purification of Recombinant mAMH

For use in *in vitro* cell culture assays, affinity-purified rmAMH was further refined by high performance liquid chromatography (HPLC) to increase purity and remove any residual endotoxin (Dudley, et al., 2003). Aliquots of Ni-NTA purified rmAMH in elution buffer were loaded onto a Beckman System Gold (Beckman Coulter,

Brea, CA) fitted with a Vydac 214TP C4 column (Grace, Columbia, MD) and run on a gradient from 100% water to 100% acetonitrile over the course of 50 minutes.

Recombinant mAMH eluted in a single major peak occurring between 32-36 minutes (64-72% acetonitrile; Figure 2.3). The peak was collected and lyophilized on a Freezone 6 Plus lyophilizer (Labconco, Kansas City, MO). Dried protein was gently resuspended in endotoxin-free water at 1 mg/mL. The identity of the eluted protein was confirmed using western blot analysis (Figure 2.2) with anti-6xHis and anti-AMH antibodies as previously described. Preparations were routinely tested for endotoxin by the Media Preparation Core (Lerner Research Institute, Cleveland, OH) using the limulus amoebocyte lysate (LAL) test and were consistently below the detectable threshold (<0.05 EU/mL). Specificity control protein recombinant mouse  $\beta$ -casein (rm $\beta$ -cas) used for *in vitro* experiments was purified and tested in the same manner as rmAMH.

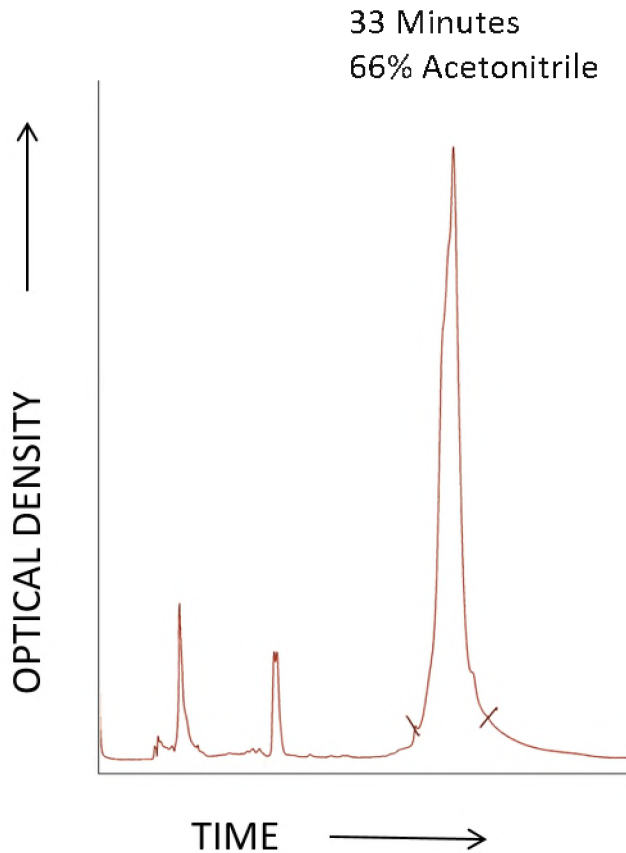


**Figure 2.3 HPLC Profile of Recombinant mAMH.** Ni-NTA-purified AMH was further refined using HPLC to increase purity and remove endotoxin. AMH eluted as the major peak centered at 33 minutes into a 50-minute linear gradient from 100% water to 100% acetonitrile. Acetonitrile content was approximately 66% at maximal elution. Optical density was measured as absorbance at 280 nm.

### **Refolding of Recombinant mAMH**

For mouse immunizations, Ni-NTA purified rmAMH in elution buffer was dialyzed in a series of gradual steps to allow proper folding of the native conformation of the protein to maintain solubility. Eluted fractions were combined and sealed inside dialysis tubing with a molecular weight cutoff (MWCO) of 25 kDa (Spectrum Laboratories, Rancho Dominguez, CA). The protein was first dialyzed against a large volume of 8 M urea, pH 8.0. Then, in a series of ten steps, the buffer was diluted 1:2

with deionized water. Finally, the protein was dialyzed against pure water, lyophilized, and stored under vacuum as a dry powder until used.

### **Quantification of Recombinant Proteins**

Each batch of recombinant protein was quantified using the Bio-Rad Protein Assay, a modified version of the Bradford assay. Bovine serum albumin (BSA) standards and samples were loaded at 10  $\mu$ L volumes on a 96-well MaxiSorp plate (Nalge Nunc, Rochester, NY). 200  $\mu$ L of 1X dye reagent (Bio-Rad) was added and mixed by pipetting and developed at room temperature for five minutes. Plates were then read at 595 nm on a Victor<sup>2</sup> spectrophotometer (Perkin Elmer, Waltham, MA) and standards were plotted as absorbance vs. protein concentration using Origin 6.0 software (OriginLab, Northampton, MA). Sample concentrations were determined from the linear portion of the standard curve.

### **Mice and Immunization**

Female C57BL/6J mice were purchased from The Jackson Laboratory (Bar Harbor, ME). At 6-8 weeks of age, mice were immunized subcutaneously (*s.c.*) in the abdominal flanks with 200  $\mu$ L of a water-in-oil emulsion of equal volumes of complete Freund's adjuvant (CFA; Difco Laboratories, Detroit, MI) containing 400  $\mu$ g of dead *Mycobacterium tuberculosis* H37RA (Difco) and water containing 1 mg/mL rmAMH. Each mouse received a total of 100  $\mu$ g of rmAMH. Control mice were immunized with an emulsion of CFA and water alone.

## **T Cell Proliferation Assays**

Ten days after immunization, mice were euthanized humanely with CO<sub>2</sub> asphyxiation followed by cervical dislocation in accordance with institutional animal care and use committee (IACUC) protocols. Axillary and inguinal lymph nodes were dissected and macerated through 40 µm nylon mesh filters to make single-cell suspensions. Cells were plated in Falcon 96-well tissue culture plates (Becton Dickinson, Franklin Lakes, NJ) at  $3.5 \times 10^5$  cells/well in Dulbecco's modified Eagle's medium (DMEM; Media Preparation Core, Cleveland Clinic) supplemented with final concentrations of 10% fetal bovine serum (FBS; Hyclone Labs, Logan, UT), 30 mM 4-(2-hydroxyethyl)-1-piperazineethanesulfonic acid (HEPES) buffer, 2 mM L-glutamine, 1 mM sodium pyruvate, 100 U/mL penicillin and 100 µg/mL streptomycin (Invitrogen). Antigen was added to the wells in a tenfold log series for a final concentration of 0.01 µg/mL to 100 µg/mL. A specificity control protein, ovalbumin (OVA; Sigma-Aldrich, St. Louis, MO) or recombinant mouse β-casein (rmβ-cas), was added to control wells in the same dilutions. Purified hamster anti-mouse CD3ε (clone 145-2C11; BD Biosciences, San Jose, CA) at 2 µg/mL was used as a positive control. Negative control wells contained no antigen. Cultures were incubated at 37°C and 5% CO<sub>2</sub> for 72 hours. All wells were then pulsed with [methyl-<sup>3</sup>H] thymidine (Perkin Elmer) at 1 µCi/well. After 16 hours, plates were harvested with a 96-well plate harvester (Tomtec, Hamden, CT) onto glass fiber filters (Perkin Elmer). Filters were dried, sealed in bags with scintillation fluid, and counted with a Betaplate liquid scintillation counter (Perkin Elmer).

### **Responses by CD4+ and CD8+ T Cell Subpopulations**

To assess the relative contributions of CD4+ and CD8+ T cells in the autoimmune response, each subset was purified and tested in a proliferation assay as described above. Ten days after immunization with rmAMH, lymph node cells (LNC) were harvested and macerated through 40  $\mu$ m nylon mesh filters to make single-cell suspensions. T cell subsets were enriched by positive selection using anti-CD4 or anti-CD8 coated magnetic beads and passage through a magnetic-activated cell sorting (MACS) LS column in a MidiMACS magnetic separator (Miltenyi Biotec, San Diego, CA). Enriched LNC were plated in 96-well plates at  $2.5 \times 10^5$  cells per well along with  $4 \times 10^5$  irradiated syngeneic splenocyte feeder cells. Feeder splenocytes were obtained from a naïve C57BL/6J mouse by maceration through a 40  $\mu$ m nylon mesh filter and were pelleted at 1500 rpm and 4°C in an Allegra X-14R centrifuge (Becton Dickinson) and resuspended in sterile water to hypotonically lyse and eliminate red blood cells (RBCs). Lymphocytes were immediately rescued by addition of 10% v/v 10X phosphate-buffered saline (PBS) to restore isotonicity and washed again with 1X PBS. The cell suspension was then subjected to 2000 rads of gamma radiation in a  $^{137}\text{Cs}$  irradiator (J.L. Shepherd & Associates, San Fernando, CA). Unsorted, CD4+, and CD8+ T cells were cultured with various doses of rmAMH and OVA in the same manner as previously described proliferation assays. Proliferation was determined by incorporation of [methyl- $^3\text{H}$ ] thymidine as described above.



### **FACS Analysis of Enriched CD4+ and CD8+ T cells**

To determine the purity of the enriched T cell subpopulations, cells were co-stained with CD3, CD4, and CD8 antibodies and analyzed using flow cytometry. LNC were washed with 1X PBS and resuspended in fluorescence-activated cell sorting (FACS) staining buffer (1% BSA in PBS) and incubated for 45 minutes at 4°C with PerCP-CD3 $\epsilon$  (clone 145-2C11), PE-CD4 (clone RM4-5), and FITC-CD8a (clone 53-6.7; BD Biosciences). To minimize non-specific binding, cells were pre-incubated for 10 minutes at 4°C with Fc Block (anti-CD16/CD32; BD Biosciences). Cells were then fixed with a 1% final concentration of paraformaldehyde and run on a FACScan flow cytometer (Becton Dickinson). Data analysis was performed post-acquisition with FlowJo version 7.0 (Flowjo, Ashland, OR). The lymphocyte population was selectively gated using forward and side scatter, and from that population, only the CD3 $^{+}$  cells were analyzed for presence of CD4 or CD8.

### **Cytokine ELISA Assays**

Ten days after immunization, mice were euthanized and lymph node cells were collected in the same manner as for proliferation assays. Cells were cultured in complete DMEM at  $2.5 \times 10^6$  cells/mL in 24-well flat-bottom plates (BD Biosciences). Each well contained 25  $\mu$ g/mL of rmAMH (stimulated) or OVA (unstimulated) control in a total volume of 2 mL per well. After 48 hours in culture, supernatants were collected and cytokine levels were determined by sandwich enzyme-linked immunosorbent assay (ELISA) in 96-well MaxiSorp plate (Nalge Nunc) using commercial recombinant mouse cytokines (BD Biosciences) as standards. Cytokine capture/detection pairs were as

follows: IL-2, clones JES6-1A12 and biotin JES6-5H4; IL-5, clones TRFK5 and biotin TRFK4; IL-10, clones JES5-2A5 and biotin SXC-1; IL-17A, clones TC11-18H10 and biotin TC11-8H4. Plates were coated with capture antibody at 4 µg/mL and blocked with a solution of 3% BSA. Standards and samples were plated at a volume of 100 µL and incubated overnight at 4°C. Biotinylated detection antibodies were used at 2 µg/mL. Avidin-peroxidase was added and plates were developed using 2,2'-azino-bis(3-ethylbenzothiazoline-6-sulphonic acid) (ABTS) substrate. For the IFN $\gamma$  assay, a commercial optimized ELISA kit was used (OptEIA; Invitrogen) in a similar manner as described above according to the manufacturer's instructions. Plates were read at 405 nm on a Victor<sup>2</sup> spectrophotometer (Perkin Elmer) and standards were plotted as absorbance vs. cytokine concentration using Origin 6.0 software (OriginLab). Sample concentrations were determined from the linear portion of the standard curve.

### **Cytokine ELISpot Assays**

Ten days after immunization, mice were euthanized and lymph node cells were collected in the same manner as for proliferation assays. Single cell suspensions in DMEM were plated at a density of  $2 \times 10^5$  cells/well on 96-well PVDF filter plates (Millipore Sigma, Burlington, MA) which had been pre-coated with the appropriate cytokine capture antibody at 4 µg/mL and blocked with a solution of 1% BSA and 5% sucrose in PBS. rmAMH antigen, as well as specificity control antigens rm $\beta$ -cas and OVA, were added to the appropriate wells at doses of 25 µg/mL and 50 µg/mL. Negative control wells contained no antigen and positive control wells contained hamster anti-mouse CD3 $\epsilon$  (clone 145-2C11, BD Biosciences) at 2 µg/mL. After 72 hours of

incubation at 37°C and 5% CO<sub>2</sub>, cells and media were aspirated and the plates were washed and the appropriate biotinylated cytokine detection antibody was added at a concentration of 2 µg/mL. Plates were then incubated overnight at 4°C. Cytokine capture/detection pairs were as follows: IL-2, clones JES6-1A12 and biotin JES6-5H4 (BD Biosciences); IFN $\gamma$ , clones AN-18 and biotin R46A2 (eBioscience, San Diego, CA); IL-5, clones TRFK5 and biotin TRFK4 (BD Biosciences); and IL-17, clones 17CK15A5 and biotin 1787 (eBioscience). After overnight incubation, plates were washed and 100 µL/well streptavidin-alkaline phosphatase (Sav-AP) enzyme (R&D Systems, Minneapolis, MN) solution was added at a working dilution of 1:60 in 1% BSA in PBS per manufacturer's instructions. Plates were then incubated for 2 hours at room temperature and washed again. 5-bromo-4-chloro-3-indolyl-phosphate/nitro blue tetrazolium (BCIP/NBT) solution was added to all wells at 100 µL/well and the plate was incubated in the dark at room temperature for 20-30 minutes until spots were clearly visible. Plates were then rinsed with deionized water and air-dried overnight at room temperature and scanned using an ImmunoSpot plate reader (CTL, Shaker Heights, OH). Data were collected and analyzed using ImmunoSpot 4.0 software (CTL).

### **qRT-PCR Analysis**

At 4 weeks, 8 weeks, and 10 months after immunization, mice were euthanized as previously described and tissues were collected for mRNA expression analysis. Ovary, spleen, heart, liver, kidney, and brain samples were removed immediately following perfusion and placed in RNAlater preservative (Sigma-Aldrich) and stored at -20°C until use. Samples were processed in Trizol reagent (Invitrogen) using a TissueMaster 240

homogenizer (Omni International, Kennesaw, GA) until completely dissociated. RNA was then extracted in chloroform and tubes were centrifuged at 12,000 x g for 15 minutes at 4°C. The upper aqueous layer containing the RNA was carefully transferred to a fresh tube and precipitated using isopropanol. RNA was pelleted by centrifugation at 12,000 x g for 15 minutes at 4°C, and the pellet was then washed with 70% ethanol made with diethyl pyrocarbonate (DEPC)-treated water. The RNA was then centrifuged at 7,500 x g for 7 minutes at 4°C and the supernatants decanted. RNA pellets were allowed to air-dry for 10-15 minutes then resuspended in 30 µL nuclease-free water. To ensure that the RNA was not contaminated with genomic DNA, DNase treatment was immediately performed using a DNA-free kit (ThermoFisher Scientific, Waltham, MA) according to the manufacturer's instructions. Briefly, samples were treated with recombinant DNase at 37°C for 30 minutes, then the enzyme was inactivated with DNase inactivation buffer for 1.5 minutes at room temperature. Samples were then centrifuged and transferred to fresh tubes and quantified using a Nanodrop 2000 spectrophotometer (ThermoFisher). cDNA was then made from the mRNA using a Superscript III first strand synthesis kit (Invitrogen) according to the manufacturer's instructions. Briefly, RNA was incubated with oligo dT primer at 65°C for 5 minutes, then placed on ice for one minute and centrifuged. The enzyme mix containing reverse transcriptase was added, and the mixture was incubated for 50 minutes at 50°C, and then transferred to ice. The cDNA was quantified using a Nanodrop 2000. Quantitative real-time polymerase chain reaction (qRT-PCR) analysis was then performed using a StepOne Plus Real-Time PCR System (Applied Biosystems, Forest City, CA) using primer pairs specific for mouse IL-1β, TNFα, IFNγ, IL-2, IL-10, IL-17A, and AMH (Table 2.2) according to the manufacturer's

protocol. Briefly, for each well, 400 ng of cDNA, 0.5  $\mu$ M primers, and 1X SYBR Green Master Mix (Applied Biosystems) were added to a MicroAmp Fast Optical 96-well plate (Applied Biosystems) and run for a total of 40 cycles with an annealing/extension temperature of 60°C. Melt curves were automatically performed at the end of each run to ensure the integrity of the data. The quality of each assay was verified by electrophoresis of the final qPCR products on agarose gels. The expression of the gene target in each sample was first normalized to the expression of the endogenous control  $\beta$ -actin for that sample ( $\Delta$ Ct). Means of samples from AMH-immunized mice were then calculated relative to the means of CFA-immunized controls ( $\Delta\Delta$ Ct) and the results plotted as the fold change in gene expression ( $2^{-\Delta\Delta$ Ct).

Target	Primer	Sequence (5' - 3')	Amplicon Length (bp)
mTNF $\alpha$ <sup>1</sup>	Forward	CGAGTGACAAGCCTGTAGCC	209
	Reverse	GTGGGTGAGGAGCACGTAGT	
mIL-1 $\beta$ <sup>2</sup>	Forward	AAGGAGAACCAAGCAACGACAAAA	213
	Reverse	TGGGGAACCTCTGCAGACTCAAAC	
mIFN $\gamma$ <sup>1</sup>	Forward	GGATATCTGGAGGAACTGGCAA	110
	Reverse	TGATGGCCTGATTGTCTTTCAA	
mIL-2 <sup>1</sup>	Forward	GCAGGCCACAGAATTGAAAG	207
	Reverse	TCCACCACAGTTGCTGACTC	
mIL-10 <sup>3</sup>	Forward	TGGCCCAGAAATCAAGGAGC	264
	Reverse	CAGCAGACTCAATACACACT	
mIL-17A <sup>2</sup>	Forward	AAGGCAGCAGCGATCATCC	150
	Reverse	GGAACGGTTGAGGTAGTCTGAG	
mAMH	Forward	CAGGCCCCCAGGTCACAGTC	213
	Reverse	AGCGGGAATCAGAGCCAAATAGAA	
m $\beta$ -actin <sup>1</sup>	Forward	GGTCATCACTATTGGCAACG	133
	Reverse	ACGGATGTCAACGTCACACT	

<sup>1</sup> (Sakalar, et al., 2015)

<sup>2</sup> (Mazumder, et al., 2017)

<sup>3</sup> (Kawane, et al., 2010)

**Table 2.2 Primers for qRT-PCR Analysis of Gene Expression.** Primer pairs specific for signature cytokines, AMH, and  $\beta$ -actin endogenous control were used to assay relative gene expression in mouse ovarian tissues using quantitative real-time PCR. All sequences are in 5' to 3' orientation. Validated primer sequences were obtained from published references as noted.

## **Immunohistochemistry**

At 4, 8, and 12 weeks after immunization, mice were euthanized by CO<sub>2</sub> asphyxiation and perfused with PBS for tissue collection. Ovaries were dissected and fixed in methanol fixative (60% methanol, 30% double-distilled deionized water, 10% acetic acid), embedded in paraffin, and sectioned at 5 µm thickness. For immunostaining, a rabbit ImmunoCruz kit (Santa Cruz Biotechnology, Dallas, TX) was used according to the manufacturer's specifications. Briefly, slides were de-paraffinized by heating to 50°C for 10 minutes, followed by washes in xylene, 100% ethanol, 95% ethanol, and finally double-distilled deionized (DDD) water. Antigens were unmasked by submerging in citric acid buffer (10 mM sodium citrate, pH 6.0) for 30 minutes in a non-pressurized steamer, then allowed to cool to room temperature. Slides were blocked with 5% normal donkey serum, and then incubated overnight at 4°C with polyclonal rabbit anti-mouse CD3 (Abcam) at 1:250 dilution. Slides were then incubated for 30 minutes with an HRP-labeled goat anti-rabbit IgG and developed using a 3,3'-diaminobenzidine (DAB) substrate. Slides were then washed in DDD and counterstained with Harris hematoxylin (Electron Microscopy Sciences, Hatfield, PA) and dehydrated with washes of 95% ethanol, 100% ethanol, and finally xylene. Slides were coverslipped with Permount medium (Fisher Scientific). Similarly, fixed ovarian sections at 4 and 8 weeks after immunization were unmasked with Trilogy reagent (Millipore Sigma) and stained with affinity-purified polyclonal rabbit anti-mouse C4d (a gift from the Baldwin Lab, Cleveland Clinic, Cleveland, OH) at 1:500 dilution and counterstained with hematoxylin (Murata, et al., 2007). All slides were scanned at 20X and imaged using an SCN400 automated slide scanner (Leica Biosystems, Buffalo Grove, IL).

### **Serum Autoantibody Isotyping**

At 4 weeks, 8 weeks, 12 weeks, and 10 months after immunization, blood was collected via terminal cardiac puncture with a 1 mL syringe with a 22 gauge 1" needle (Becton-Dickinson) under general anesthesia using a vaporizer (Ohmeda, Madison, WI) delivering a constant supply of oxygen with 2.5% isoflurane (Baxter, Deerfield, IL). After blood collection, mice were euthanized via cervical dislocation in accordance with IACUC protocols, and blood was allowed to clot for one hour at room temperature, then transferred to 4°C overnight. After 16 hours, the blood samples were centrifuged for one minute at 2,500 x g at 4°C, then sera were carefully transferred to clean microcentrifuge tubes. Tubes were then centrifuged at 1,500 x g for 10 minutes at 4°C, and again transferred to clean microcentrifuge tubes. Cleared sera were then transferred to clean tubes and stored at -20°C until use. Sera were tested for the presence of AMH-specific IgG isotypes using a Mouse Typer Sub-Isotyping Kit (Bio-Rad) according to the manufacturer's specifications. Briefly, HPLC-purified rmAMH or rm $\beta$ -cas was plated in 96-well flat bottom MaxiSorp plates (Nalge Nunc) at 10  $\mu$ g/mL in a volume of 50  $\mu$ L PBS and incubated overnight at 4°C. Wells were washed and blocked with 1% BSA in PBS for 1 hour at room temperature. Serum samples were diluted serially with 1% BSA in a 1:2 scheme from 1/256 to 1/8192 and added to the plate in duplicate wells in 100  $\mu$ L volumes and incubated overnight at 4°C. Negative control wells contained diluent alone and positive control wells contained a rabbit polyclonal mAMH (Abcam) antibody at 1:1000 dilution. Plates were washed and pre-diluted rabbit anti-mouse IgG isotype detection antibodies added: IgG<sub>1</sub>, IgG<sub>2a</sub>, IgG<sub>2b</sub>, and IgG<sub>3</sub>. Plates were incubated for one hour at room temperature, then washed again. Wells were then treated with horseradish



peroxidase (HRP) conjugated goat anti-rabbit IgG and exposed to peroxidase substrate solution for 30 minutes and absorbance at 405 nm was measured with a Victor<sup>2</sup> 1450 spectrophotometer (Perkin Elmer). Mean absorbances for each isotype were plotted vs. antibody titer.

### **Serum Hormone ELISAs**

To evaluate circulating levels of AMH in the bloodstream, blood from mice immunized with rmAMH or CFA was collected via terminal cardiac puncture as previously described at 10 months after immunization. Sera were kept frozen at -20°C until use and evaluated for AMH levels using a commercially-available mAMH competitive ELISA kit (Cusabio, College Park, MD) according to the manufacturer's instructions. Briefly, serum samples were thawed and diluted 1:3 with PBS, then added in duplicate to wells in a 96-well plate pre-coated with capture antibody. AMH standards supplied with the kit were also added in separate wells in duplicate. The volume of all samples and standards was 50 µL. Unlabeled standards and samples competed with HRP-labeled AMH for 1 hour at 37°C. After a final wash, 3,3',5,5'-tetramethylbenzidine (TMB) substrate was added and the plate was developed for 15 minutes at 37°C. 50 µL of stop solution was then added to the plate to halt development, and the absorbance at 450 nm was read on a Victor<sup>2</sup> spectrophotometer (Perkin Elmer). Means of the standards were plotted vs. absorbance, and the mean AMH concentrations of samples were determined from the linear portion of the standard curve. Serum FSH levels were similarly assessed at 8 weeks and 10 months after immunization using a commercial non-competitive sandwich ELISA kit (Aviva Systems Biology, San Diego, CA) according to

the manufacturer's instructions. Briefly, serum samples were diluted 1:100 with kit diluent and added in duplicate to wells in the 96-well assay plate pre-coated with capture antibody along with along with the kit FSH standards in a volume of 100  $\mu$ L and incubated for two hours at 37°C. The plate was then washed and 100  $\mu$ L of biotinylated detection antibody was added and the plate was incubated for one hour at 37°C. The plate was washed again and 100  $\mu$ L of avidin-HRP conjugate was added and the plate was again incubated for one hour at 37°C. After a final wash, TMB substrate was added and the plate was developed at 37°C for 15 minutes in the dark. The reaction was halted with kit stop solution and the absorbance at 450 nm was read, the standard curve was plotted, and sample values determined in the same manner as described for the ELISA for AMH.

### **Fertility Assessments**

To evaluate the impact of AMH autoimmunity on fertility, 8-week old female mice were immunized with rmAMH or CFA alone and serially mated to the same age-matched C57BL/6J males for four mating cycles (Figure 2.4). Matings began 14 days after immunization, and females were rested for two weeks between parturition and the next mating cycle. Mice were checked daily for litters. Total litter weights, individual pup weights, and numbers of pups per litter were assessed at birth.

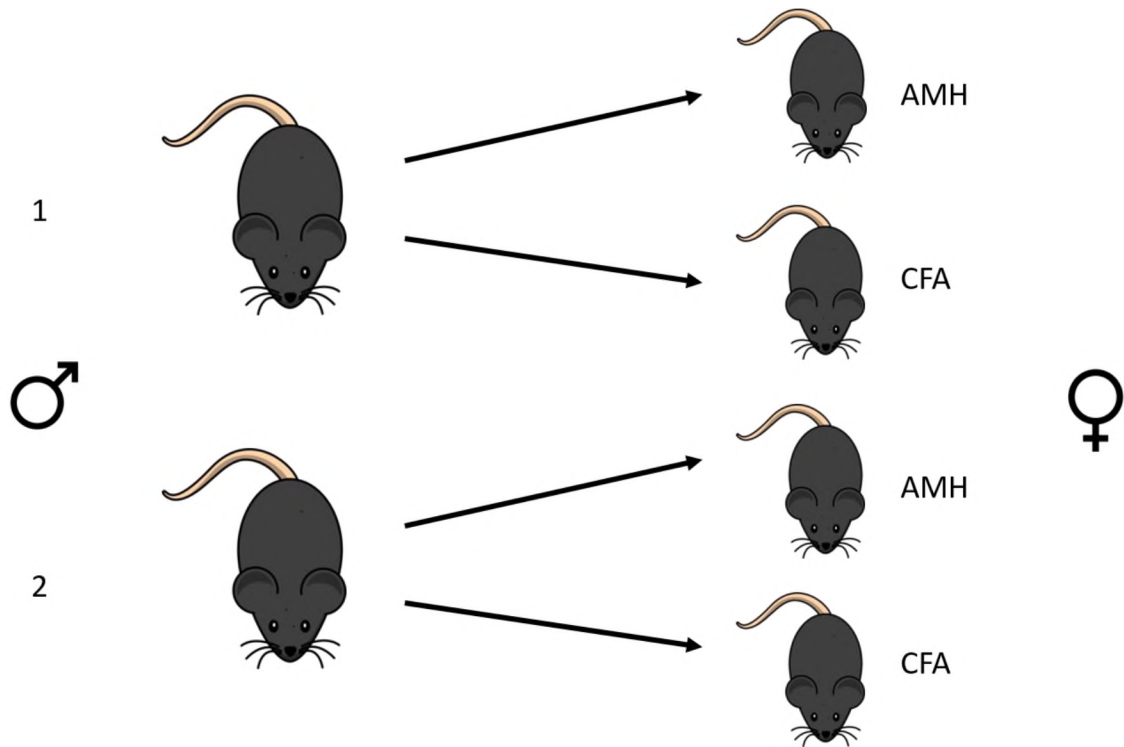


**Figure 2.4 Fertility Assessment Mating Scheme.** To assess fertility, female C57BL/6J immunized with either AMH or CFA control were mated with normal age- and strain-matched males. Males mated with equal numbers of AMH and CFA immunized mice. Each male mated with the same females for every mating round.

### Follicle Quantification and Ovary Measurements

At 4 weeks, 8 weeks, and 10 months after immunization, mice were euthanized, perfused with PBS, and ovaries were dissected and weighed. Ovaries were then fixed in methanol fixative (60% methanol, 30% DDD water, 10% acetic acid) and embedded in paraffin and serially sectioned completely through the organ. Every tenth 5  $\mu$ m section was mounted to avoid counting any follicle more than once. Sections were stained with hematoxylin and eosin (H&E) and slides were imaged using a SCN400 automated slide scanner (Leica Biosystems). Images were analyzed in ImagePro 7.0 software (Leica Biosystems) and follicles were manually tagged and counted using the following criteria: small, an oocyte surrounded by a single layer of granulosa cells; medium, an oocyte

surrounded by 2-3 layers of granulosa cells; large, an oocyte surrounded by more than three layers of granulosa cells and/or the presence of antra (Figure 2.5). Involved follicles as well as any large follicles showing signs of involution and/or pyknotic nuclei were considered atretic. Corpora lutea were identified as large, light-colored bodies with a slim central cavity containing a blood clot. The area of each serial section analyzed was measured by manually outlining the perimeter in ImagePro. The mean area of each ovary was determined as the average area of the four largest consecutive sections. Ovary weights were normalized to body weight just prior to euthanization.

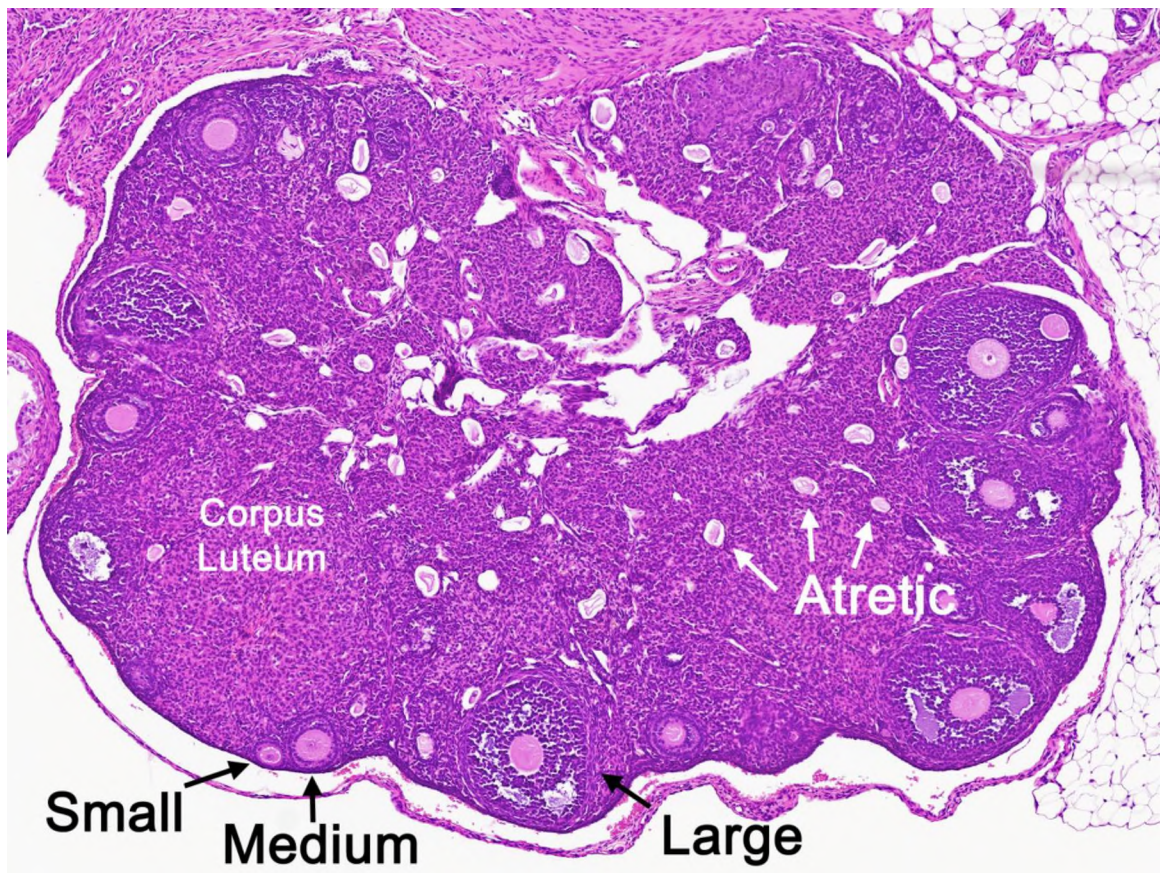
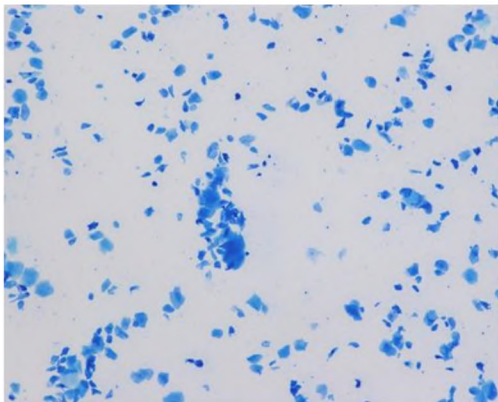


**Figure 2.5 Follicle Quantification Scheme.** For each H&E stained ovarian section, follicles were quantified according to morphology. Small, medium, large, and atretic follicles, as well as corpora lutea were counted and ovarian measurements were taken manually using ImagePro software.

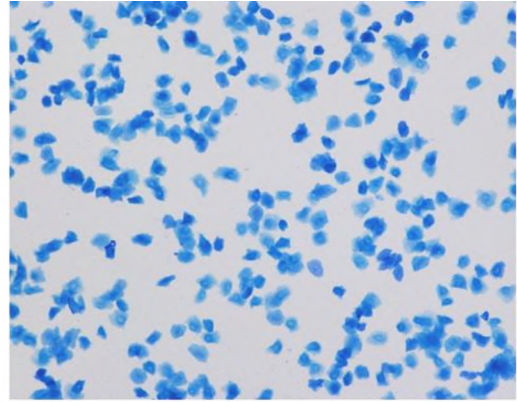
### **Estrous Cycle Staging**

Four weeks after immunization with rmAMH or CFA, vaginal smears were taken at the same time daily for a total of 52 consecutive days by flushing the vagina with 20  $\mu$ L of sterile PBS and transferring to a glass slide. Slides were air-dried, then fixed in 100% methanol and allowed to dry. Slides were then stained with methylene blue in 9.5% ethanol, then washed with DDD water and then 75% ethanol. Slides were air-dried and coverslipped with Permount (Fisher Scientific). Slides were examined with light microscopy and estrous stage was determined as follows: proestrus, predominantly round nucleated epithelial cells with presence of leukocytes; estrus, cornified non-nucleated epithelial cells with absence of leukocytes; metestrus, roughly equal numbers of cornified epithelial cells and leukocytes; diestrus, a predominance of leukocytes (80-100%; Figure 2.6).

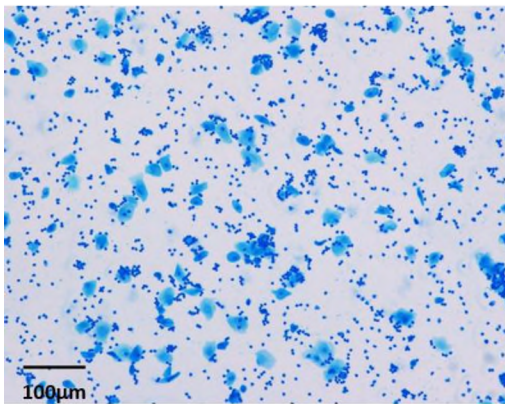




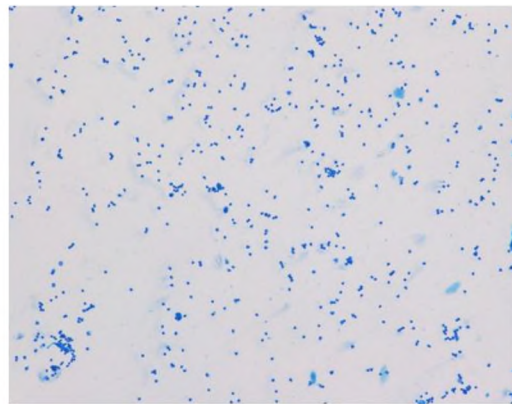
**Day 1 - PROESTRUS**



**Day 2 - ESTRUS**



**Day 3 - METESTRUS**



**Day 4 - DIESTRUS**

**Figure 2.6 Estrous Cycle Staging Scheme.** Vaginal samples were collected at the same time daily, smeared on slides, methanol fixed, and stained with methylene blue. Slides were examined under the microscope and estrous stage was determined by the relative numbers of cell types and their morphologies. Panels represent the typical appearance of each stage, each of which lasts approximately one day. Scale bar represents 100  $\mu\text{m}$ .

### **Passive Transfer of Autoimmunity**

To assess the contributions of various components of the immune system to the observed phenotype, passive transfer was performed. Eight-week-old female C57BL/6J donor mice were actively immunized *s.c.* with 100 µg rmAMH or OVA control as previously described. After four weeks, spleens were harvested and single-cell suspensions were made. Suspensions from each immunizing antigen were pooled and populations of CD4<sup>+</sup> T cells and B cells were enriched using MACS separation as previously described with CD4-specific and B220-specific beads, respectively (Miltenyi Biotec). Purities of enriched populations were confirmed using FACS analysis as previously described. B cells were washed with PBS and immediately transferred by intraperitoneal (*i.p.*) injection to naïve age and sex matched syngeneic recipients, with each mouse receiving a total of  $2 \times 10^7$  cells. Prior to transfer, CD4<sup>+</sup> enriched T cells were cultured and activated in 24-well plates with syngeneic irradiated splenocyte feeder cells for four days with HPLC-purified rmAMH or OVA recall antigen at 25 µg/mL. T cells were then harvested, washed with PBS, and injected *i.p.* into naïve recipients at  $2 \times 10^7$  cells per mouse. In addition, blood from mice immunized with rmAMH or OVA was collected at 4 weeks via terminal cardiac puncture as previously described. Sera were transferred to naïve recipient mice via intravenous (*i.v.*) tail vein injection using a 1 mL syringe with a 30 gauge needle (Becton-Dickinson). Each mouse received a total of four injections of 200 µL serum every third day. Seven days after initial transfer, mice were evaluated every day for estrous cycle stage using vaginal smears as previously described.

### **Statistical Analyses**

The unpaired Student's *t*-test was used to analyze differences in fertility, estrous cycle, follicle numbers, gene expression, and hormone levels between mice immunized with CFA containing rmAMH and control mice immunized with CFA alone.



## CHAPTER III

### RESULTS

#### **Immunization with AMH Elicits a Robust Antigen-Specific T Cell Response**

To determine the T cell response to rmAMH, ten days after immunization with 100  $\mu\text{g}$  rmAMH in CFA, inguinal and axillary LNC were cultured in the presence of antigen over a wide logarithmic dose range for 72 hours. Cells were radiolabeled with tritiated thymidine, and the degree of cell division was expressed as the stimulation index (SI), defined as the counts per minute (cpm) of sample divided by the cpm of negative control wells with no antigen. The results show that rmAMH elicited a significant T cell response ( $>20$  SI units) at 10  $\mu\text{g}/\text{mL}$  and an extremely robust T cell response ( $>100$  SI units) at 100  $\mu\text{g}/\text{mL}$  (Figure 3.1). Not only was this response dose-dependent, but it was antigen-specific, as there was no measurable response to the immunologically-irrelevant antigen OVA across the entire dose range.

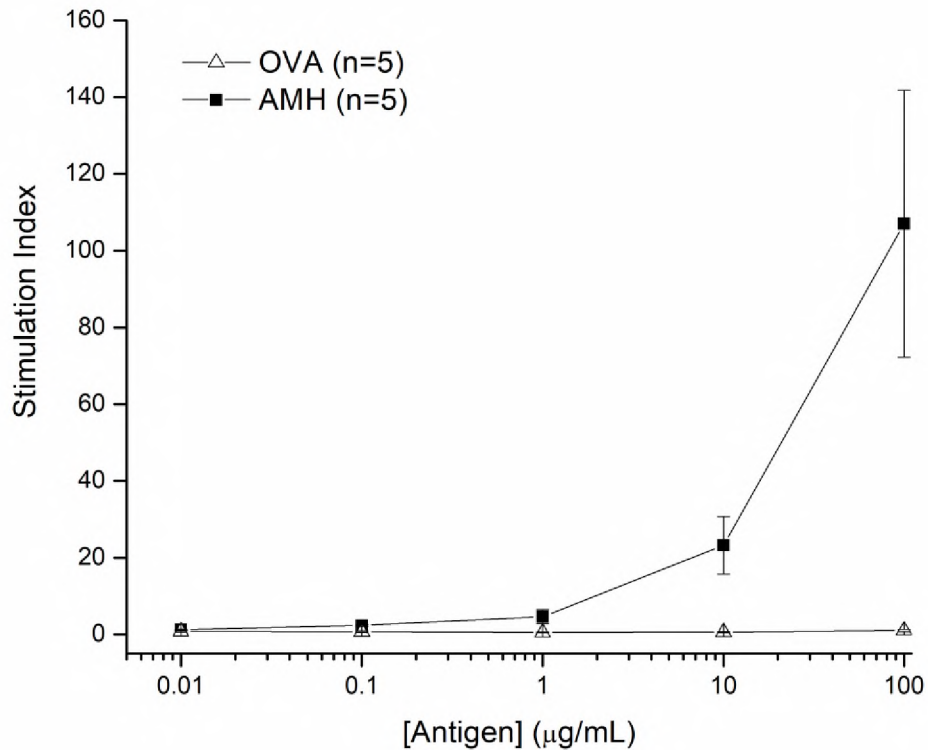


**FIGURE 3.1 T cell proliferation response to AMH.** Ten days after immunization with rmAMH, LNC were harvested and tested in culture for response to antigen. T cells showed a robust, dose-dependent response to HPLC-purified rmAMH, but not to the irrelevant control antigen OVA. Error bars represent  $\pm$ SEM.

### **AMH-reactive T Cells are Primarily of the CD4+ Phenotype**

To further characterize the phenotype of AMH-reactive T cells, ten days after immunization with rmAMH, LNC were harvested and enriched for either CD4+ or CD8+ T cells by positive selection using MACS magnetic separation beads. To verify the purity of the enriched populations, flow cytometry was performed on samples using fluorochrome-tagged antibodies specific for mouse CD4 and CD8. Analysis of results confirmed high homogeneity of the enriched populations, with CD4+ cells >98% pure and CD8+ >97% pure (Figure 3.2). Enriched and unsorted cells were then cultured for

72 hours in the presence of antigen and with irradiated syngeneic splenocyte feeders, and T cell proliferation was measured as previously described with radiolabeling. The data showed a robust response to rmAMH in the unsorted LNC, which was greatly enhanced in the enriched CD4<sup>+</sup> population (Figure 3.3). In contrast, the CD8<sup>+</sup> population showed little response to cognate antigen. In all cases, positive responses were dose-dependent. No significant proliferation was observed in response to the irrelevant control antigen OVA, confirming antigen-specificity. These data indicate that the T cell immune response to AMH is primarily of the CD4<sup>+</sup> phenotype, which represents the T helper (T<sub>H</sub>) subset. The responses elicited by CD4<sup>+</sup> T cells are restricted to antigens presented by major histocompatibility (MHC) class II molecules, which suggests that this is the primary form of T cell activation following immunization with rmAMH.

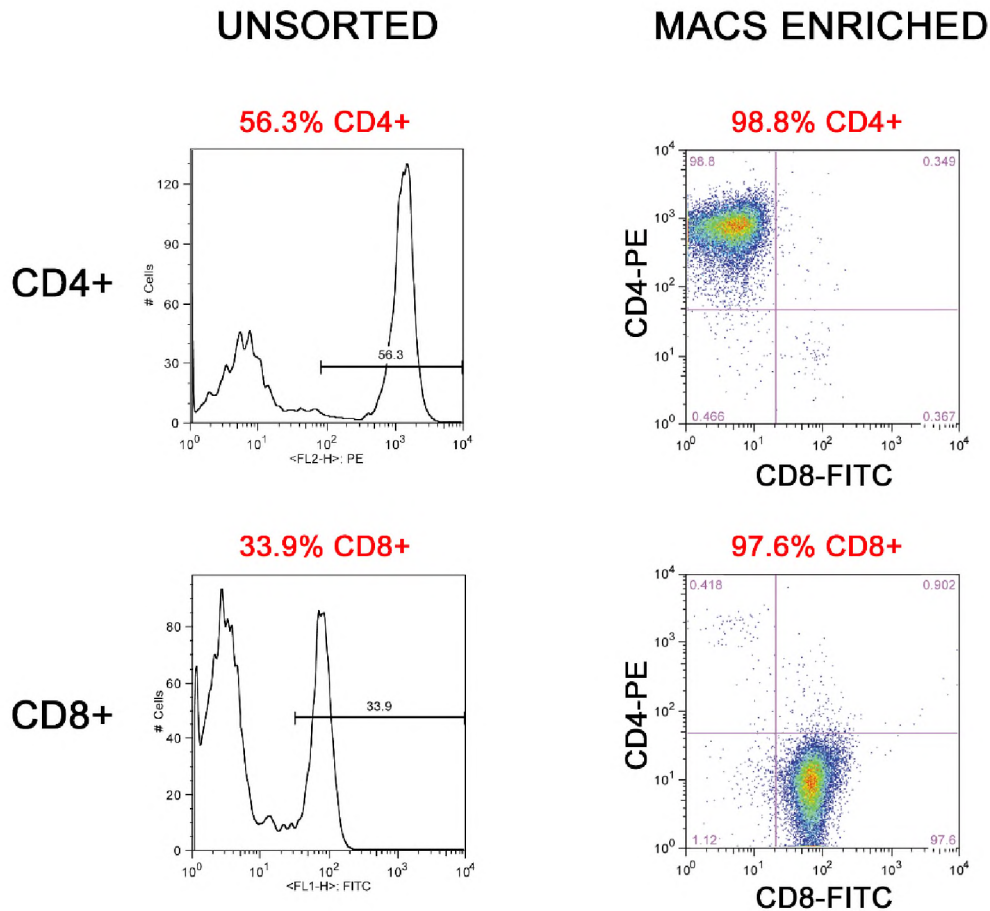


**Figure 3.2 Flow Cytometry Analysis of Enriched CD4+ and CD8+ T Cells.** LNC were harvested from rmAMH-immunized mice and analyzed by flow cytometry before (unsorted, left) and after (MACS enriched, right) positive selection using CD4 or CD8 MACS beads. Cells were triple-stained with fluorochrome-labeled antibodies to CD4, CD8, and the T cell marker CD3. The target population was gated using forward and side scatter, and further gated on the CD3+ population. After enrichment, the purity of CD4+ and CD8+ increased from 56.3% to 98.8% and from 33.9% to 97.6%, respectively.

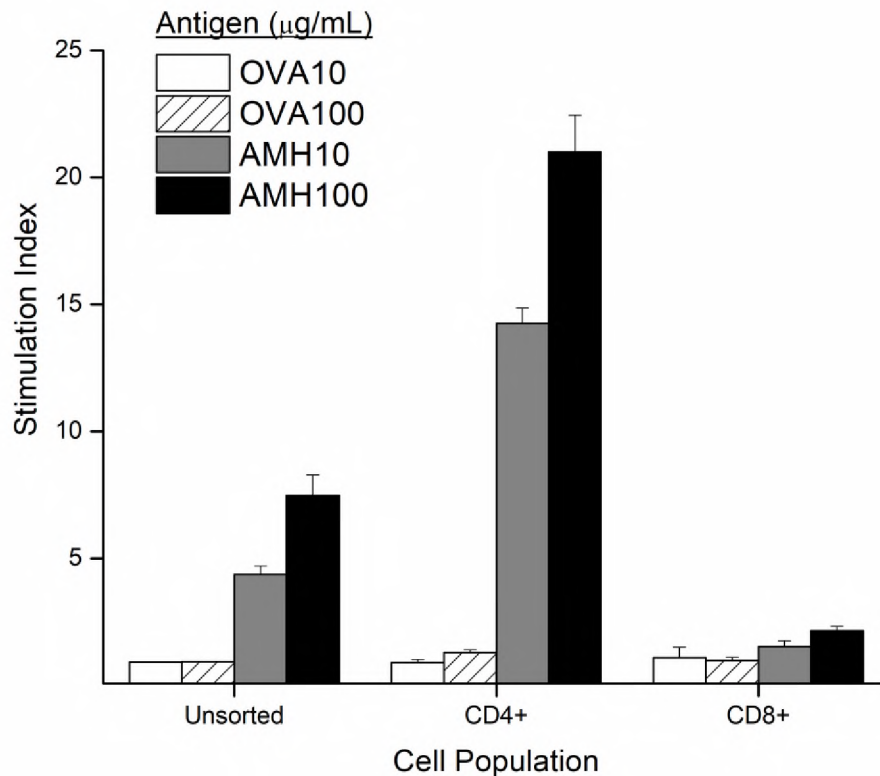


**Figure 3.3 Proliferation Assays.** Ten days after immunization with rAMH, LNC were harvested and a portion were purified by MACS positive selection for CD4 or CD8. Cells were cultured for 72 hours with rAMH or OVA control on a monolayer of irradiated syngeneic splenocyte feeders. Unsorted splenocytes and CD4+ T cells showed robust, dose-dependent, antigen-specific responses. A negligible response was observed in the CD8+ population. Error bars represent  $\pm$ SEM.

### **AMH Immunization Elicits a Type-1/Type-17 Cytokine Profile**

To assess the cytokine profile of the T cell response to AMH, ten days after immunization with rAMH, LNC were cultured at  $2.5 \times 10^6$  cells/mL in 24-well flat-bottom plates in the presence of 25  $\mu$ g/mL rAMH or OVA negative control for 48 hours. Supernatants were then collected and analyzed by sandwich ELISA for a panel of type-1, type-2, and type-17 cytokines. The rAMH-stimulated wells showed a predominance of the definitive type-1 cytokine IFN $\gamma$ , as well as significant expression the

type-1 associated T cell growth factor IL-2 (Figure 3.4). In addition, there was robust expression of the archetypal type-17 cytokine IL-17. There was no measurable production of the type-2 cytokines IL-4 or IL-5, and only a trivial amount of the type-2 cytokine IL-10 was detected. There was no observable cytokine production in wells stimulated with the OVA control. Taken together, these data indicate that immunization with AMH elicits a strong, antigen-specific type-1/type-17 cytokine profile, which is typical of an autoimmune response (Raphael, et al., 2015).

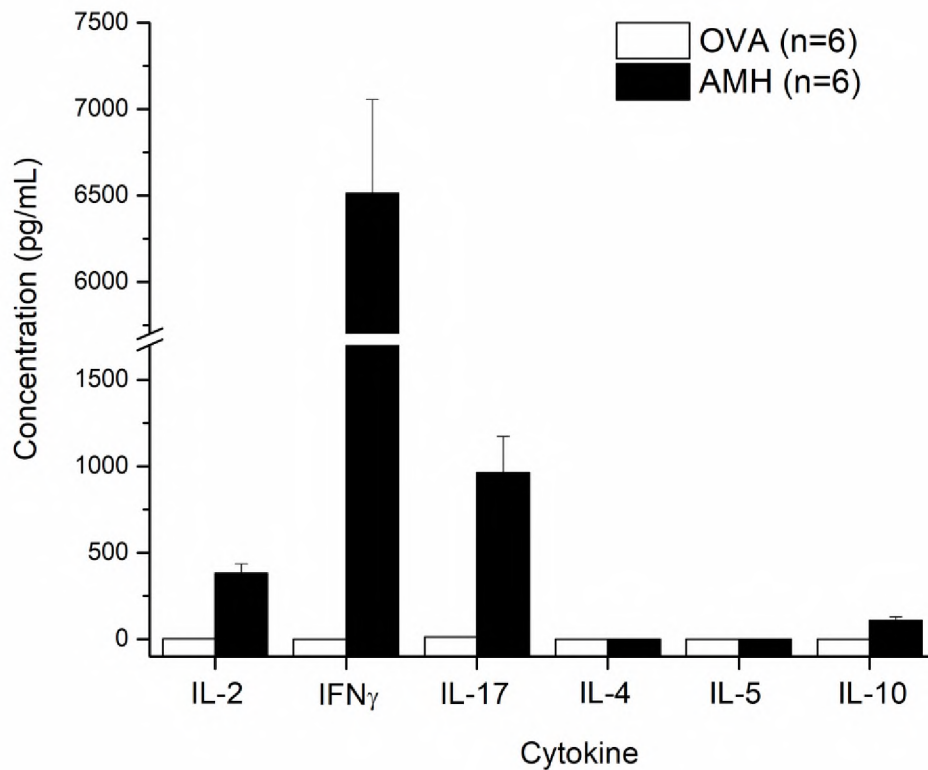


**Figure 3.4 Cytokine ELISA Profile of AMH-Specific T Cells.** Ten days after immunization with rmAMH, LNC were cultured in the presence of HPLC-purified rmAMH or OVA control. Culture supernatants were collected and tested for a panel of cytokines by sandwich ELISA. Results indicate a strong antigen-specific type-1/type-17 immune response. Error bars represent  $\pm$ SEM.

### **ELISpot Analysis of Type-1/Type-17 T Cell Frequencies**

To further evaluate the type-1/type-17 profile evident in the culture supernatants by ELISA, ELISpot analysis was performed to assess the frequencies of T cells secreting IL-2, IFN $\gamma$ , IL-5, and IL-17. Ten days after immunization with rmAMH, LNC were harvested and seeded at  $2 \times 10^5$  cells/well in 96-well PVDF filter plates. Plates were cultured for 72 hours in the presence of 25  $\mu\text{g}/\text{mL}$  or 50  $\mu\text{g}/\text{mL}$  antigen. For these experiments, mouse  $\beta$ -casein (rm $\beta$ -cas), a recombinant protein prepared from *E. coli* using the same protocol for generating rmAMH, was used in addition to the OVA control to rule out non-specific stimulation from bacterial contaminants. As in the ELISA analysis, the dominant cytokine secreted was IFN $\gamma$ ; T cells producing this cytokine exhibited a frequency of over 100 cells per million at the 50  $\mu\text{g}/\text{mL}$  dose (Figure 3.5). Also congruent with the ELISA results, substantial IL-2 and IL-17 activity was detected, with no measurable contribution from cells secreting IL-5. No significant responses were observed with either control protein, affirming once again that the responses to rmAMH are antigen-specific. Moreover, in accord with T cell proliferation assays, antigen-specific responses were positively dose-dependent. Taken together, these data reinforce the type-1/type-17 characterization of the AMH immune response.

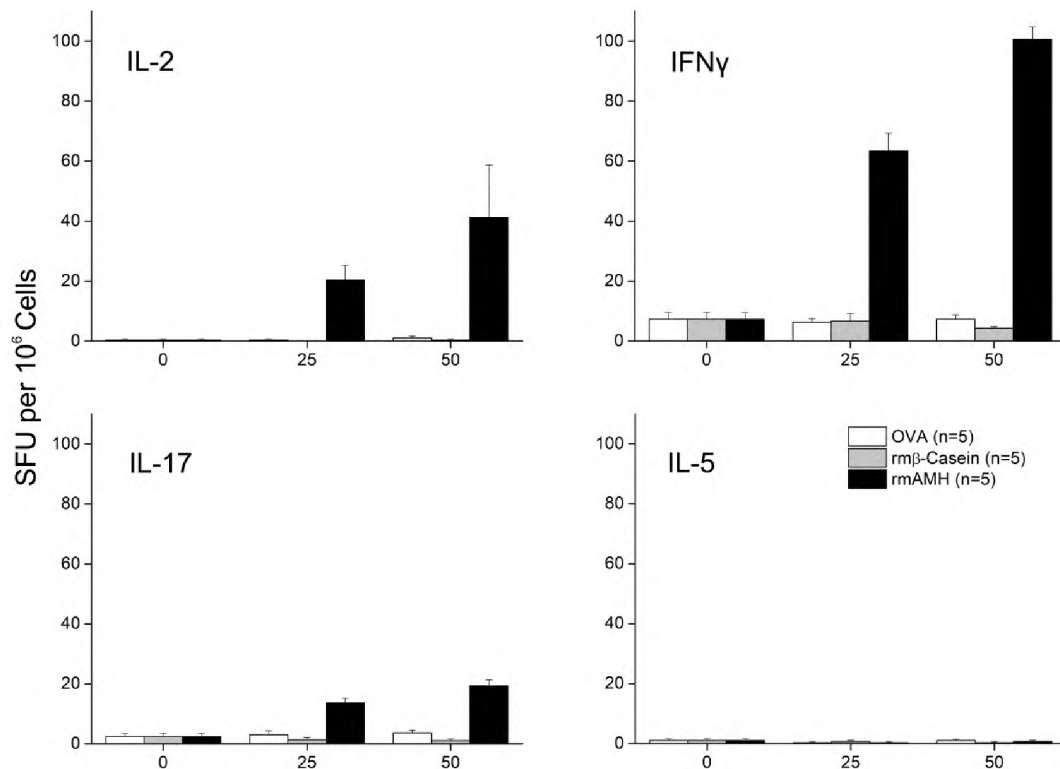


**Figure 3.5 Cytokine ELISpot Profile of AMH-Specific T Cells.** Ten days after immunization with rmAMH, LNC were cultured in ELISpot plates for 72 hours in the presence of antigen or control and tested for the frequencies of T cells producing cytokines IL-2, IFN $\gamma$ , IL-17, and IL-5. Data are expressed as spot-forming units (SFU) per million cells at each dose for each recall antigen. Results indicate a dose-dependent antigen-specific type-1/type-17 response. Error bars represent  $\pm$ SEM.

### **qRT-PCR Analysis Reveals Expression of Type-1/Type-17 Inflammatory Genes**

Multiple lines of *in vitro* evidence have shown that AMH immunization produces a robust type-1/type-17 T cell response that is characteristic of autoimmunity. To assess the AMH immune response at a molecular level in the host, ovarian tissues were harvested from mice at 4 weeks, 8 weeks, 12 weeks, and 10 months after immunization with rmAMH or CFA. Expression of a panel of signature cytokines (Table 2.2) was evaluated using quantitative real-time RT-PCR (qRT-PCR). Each sample was first



normalized to its endogenous  $\beta$ -actin control, and gene expression for each target cytokine in the AMH-immunized mice was quantified relative to age-matched CFA-immunized controls. The data reveal a pattern of transient initial upregulation of the innate inflammatory cytokines IL-1 $\beta$  and TNF $\alpha$ , with TNF $\alpha$  expression being the most prominent, peaking early and subsiding by 12 weeks. The inflammatory type-1/type-17 cytokines IFN $\gamma$  and IL-17 were also expressed abundantly from 4 weeks through 12 weeks. Very little expression of the type-2 cytokine IL-10 was observed at any time point. This predominantly type-1/type-17 inflammatory *in vivo* tissue profile is consistent with *in vitro* ELISA and ELISpot assays. IL-2, while detected in minor quantities *in vitro* in LNC harvested ten days after immunization, was generally not observed in significant quantities in the tissues examined at 4 weeks and beyond. This is probably due to the role of IL-2 as an early-expressed factor driving the differentiation of naive T cells to effector cells (Liao, et al., 2011). Expression of all cytokines had subsided by 10 months, indicating a late waning of the cellular immune response.

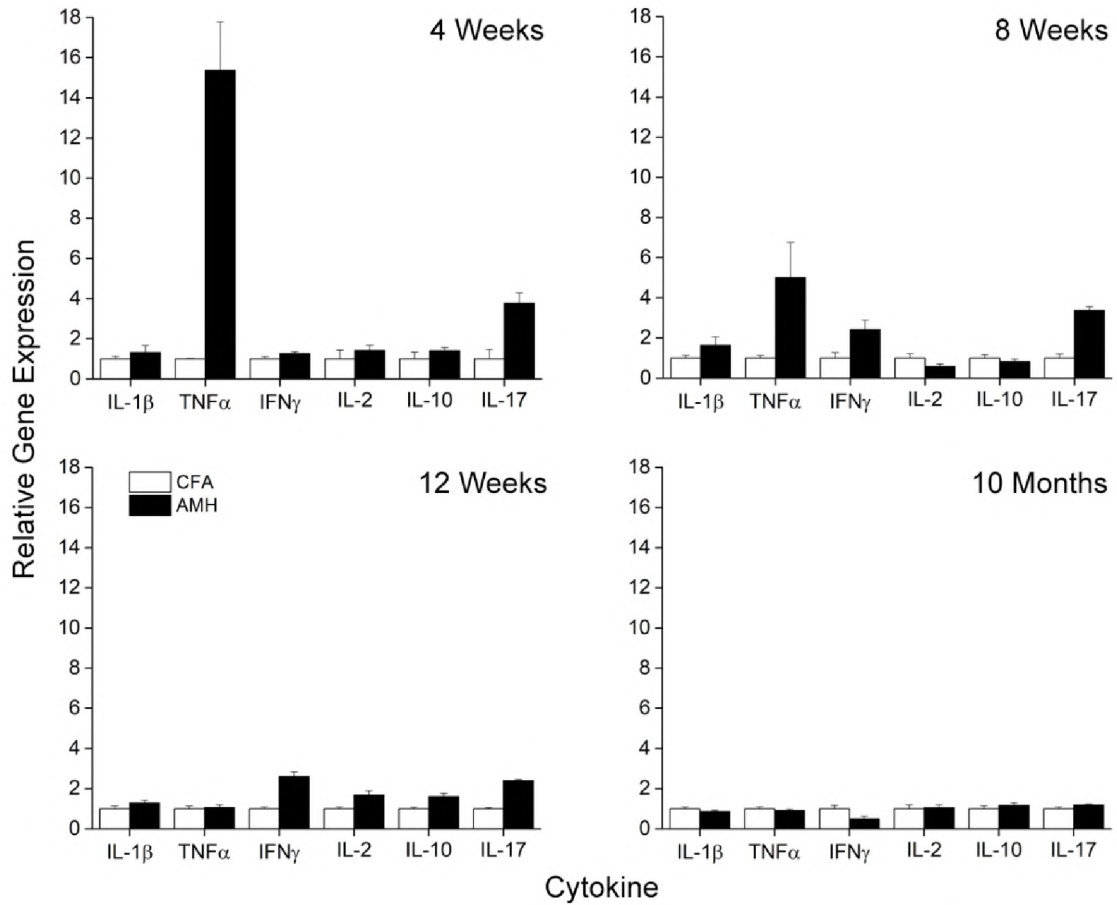


**Figure 3.6 qRT-PCR Inflammatory Marker Profile of Ovarian Tissue.** qRT-PCR analysis was performed on ovarian tissue harvested from mice immunized with rmAMH or CFA. Data were normalized to internal  $\beta$ -actin controls and plotted relative to age-matched CFA controls. Innate inflammatory cytokines IL-1 $\beta$  and TNF $\alpha$  were expressed early and transiently. Consistent with *in vitro* assays, significant upregulation of type-1 and type-17 cytokines was observed, while type-2 cytokine IL-10 remained low. Error bars represent  $\pm$ SEM.

### **Immunohistochemistry Shows Mild Transient T cell Infiltration of Ovarian Tissues**

To further explore the effect of the AMH immune response *in vivo*, immunohistochemistry (IHC) was performed on tissue sections from the ovaries of mice 4, 8, and 12 weeks after immunization with rmAMH or CFA. Methanol-fixed paraffin-embedded sections were immunostained with polyclonal rabbit anti-mouse CD3 and analyzed by light microscopy for evidence of T cell infiltration. At 4 weeks, a mild diffuse CD3<sup>+</sup> infiltration was detected in sections from mice in the AMH group (Figure 3.7 A). These cells were primarily found associated with granulosa cells of follicles (black arrows). No infiltrates were detected in sections from CFA control mice (Figure 3.7 B). This early infiltration was transient, as no significant infiltrates were observed in CD3<sup>+</sup> sections at 8 and 12 weeks (data not shown). Complement activation was absent as evidenced by negative staining for complement component 4d (C4d; Appendix, Figure S1). No gross pathology or anatomical abnormalities were observed in the tissues of any of the samples in either group.

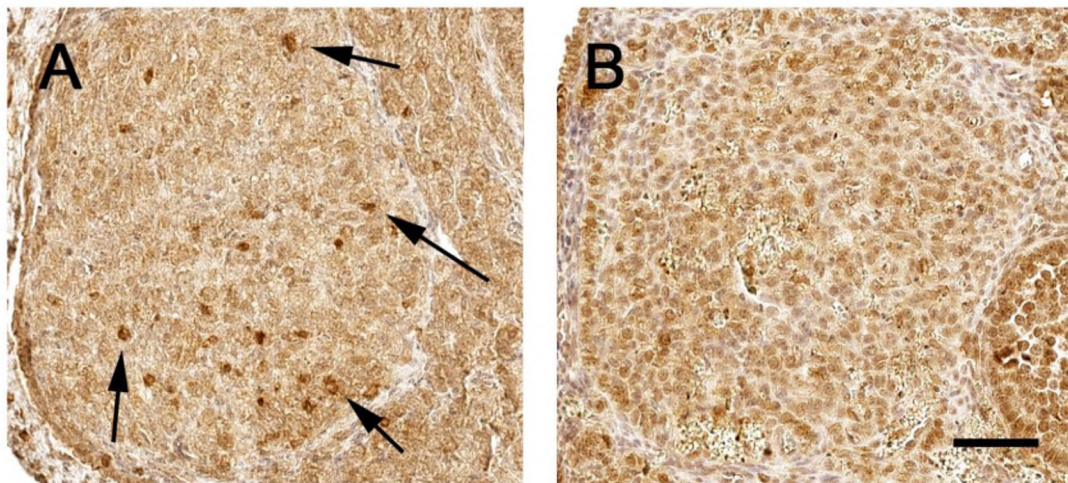


**Figure 3.7 CD3<sup>+</sup> T Cell Infiltration of Ovarian Tissue.** Sections of ovaries from mice immunized with rmAMH or CFA were immunostained with CD3 antibody and analyzed by light microscopy. (A) At 4 weeks, mild diffuse T cell infiltrates were evident (black arrows). (B) No infiltrates were observed in immunostained sections of CFA controls. Scale bar represents 50  $\mu$ m.

## **AMH Immunization Produces Long-Lasting High Titers of Antigen-Specific**

### **Autoantibodies**

To this point, a robust type-1/type-17 cellular immune response to immunization with rmAMH has been characterized. To assess whether AMH immunization also induces a humoral response, sera were obtained from mice by cardiac puncture at 4 weeks, 8 weeks, 12 weeks, and 10 months after immunization with AMH or CFA control. Sera were diluted with PBS in a 1:2 series and tested by ELISA for the presence of AMH-specific antibodies for each IgG subclass. At 8 weeks, mice exhibited a robust humoral response to AMH primarily of the IgG<sub>1</sub> and IgG<sub>2b</sub> isotypes, with titers detectable at 1/8192 dilution (Figure 3.8 A). These positive reactions were antigen-specific, as there was no significant response of any IgG isotype to either PBS alone or the control antigen rm $\beta$ -casein. Moreover, sera from mice immunized with CFA alone did not react to AMH or controls, even at the highest serum concentration of 1/256 (Figure 3.8 B).

The C57BL/6J mouse is unusual in that the gene for IgG<sub>2a</sub> is absent; it instead produces an IgG<sub>2c</sub> isotype. Accordingly, there was no significant IgG<sub>2a</sub> detected in any sample (data not shown). To date, there are no commercially available isotyping reagents to specifically detect IgG<sub>2c</sub> (Martin, et al., 1998). No IgG<sub>3</sub> was detected in any sample.

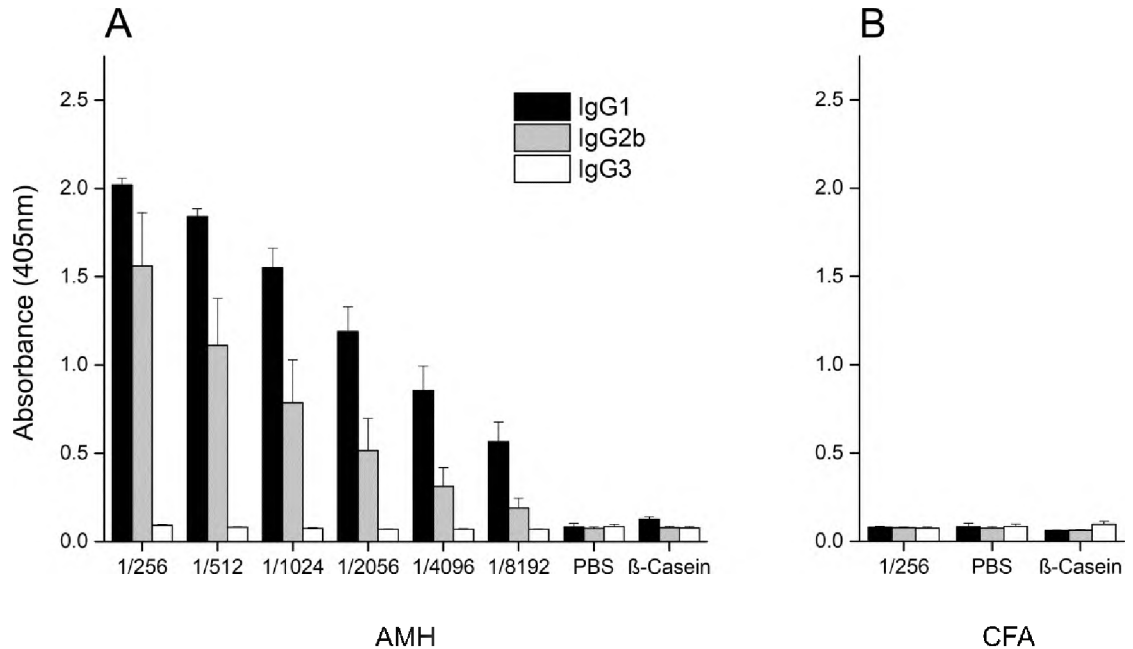


**Figure 3.8 Serum AMH Autoantibody Titers at 8 Weeks.** Serum was obtained from cardiac blood and tested for antibody response to rAMH and controls. (A) Mice immunized with rAMH demonstrated high IgG<sub>1</sub> and IgG<sub>2b</sub> titers at 8 weeks in response to rAMH but not in response to PBS or r $\beta$ -casein controls. (B) Mice immunized with CFA alone showed no response to controls or rAMH even at the maximum concentration of 1/256. Titers represent 1:2 dilutions of serum in PBS from 1/256 to 1/8192. Serum dilution for PBS and r $\beta$ -casein controls is 1/256. For all titers n=4. Error bars represent  $\pm$ SEM.

This signature humoral response was also consistently detected at 4 and 12 weeks after immunization, and was found to persist at high levels at 10 months (Figure 3.9). At this late stage, IgG<sub>1</sub> levels dropped by approximately half, while IgG<sub>2b</sub> remained stable. At all time points tested, responses were vigorous and antigen-specific, indicating that AMH immunization generated a robust and long-lasting antibody response.

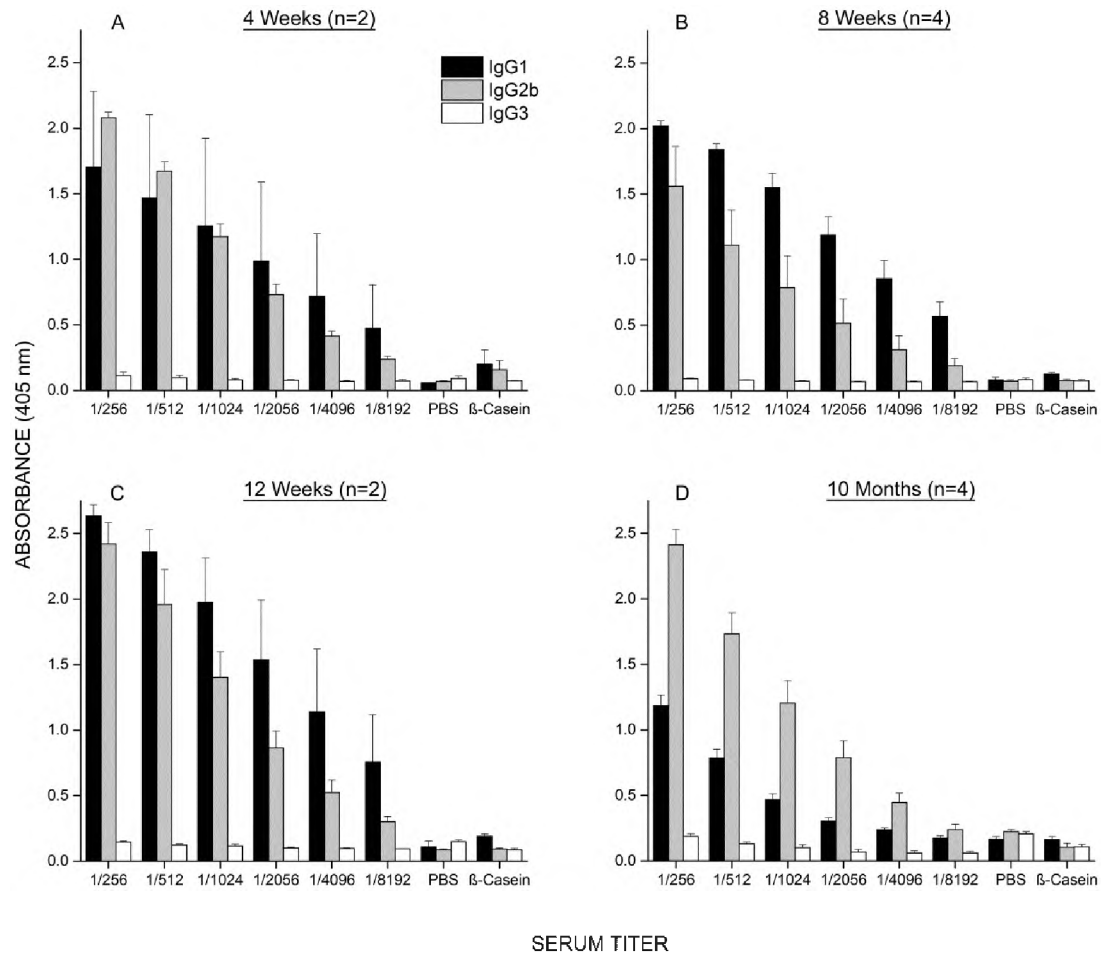


**Figure 3.9 Long-Term Serum AMH Autoantibody Titers.** Serum was obtained from cardiac blood and tested for antibody response to rAMH and controls. A strong consistent IgG<sub>1</sub> and IgG<sub>2b</sub> profile was observed at (A) 4 weeks, (B) 8 weeks, (C) and 12 weeks after immunization with rAMH. (D) This response was long-lived and detectable at 10 months. At this late stage, titers of IgG<sub>1</sub> fell approximately 50%, while IgG<sub>2b</sub> remained steady at high levels. Titers represent 1:2 dilutions of serum in PBS from 1/256 to 1/8192. Serum dilution for PBS and r $\beta$ -casein controls is 1/256. Error bars represent  $\pm$ SEM.

### Immunization with AMH Extends Fertility

A strong cellular and humoral autoimmune response has been demonstrated in mice immunized with AMH, an ovarian regulatory hormone. To assess the effect of this immune attack on fertility *in vivo*, a serial mating study was conducted. Two weeks after immunization with rAMH in CFA or with CFA alone, female mice were serially mated

to age- and strain-matched males for four breeding cycles. Males mated with equal number of AMH and CFA control mice, and were mated to the same females for each round. Initially, mice in both groups regularly produced litters of average size, and there were no significant differences in the numbers of pups in each litter. Over the duration of this long-term fertility study, a natural and gradual decline in fertility was observed in both groups. However, this decline appeared to be slowed in the AMH-immunized mice (Figure 3.10), and by the fourth mating, when the mice were approximately ten months of age, the mean numbers of pups per litter in the AMH group was more than double the number in the CFA control group, averaging 7.0 and 3.3 pups per litter, respectively. This difference was highly statistically significant ( $P < 0.006$ ).

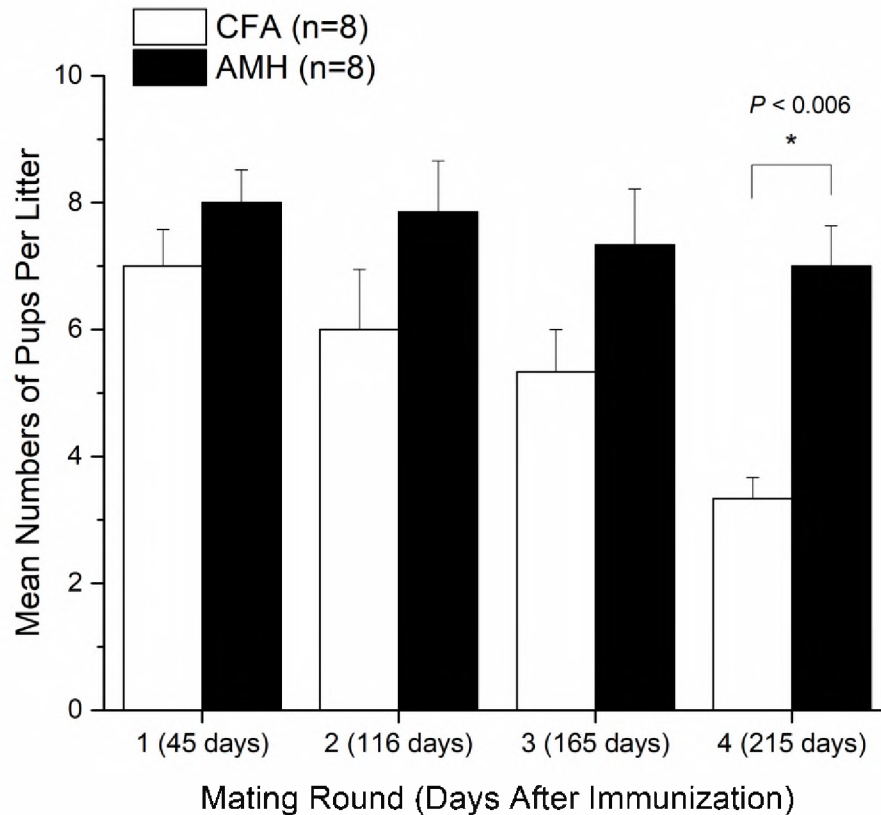


**Figure 3.10 Mean Numbers of Pups Per Litter.** Female mice immunized with rmAMH or CFA control were mated for four rounds with the same males. Numbers of pups in each litter were assessed at birth. The CFA group showed a gradual natural decline in fertility over time. In the AMH group, this decline was significantly moderated, resulting in a two-fold greater pup production by the fourth round. Error bars represent  $\pm$ SEM.

This disparity in fertility decline was also evident when litters were compared by total weights instead of numbers of pups (Figure 3.11 A) which yields a nearly identical result and was also highly significant ( $P < 0.007$ ). Importantly, throughout the entirety of the study, mice in both groups consistently gave birth to healthy pups of normal weight, and there were no significant differences in mean pup birth weights between the groups or between mating rounds (Figure 3.11 B).



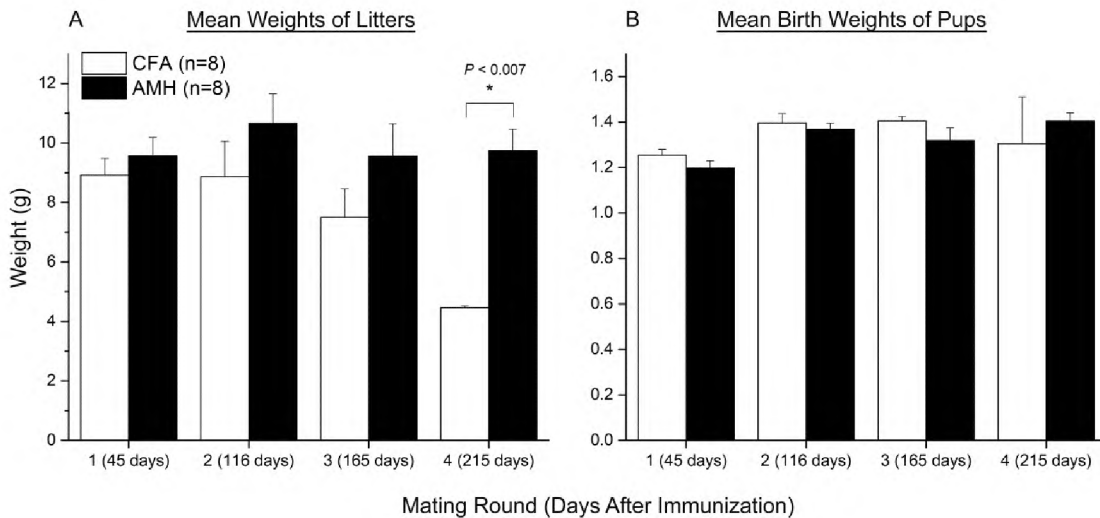


**Figure 3.11 Mean Weights of Litters and Birth Weights of Pups.** Female mice immunized with rAMH or CFA control were mated for four rounds with the same males. Weights of entire litters and individual pups were assessed at birth. (A) Mean weights of litter declined dramatically in the CFA group, but were relatively unchanged in the AMH group. (B) Weights of pups at birth were normal in both groups at each round, confirming that litter weight differences were due to differences in numbers of pups and not due to pup weight disparities. Immunization of the female with rAMH did not alter pup weight, and no other abnormalities in pups were observed. Error bars represent  $\pm$ SEM.

It is important to note that litter size and weight assessments by definition include only fertile mice producing litters. Equally critical is the proportion of total mice that are fertile at each mating round. These data show that in addition to maintaining a greater level of fertility in terms of litter sizes, AMH immunization substantially preserves the number of fertile females producing litters over time (Figure 3.12). This appraisal yields a very similar profile to the litter size and weight data, with roughly equal proportions of females producing litters in the first two rounds, and a marked difference in fertility becoming evident in the latter two rounds. Again, fertility in aged mice was extended in the AMH-immunized group. This enhancement is also evident in the raw data (Table

3.1). Both groups showed similar attrition due to natural aging factors that were not associated with treatment.

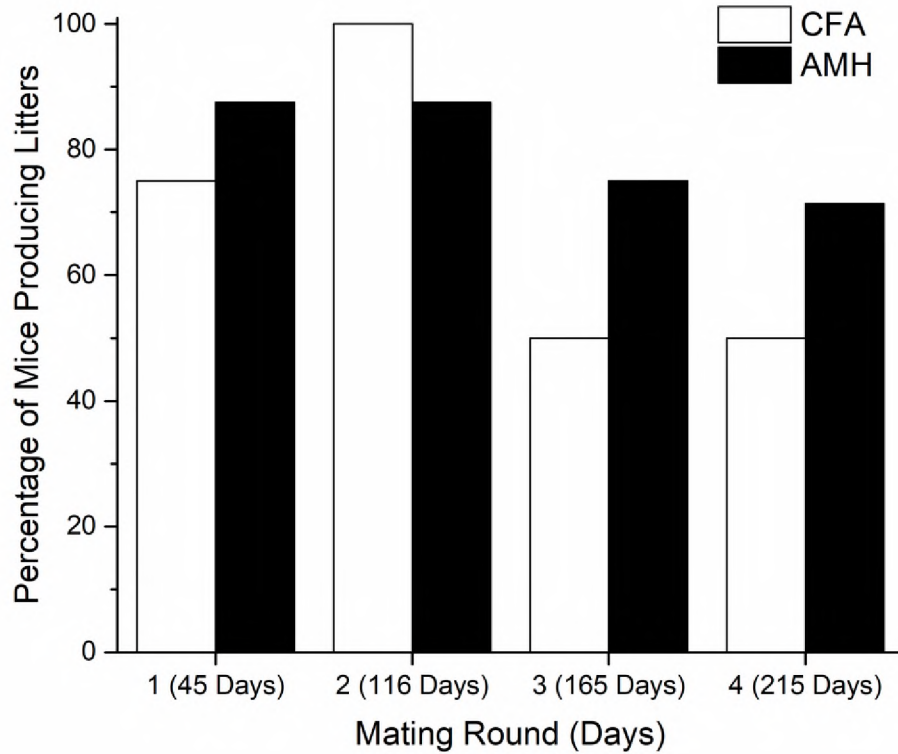


**Figure 3.12 Percentage of Mice Producing Litters.** Female mice immunized with rmAMH or CFA control were mated for four rounds with the same males. Over time, a natural decline in fertility resulted in fewer females producing litters. The AMH group exhibited enhanced fertility with a greater percentage of mating females producing litters in the latter two rounds.

### Mating Round

Immunogen	1	2	3	4
CFA Alone	6/8	7/7	3/6	3/6
AMH/CFA	7/8	7/8	6/8	5/7

**Table 3.1 Proportion of Fertile Females in Each Mating Round.** Female mice immunized with rmAMH or CFA control were mated for four rounds with the same males. Over time, a natural decline in fertility resulted in fewer females producing litters. The AMH group exhibited enhanced fertility with a greater percentage of mating females producing litters in the latter two rounds. In both groups, there was roughly equal attrition due to natural causes not associated with treatment.

### Immunization with AMH Conserves Ovarian Follicles

To evaluate the effects of AMH immunization on ovarian follicles, histologic serial section analysis was performed. Ovaries dissected from mice at 4 weeks, 8 weeks, and 10 months after immunization with rmAMH or CFA were weighed, fixed in methanol, and embedded in paraffin. Ovaries were then serially cross-sectioned through the entire organ, with every tenth section mounted and stained with H&E. This allowed active follicles in three-dimensional space to be classified and tallied without counting any follicle more than once. Sections were digitally scanned, the images were measured, and follicles were manually identified and tagged in software. A grand total of 662 sections were analyzed. The profiles of ovary weights (Figure 3.13 A) and cross-sectional area (Figure 3.13 B) are remarkably similar, showing consistent similar metrics in both groups at 4 and 8 weeks after immunization, but exhibiting a dramatic drop to

approximately half their values at 10 months in both groups. These data are consistent with the natural atrophy of the aging human ovary (Laszczynska, et al., 2008). Treatment had no discernible effect on either ovarian weights or cross-sectional areas. A minor increase in weight and size in the AMH group at 4 weeks may have been due to mild transient inflammation previously noted at that time point; however, this was not statistically significant ( $P > 0.3$ ).

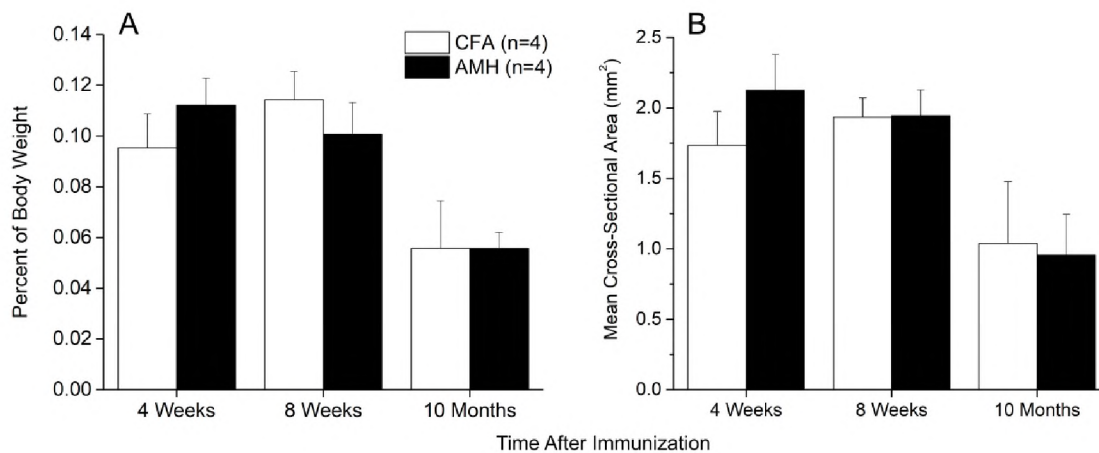


**Figure 3.13 Ovary Weight and Size Decline with Age.** Ovaries were dissected from mice at 4 weeks, 8 weeks, and 10 months after immunization with rmAMH or CFA. The entire organ was weighed, then fixed and sectioned for measurement. Ovary weight was normalized to body weight at harvest. (A) Mean weights were stable at 4 and 8 weeks, then dropped by approximately half by 10 months. (B) Mean cross-sectional area measurements roughly paralleled weight data. Treatment did not significantly affect either metric. Error bars represent  $\pm$ SEM.

In contrast, although ovary weights and cross-sectional areas were similar between the groups, there was a dramatic difference observed in the numbers of active follicles present. Again, data were similar between the groups at 4 and 8 weeks, and a natural decline in follicle numbers was evident in both groups at 10 months. However, the total numbers of active follicles at 10 months were much greater in mice immunized

with AMH despite the ovaries having a similar size (Figure 3.14). When quantified by serial section, mice in the AMH group had an average of 9.25 total follicles per  $\text{mm}^2$  compared with 3.20 follicles per  $\text{mm}^2$  in controls, and this difference was significant (Figure 3.15;  $P = 0.039$ ).

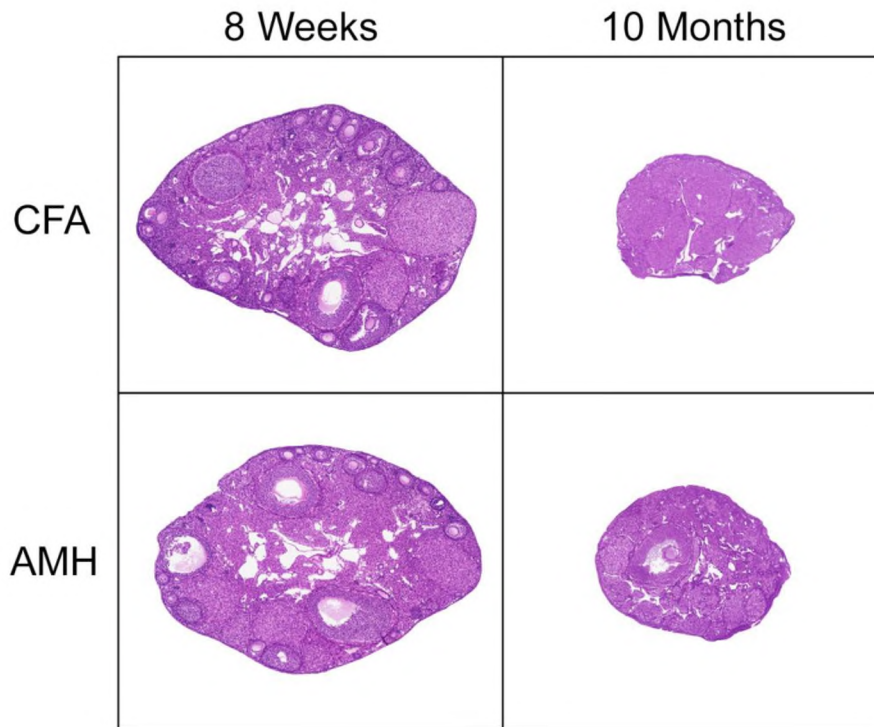


**Figure 3.14. AMH Immunized Mice Have More Active Follicles at Ten Months.**

Ovaries were dissected from mice at 4 weeks, 8 weeks, and 10 months after immunization with rmAMH or CFA. Cross sections were stained with H&E and digitally imaged. A natural age-related ovarian atrophy was observed at 10 months that affected both groups approximately equally; however, sections from AMH-immunized mice revealed greater numbers of active follicles. Representative sections are shown. Sections from 4 weeks were nearly identical to 8 week sections and are omitted for clarity.

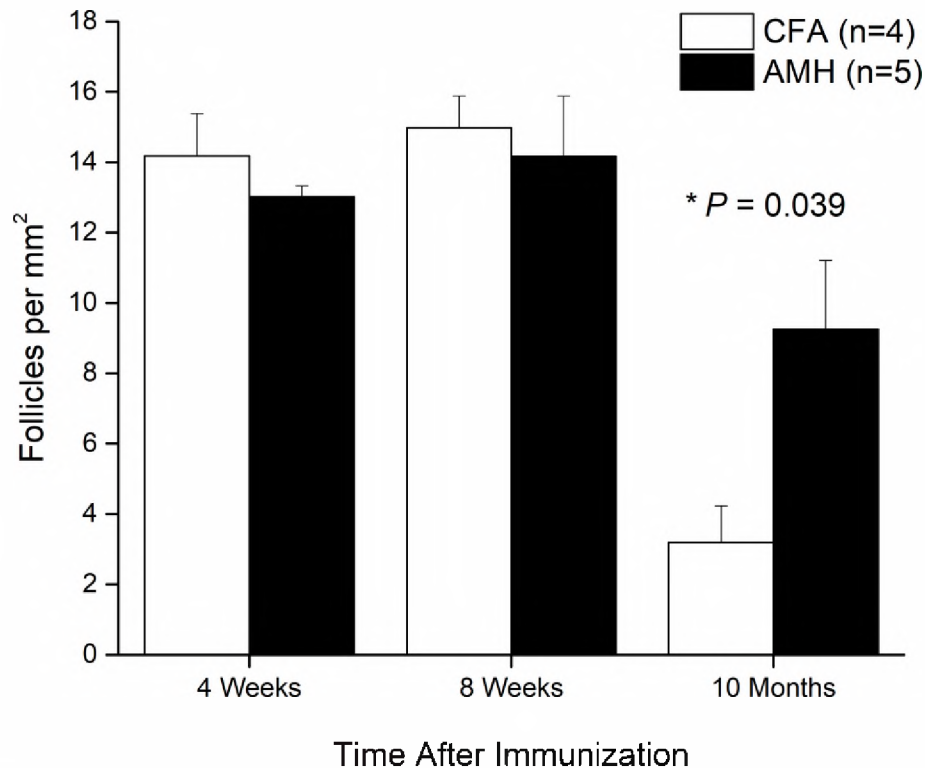


**Figure 3.15 AMH Immunized Mice Have Greater Numbers of Total Follicles at Ten Months.** Ovaries were dissected from mice at 4 weeks, 8 weeks, and 10 months after immunization with rmAMH or CFA. The entire organ was weighed, then fixed and sectioned and ovarian follicles manually quantified. Total follicle numbers were similar between the groups at 4 and 8 weeks. At 10 months, a natural decline in follicles was observed in both groups, but AMH-immunized mice had significantly greater numbers ( $P = 0.039$ ). Error bars represent  $\pm$ SEM.

The difference detected in total follicle numbers between AMH-immunized mice and CFA controls was further analyzed by follicle subtype. Small, medium, large, and atretic follicles, as well as corpora lutea (CL), were quantified and compared (Figure 3.16). The AMH group had more follicles in every category, with the greatest divergence observed in the small and atretic follicle types. While none of these differences

individually reached statistical significance, they indicate a trend toward follicle preservation across all subtypes after immunization with AMH.

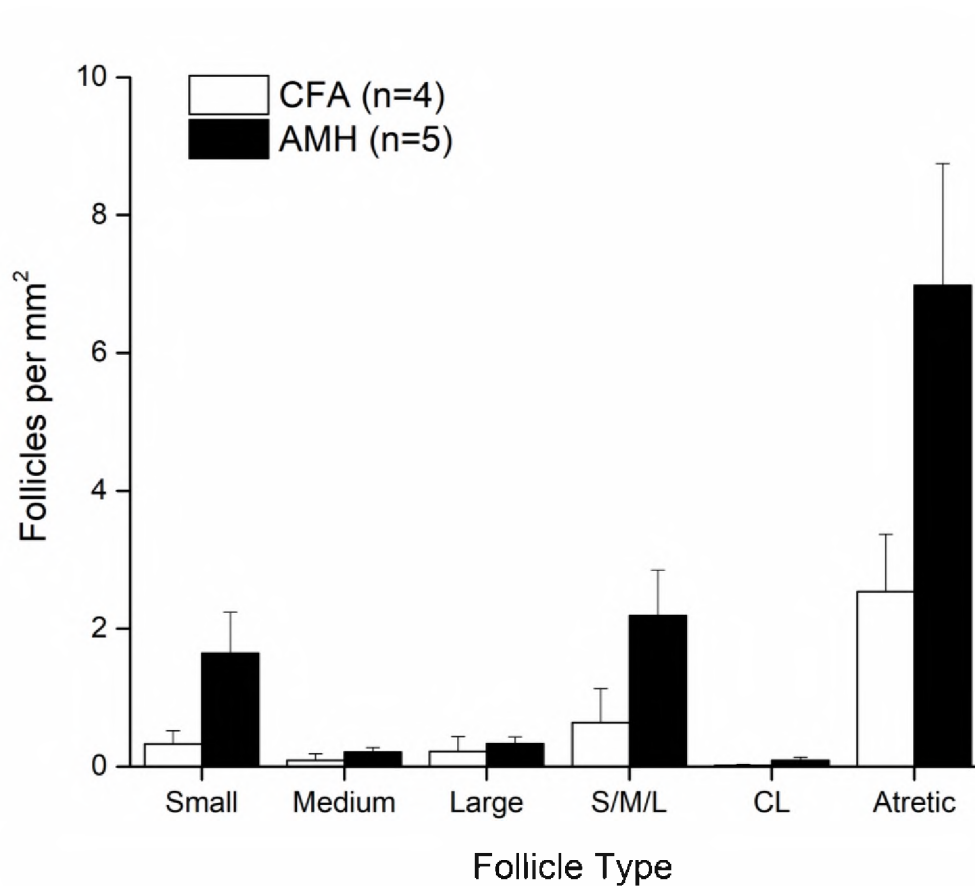


**Figure 3.16 Follicle Differences by Subtype at 10 Months.** Ovaries were dissected from mice ten months after immunization with rmAMH or CFA. The entire organ was weighed, then fixed and sectioned and ovarian follicles manually quantified by type: small; medium; large; total of small, medium, and large (S/M/L); corpora lutea (CL); and atretic. AMH-immunized mice had greater counts in all categories with the largest differences in the small and atretic subtypes. Error bars represent  $\pm$ SEM.

Because AMH gene expression is proportional to the ovarian reserve (Skiadas, et al., 2012), the histological findings were further assessed at the molecular level by measuring AMH gene expression via qRT-PCR. At 8 weeks and 10 months after immunization, RNA was extracted from the ovaries of mice immunized with rmAMH or CFA. cDNA was then made from purified RNA, and it was used as a template for qRT-PCR using primers specific for mAMH. Gene expression in each sample was normalized to endogenous  $\beta$ -actin controls, and relative gene expression among samples was compared. Consistent with the normal age-related decline in ovarian follicles observed by direct count, AMH gene expression at 10 months dropped to less than one tenth of 8 week levels in both groups ( $P = 0.001$  and  $P < 0.001$ ; Figure 3.17 A). Also consistent with histological analysis, AMH-immunized mice exhibited a significant preservation of the ovarian reserve at 10 months compared to CFA controls, demonstrating 90-fold greater expression of the AMH gene ( $P = 0.01$ ; Figure 3.17 B). Despite the differences in AMH expression between the two groups observed directly in ovarian tissue by qRT-PCR, no significant difference in serum AMH levels was observed at 10 months by ELISA (Appendix; Figure S2). Serum FSH levels were similarly assessed by ELISA at 8 weeks and 10 months after immunization. While the data showed the expected natural age-related increase in FSH in both groups due to the lack of negative feedback from diminished ovarian reserves (Appendix; Figure S3) and this rise was significant in the AMH-immunized group ( $P < 0.05$ ), no significant difference between the groups at either time point was observed. The seeming disparity between the significantly higher level of AMH expression in AMH-immunized mice in versus control mice at 10 months demonstrated by qRT-PCR in ovarian tissues compared with the nearly equal amounts of



circulating serum AMH shown by ELISA can be explained by the fact that the qRT-PCR test in this case directly measures the ovarian reserve, and is considerably more sensitive in this regard than the serum ELISA. There is no evidence to support a possible compensatory response to the autoimmunity directed at the AMH protein.

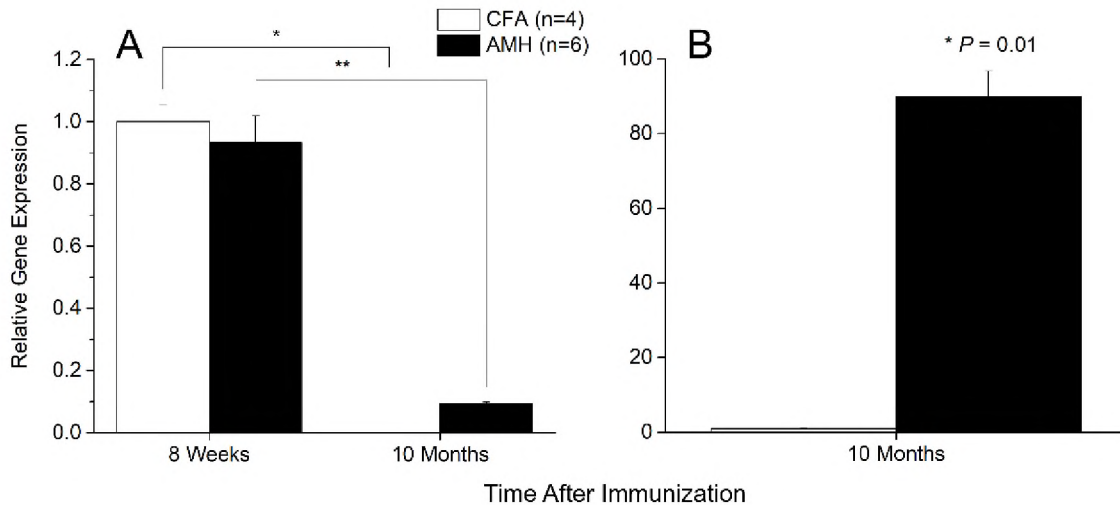


**Figure 3.17 AMH Immunized Mice Express Greater Levels of the AMH Gene at 10 Months.** qRT-PCR analysis of AMH gene expression was performed on cDNA from ovaries of mice immunized with rmAMH or CFA. (A) Relative AMH gene expression dropped dramatically and significantly from 8 weeks to 10 months ( $*P = 0.001$ ;  $**P < 0.001$ ), but AMH gene expression at 10 months was greater in the AMH-immunized group. (B) Compared to CFA controls, AMH-immunized mice showed a 90-fold greater AMH gene expression at 10 months ( $P = 0.01$ ).

### **Immunization with AMH Significantly Lengthens the Estrous Cycle**

To further explore the *in vivo* reproductive physiologic changes mediated by immunization with AMH, the estrous cycle was analyzed for 52 consecutive days, capturing an average of ten complete cycles in all mice studied. Four weeks after immunization with rmAMH or CFA control, vaginal smears were collected at the same time daily. Samples were methanol fixed, stained with methylene blue, and analyzed by light microscopy. Estrous stage was determined by the types and numbers of cells present. The data show striking differences in the cycles of the individual mice between the groups (Figure 3.18). All of the CFA-immunized mice exhibited a highly regular pattern of follicular (proestrus + estrus) phases and luteal (metestrus + diestrus) phases. However, at least half of the AMH-immunized mice demonstrated obvious erratic patterns with greatly extended follicular and/or luteal phases. The remaining mice in this group exhibited a subtle lengthening of one or both phases. This elongation of the cycle resulted in the AMH-immunized group completing significantly fewer cycles over the duration of the study. This effect is evident in the figure when follicular phase 10 is highlighted. Only 4/8 mice in the AMH-immunized group reached follicular phase 10, whereas 8/8 control mice reached follicular phase 10 during the 52 days of observation.

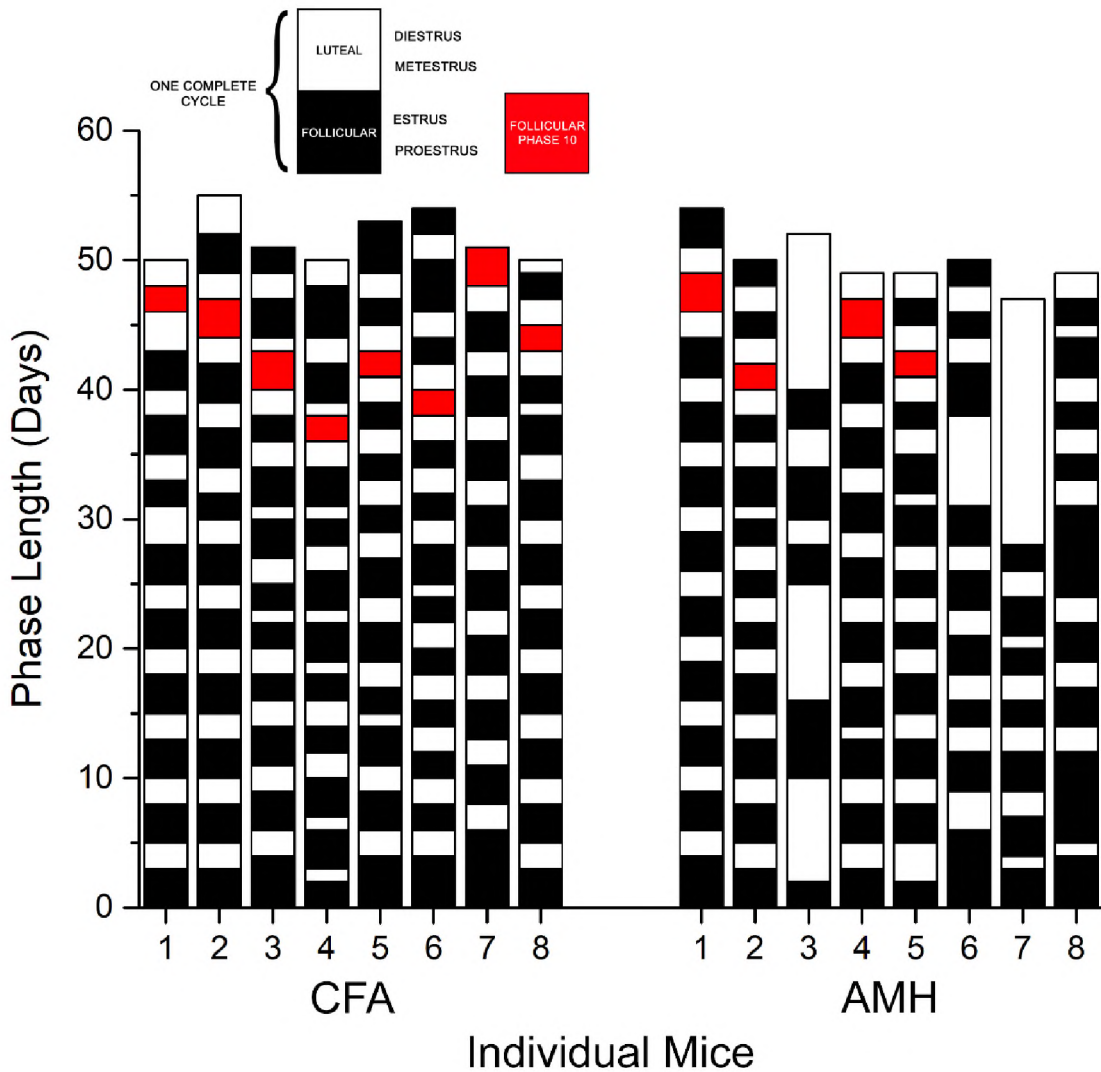


**Figure 3.18 AMH Immunization Disrupts the Estrous Cycle.** Vaginal smears taken at the same time daily for 52 consecutive days were analyzed to determine the stage of estrous in mice immunized with AMH/CFA or with CFA alone as control. Each completed cycle consists of the follicular phase (proestrus + estrus; black boxes) and luteal phase (metestrus + diestrus; white boxes). Follicular phase 10 (if completed) is highlighted in red. Completed cycles for individual mice are shown stacked with the first day of the first full cycle aligned at day zero. Mice immunized with AMH/CFA exhibited significant disruption of the estrous cycle with prominent or subtle elongation of phases evident. This estrous elongation led to fewer overall cycles completed during the study period. Only 4/8 mice in the AMH/CFA group reached follicular phase 10, whereas 8/8 control mice reached follicular phase 10.

The differences in the number of cycles completed between the means of the two groups for the duration of the study was significant (Figure 3.19). The CFA controls completed an average of 11.4 cycles in 52 days, while the AMH/CFA group completed a significantly fewer average of only 8.9 cycles, a 22% decrease ( $P = 0.007$ ).

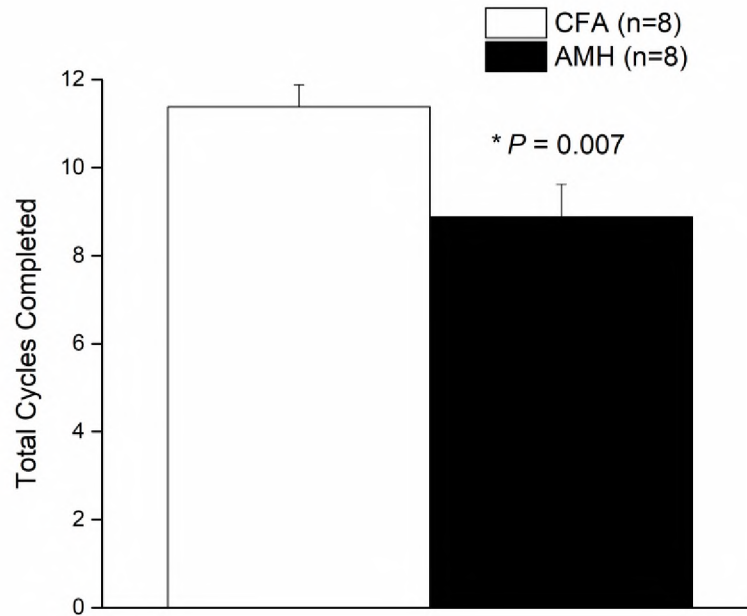


**Figure 3.19 AMH Immunization Results in Fewer Estrous Cycles.** Vaginal smears taken at the same time daily for 52 consecutive days were analyzed to determine the stage of estrous in mice immunized with rmAMH or CFA control. Total numbers of fully completed estrous cycles within the study period were tallied for each individual mouse. The means of each group are represented. Mice immunized with rmAMH completed an average of 2.5 fewer cycles than CFA controls ( $P = 0.007$ ).

The elongation of the estrous cycles observed in the profiles of individual mice was quantified and averaged for each group. In CFA control mice, the mean cycle length was 4.5 days. However, mice in the AMH group took about one full day longer for an average of 5.5 days (Figure 3.20). This 22% increase in length was highly significant ( $P < 0.003$ ).

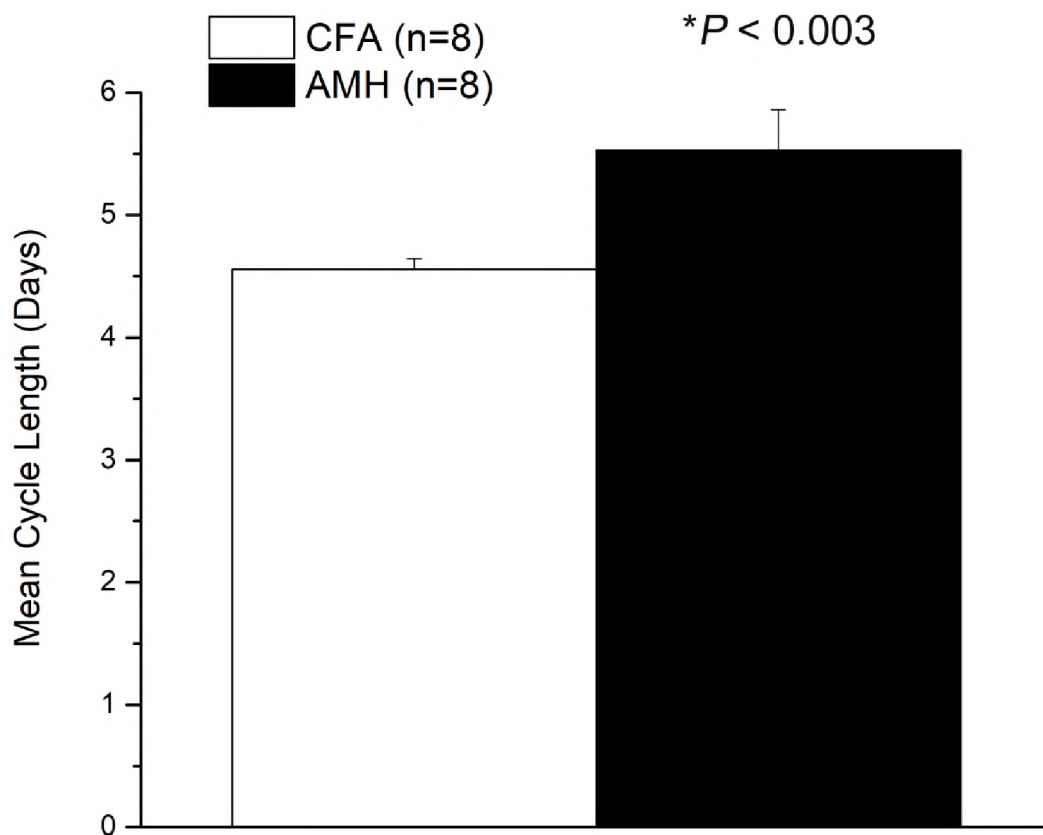


**Figure 3.20 AMH Immunization Lengthens the Estrous Cycle.** Estrous staging was determined by vaginal smear at the same time daily. Total cycle lengths consisting of all four stages of estrous were averaged for each group. Mice immunized with AMH displayed a significant increase in cycle length an average of one full day ( $P < 0.003$ ). Error bars represent  $\pm$ SEM.

The differences detected in total cycle length were further subdivided by estrous phase to determine the individual follicular and luteal contributions (Figure 3.21). The data show that while the follicular phase was somewhat elongated in the AMH-immunized group, the majority of the difference observed in total cycle length was due to significant lengthening of the luteal phase by an average of 0.72 days, a 36% increase ( $P < 0.02$ ).

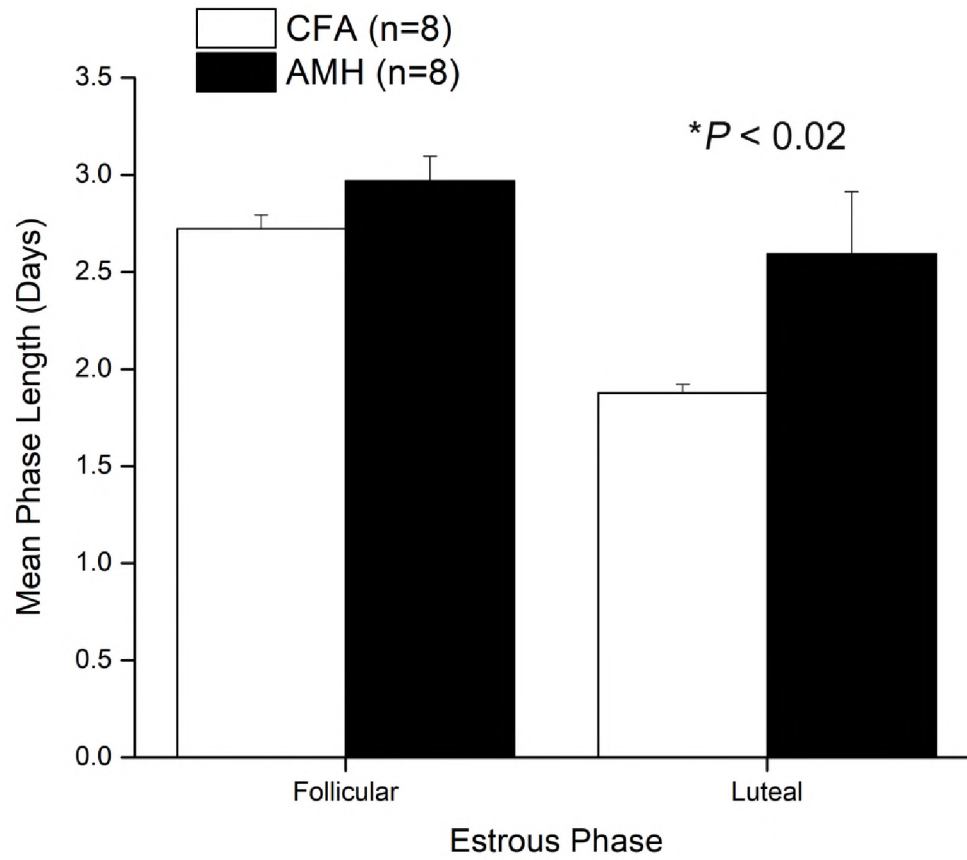


**Figure 3.21 Mean Estrous Phase Length.** Estrous staging was determined by vaginal smear at the same time daily. Mean phase lengths consisting of follicular (proestrus + estrus) and luteal (metestrus + diestrus) were averaged for each group. Mice immunized with AMH displayed significantly longer luteal phases by an average of 0.72 days ( $P < 0.02$ ). Error bars represent  $\pm$ SEM.

## **CHAPTER IV**

### **DISCUSSION**

These experiments have shown that immunization of C57BL/6 female mice with AMH/CFA results in the following: 1) a T cell response characterized by high frequencies of type-1 and type-17 antigen-specific CD4+ T cells; 2) a significant antigen-specific serum antibody response with dilutions exceeding 1:8,000 even at 10 months following immunization with AMH/CFA; 3) a transient mild oophoritis characterized by T cell infiltration of the ovary at 4 weeks but not 8 weeks or 12 weeks after immunization; 4) a significant extension of fertility characterized by a significant increase in litter sizes in the fourth mating cycle after immunization, at a time when fertility normally declines; 5) the extended period of increased fertility is due to a significant elongation of the estrous cycle confined to the luteal phase; 6) the elongated estrous cycles in AMH-immunized mice resulted in significantly fewer cycles over the 52 days of experimental observation and thereby, significantly increased follicle numbers and a preservation of the ovarian reserve. These data are consistent with the view that AMH-targeted autoimmunity lengthens the estrous cycle and extends fertility long after the anticipated age-related decline. These observed effects on estrous cycle elongation

and ovarian reserve preservation are unique for this model of AMH-targeted disruption and have shed light on the poorly understood role of AMH in controlling fertility and the ovarian reserve. Thus, these experiments have shown that AMH is a potent immunogen and that it yields a novel form of EAO which has not been previously described. While the current model bears some similarities to established models, no immunologic study to date has demonstrated prolonged fertility during the stage of life commonly associated with menopause.

### **Evaluating the Immune Response and Phenotype of AMH Autoimmunity**

Immunization with AMH produces a robust antigen-specific CD4<sup>+</sup> T cell response primarily of the type-1/type-17 profile, which is characteristic of autoimmune disease both in mouse models and in humans (Raphael, et al., 2015). While mild T cell infiltration was detected in follicles, it was far less pronounced than in the ZP3 and inhibin- $\alpha$  models (Rhim, et al., 1992; Altuntas, et al., 2006), and it did not result in observable gross pathology, which stands in contrast to the severe follicular tissue destruction typical of the NTx model (Taguchi & Nishizuka, 1980). Coupled with the fact that transfer of T cells alone into naive recipient mice was not sufficient to induce changes in the estrous cycle (Appendix; Figures S4-S6), these data suggest that the T cell response is not directly responsible for the phenotype, and that it may only participate indirectly by providing help to B cells. This hypothesis is further evidenced by the predominance of high, long-lasting serum titers of AMH-specific antibodies of the IgG<sub>1</sub> and IgG<sub>2b</sub> subtypes, which require the aid of T helper cells to initiate class switching. These antibodies persist at least 10 months after initial immunization, despite the absence



of detectable signature cytokines of inflammatory T cells in the ovarian tissue at this extreme time point. While the type-1 response is traditionally associated with the development of IgG<sub>2a</sub>, the C57BL/6 strain used in the study notably cannot produce this isotype (Martin, et al., 1998). However, it has been shown experimentally that type-17 T cells alone are capable of driving class switching to all IgG subclasses, including IgG<sub>1</sub> and IgG<sub>2b</sub> (Mitsdoerffer, et al., 2010). Interestingly, these two isotypes also predominate the humoral response to inhibin- $\alpha$  in SWXJ females in the EAO model (Altuntas, et al., 2006) and in BALB/c males when inhibin- $\alpha$  is used to vaccinate against testicular cancer (Aguilar, et al., 2017).

Phenotypically, AMH-immunized mice exhibit unique traits not associated with existing EAO/POI models. Most strikingly, these mice remain fertile and continue to produce more litters and larger litters late in life when normal controls begin to exhibit reproductive senescence. All currently known autoimmune models yield quite the opposite effect, with fertility diminishing earlier than would be expected for a natural age-related decline, consistent with human POI. The inhibin- $\alpha$  EAO model shows biphasic features in that the later decline in fertility is preceded by an earlier phase of superfertility at 7-9 weeks after immunization. During this same early period, AMH-immunized mice did not exhibit any statistically-significant increase in pup production. Concomitant with fertility extension, the AMH EAO model demonstrates enhanced conservation of follicles late into life, as opposed to the POI-like early depletion seen in other models. And whereas the inhibin- $\alpha$  EAO model exhibits early-phase superovulation preceded by a later stage follicle depletion, superovulation was not detected in the AMH model at any time point tested. Therefore, the steady and extended

follicle production and the concomitant extension of fertility with advancing age appear to be distinct and novel features of the AMH EAO model.

Another unique feature of this model is that the delay in the decline of fertility and the ovarian reserve in AMH-immunized mice was accompanied by a significant lengthening of the estrous cycle, with the majority of the extra length occurring in the luteal (metestrus-diestrus) phase. Estrous disruption is common to many mouse models of infertility, including the inhibin- $\alpha$  EAO model and the non-ovarian experimental autoimmune encephalomyelitis (EAE) model, as well as in non-autoimmune ovarian experimental systems such as the FSH-R (+/-) mouse. However, while both the AMH and inhibin- $\alpha$  EAO models demonstrated extended luteal phases and longer cycles overall (Altuntas, et al., 2006), immunization with inhibin- $\alpha$  did so while significantly shortening the follicular phase (proestrus-metestrus), which was slightly lengthened in the AMH mouse. In mice immunized with the CNS myelin peptide PLP 139-151 to produce EAE, a model for human multiple sclerosis (MS), estrous cycles were found to be shortened overall with the reduction occurring in the follicular phase (Jaini, et al., 2015); this effect stands in direct contrast to the AMH EAO model, despite the lengthening of the luteal phase that was common to both models. And finally, while the FSH-R (+/-) mice initially exhibited lengthened estrous cycles similar to the AMH-immunized mice, they did so at the expense of early depletion of the ovarian reserve resulting in cessation of estrous (Danilovich & Sairam, 2002), which was opposite to the effect of ovarian conservation and extended fertility seen in mice immunized with AMH. Thus, the specific mode of estrous disruption observed following AMH immunization appears to be novel.

### **Possible Mechanisms of AMH Autoimmunity-Mediated Fertility Extension**

It is plausible that the lengthening of the estrous cycle and concurrent decrease in estrous cycle frequencies could be the primary mechanism by which follicles are conserved and fertility is extended. Control mice immunized with CFA alone showed a mean estrous cycle length of 4.5 days and completed a total of 91 complete cycles in the experimental observation period of 52 days. In contrast, the AMH-immunized mice showed a mean estrous cycle length of 5.5 days and completed a total of 71 cycles in the experimental observation of 52 days (Figures 3.19 & 3.20). Thus, the AMH-immunized mice as a group experienced 20 fewer estrous cycles than the control immunized mice during the 52 days of observation, for an average of approximately 2.5 fewer cycles per mouse. This significant decrease in estrous cycle frequency in the AMH-immunized mice indicates that fewer ovarian follicles were expended, thus conserving the finite ovarian reserve. This preservation of the ovarian reserve is clearly demonstrated by histologic follicle counts at 10 months following AMH immunization (Figures 3.14–3.16). The preservation of the ovarian reserve could directly account for the longer duration of intact fertility. Although the estrous cycle was significantly lengthened, these elongated cycles did not negatively impact the numbers of litters produced. This is perhaps a function of the overall rapid nature of the murine estrous cycle itself; because a female mouse ovulates on average every four days, it is nearly always fertile. The lengthening of the cycle by one day would not be expected to significantly reduce the probability of fertilization with the mating male. In addition, since mean litter sizes were normal, the longer cycle did not appear to affect the number of eggs released during each ovulation.

If the elongation of the estrous cycle represents the proximal cause of fertility extension, the distal cause is the mechanism by which the estrous cycle is lengthened. One possibility is that the bioactivity of AMH is neutralized by autoantibody that inhibits the binding of AMH to AMHR2 and/or prevents the enzymatic cleavage of full-length AMH into its active form. This effect in turn would lower the bioavailable amount of AMH without necessarily causing a detectable change in serum levels of AMH. A reduction in active AMH could affect the estrous cycle in multiple ways. Firstly, as the gatekeeper of the entry and exit of primordial follicles into the developing pool with each cycle, neutralization of AMH might result in “lifting the brake” on the follicular phase, allowing more oocytes to participate in each cycle. This effect was observed in the AMH (-/-) model, in which excessive follicle recruitment early in life caused a premature depletion of the ovarian reserve (Durlinger, et al., 1999). This finding stands in contrast to the normal follicle counts early in life and the late-stage conservation of the ovarian reserve seen in the AMH model. However, the physiologic environment in an autoimmune model is considerably more nuanced than in a knockout. Autoantibody neutralization of AMH would not completely eliminate AMH activity, but would most likely diminish it; the effect may be more akin to the AMH (+/-) mouse, which had an intermediate phenotype to the AMH (-/-) and wild-type mice in the Durlinger study. More importantly, AMH knockout mice are completely devoid of any AMH expression from the moment of conception, and this absence must have significant consequences on the ovarian reserve during pre-natal development and in the time prior to adulthood. In the current study, AMH-immunized mice may be considered more of a "functional conditional knockout/knockdown" that have normal ovarian development and function

until they are immunized at full maturity, and thus fundamentally differ from AMH (-/-) mice. Alternatively, in the AMH EAO model it is possible that a reduction of AMH activity may in essence relieve apoptotic pressure—instead of simply lifting the brake to allow greater numbers of oocytes to enter and exit the developing pool, it may cause fewer oocytes per cycle to undergo apoptosis. In this scenario, reduction of AMH activity would allow normal ovulation rates and typical litter sizes while preserving the absolute numbers of primordial follicles in the reserve, thus extending the fertile lifespan of the mouse. This mechanism would best fit the phenotype of AMH autoimmunity in the current study; moreover, a similar phenotype of extended fertility due to conservation of the ovarian reserve was described in a mouse model in which the pro-apoptotic gene *Bax* was knocked out (Perez, et al., 1999).

While the effect of a reduction of bioavailable AMH on follicular development may help explain the extended conservation of the ovarian reserve, it does not directly account for the lengthening of the estrous cycle in AMH-immunized mice. The estrous cycles of *Bax* (-/-) mice were not analyzed, and AMH (-/-) mice did not exhibit significant differences in the estrous cycles from their wild-type counterparts until they became acyclic from exhaustion of the ovarian reserve. The elongation of the estrous cycle evident in the AMH EAO model clearly cannot be explained by modulation of apoptosis alone. However, a reduction of AMH activity could also exert influence on the hormonal control of the estrous cycle. It has been reported that AMH inhibits aromatase activity, thereby opposing production of estrogen from precursor androgens (Pellatt, et al., 2011; Sacchi, et al., 2016). A decrease in AMH activity would therefore lead to greater estrogen levels, which in turn would increase negative feedback on the pituitary

gland—which ultimately drives the cycle by secreting FSH and LH. Therefore, it is plausible that increased negative feedback on the pituitary could be the means by which AMH autoimmunity slows the cycling process and thereby lengthens the estrous cycle. In the current study, the mean FSH levels in the serum of mice immunized with AMH were slightly lower than CFA controls at 8 weeks, although this effect did not reach significance (Appendix; Figure S3). Further investigation with larger numbers of mice and time points matched to specific stages of estrous may be necessary. In addition, direct measurement of estradiol at these time points may shed further light on this process.

Although the ultimate mechanism by which AMH autoimmunity exerts its effect remains speculative, multiple lines of evidence suggest that the physiologic effect is mediated by autoantibody neutralization of AMH. As previously mentioned, persistently high antibody titers were observed as late as ten months after immunization, and T cell infiltration of ovarian tissues was mild and transient. Additionally, *in vitro* evidence revealed negligible CD8<sup>+</sup> activation, which suggests that cytotoxic T cells are not a relevant effector cell in the AMH immune response. Furthermore, no gross pathology or tissue damage was evident in the ovaries at any time point. Thus, it is likely that the mechanism of action is non-destructive, and therefore does not involve antibody-dependent cellular cytotoxicity (ADCC) or complement fixation. The lack of complement involvement is further evidenced by negative staining for C4d, a definitive marker for antibody-mediated complement fixation (Murata & Baldwin III, 2009). Lastly, antibody neutralization is the mechanism of action in the inhibin- $\alpha$  EAO model, which also exhibits high titers of the isotypes IgG<sub>1</sub> and IgG<sub>2b</sub>. Although there is much evidence to

suggest that antibody neutralization of AMH is the ultimate cause of fertility extension, it was not demonstrated directly in the current study and it remains an area of focus for future research. Although many questions remain to be addressed, taken together, the findings in the current study suggest a possible mechanism by which AMH autoantibodies may exert their influence to lengthen the estrous cycle, preserve ovarian follicles, and ultimately extend fertility. A working model of these processes is proposed in Figure 4.1.

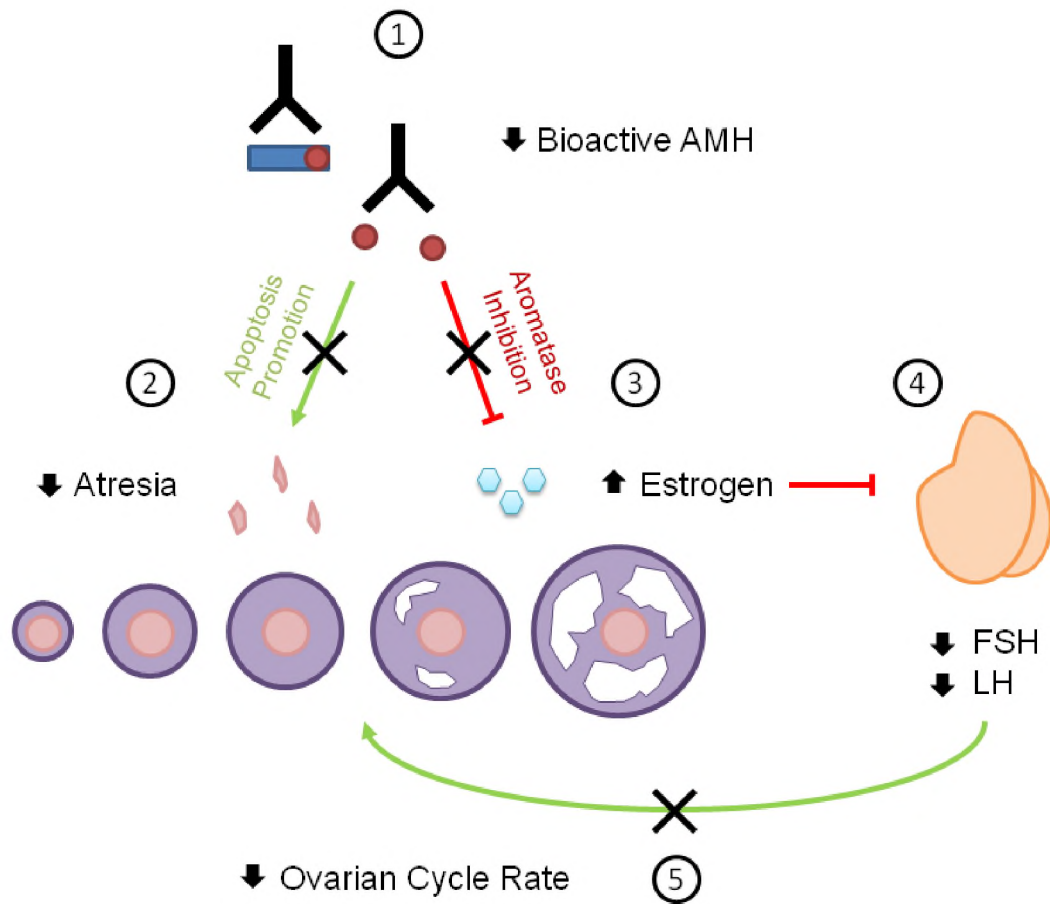


**Figure 4.1 Proposed Mechanism for AMH Autoantibody-Mediated Fertility Extension.** High titers of circulating AMH autoantibodies lower the bioactive amount of AMH by direct neutralization of its activity and/or preventing cleavage to the active form (1). With less bioactive AMH in the ovarian microenvironment, apoptosis is reduced and fewer follicles undergo atresia (2). Simultaneously, the natural inhibition of aromatase by AMH is diminished, allowing greater production of estrogen by the ovarian follicles (3). An elevated level of estrogen exerts negative feedback on FSH and LH production by the pituitary (4), which in turn causes a slowing of the ovarian cycle rate (5). Taken together, the preservation of the ovarian reserve by reduced atresia and fewer cycles over time may account for the extension of fertility observed in AMH-immunized mice.



## **Insights Gained into the Natural Functions of AMH**

The knowledge acquired in the AMH autoimmunity model may be useful in elucidating the true physiologic role of AMH. As previously noted, although an AMH knockout mouse has long existed, these mice lack AMH production from the moment of their conception, and therefore do not accurately represent women who are born fertile but develop POI later in life. Immunization with AMH offers a convenient method of creating a “functional conditional knockout/knockdown” system in which AMH can be targeted at any stage of life after normal development has occurred. And surprisingly, despite the abundance of current *in vivo* and *in vitro* models, and after nearly 40 years of research on AMH in the ovary, its precise role in females remains a topic of debate. In fact, even the most basic molecular function of AMH—whether it inhibits or promotes cell growth—remains controversial. Although the majority of scientific literature describes AMH as a pro-apoptotic, there is also considerable published evidence to suggest exactly the opposite (Pankhurst, 2017). The accumulation of contradictory evidence regarding the basic function of AMH, as well as its role in the mature female, has shaped a murky understanding of the hormone and its physiologic significance. However, a unified concept of AMH as a subtle yet essential regulator of the ovarian reserve has begun to emerge.

The earliest known function of AMH—to cause regression of the Müllerian ducts in the male fetus—clearly demonstrates its ability to promote apoptosis (Roberts, et al., 1999; Xavier & Allard, 2003). Moreover, it has been shown that the canonical pathway of AMH/AMHR2 signaling in adult tissues leads to cell cycle arrest and apoptosis (Namkung, et al., 2012; Zhang, et al., 2018) as well as to the induction of pro-apoptotic

genes such as *Bax* (Mazumder, et al., 2017). As it belongs to the TGF $\beta$  superfamily, it is not surprising that AMH would share this capacity with the namesake member.

However, the actions of TGF $\beta$  itself are diverse, ranging from apoptosis to cell growth, cell differentiation, and immunomodulation (Clark & Coker, 1998; Shi & Massague, 2003). Therefore, it follows that AMH may also have pleiotropic effects, some of which may not yet be defined.

The outcomes of *in vitro* studies designed to test the effects of AMH have varied enormously. AMH has been shown to inhibit the growth of AMHR2-expressing human GCTs by activating apoptosis (Anttonen, et al., 2011). Furthermore, AMH treatment can inhibit chemotherapy-resistant ovarian cancer progenitor cells (Meirelles, et al., 2012) as well as cervical cancer (Barbie, et al., 2003). In addition to its efficacy against gynecologic tumors, AMH treatment is effective against cancers originating from AMHR2-expressing neural-derived tissues, such as human ocular melanoma (Parry, et al., 1992). However, in stark contrast to these pro-apoptotic effects, Schmidt and colleagues demonstrated that AMH added to human ovarian explants in culture stimulated growth of primordial follicles (Schmidt, et al., 2005). From these diverse studies, it is not clear if the functions of AMH vary depending on context, or if differences in methodologies may account for the observed contrasting effects.

Similarly, *in vivo* murine models have produced conflicting results. The AMH *null* mouse model surprised investigators in that AMH (-/-) females are initially fertile; the early implication was that AMH is not required for fertility and therefore rather unimportant in the ovarian cycle. However, as these mice eventually show premature depletion of their ovarian reserve, AMH became appreciated as an essential regulator of

the oocyte supply (Durlinger, et al., 1999). It was subsequently demonstrated that this effect was mediated through opposing FSH recruitment of preantral follicles, allowing AMH to influence management of the reserve (Durlinger, et al., 2001). More recently, a contrasting animal model has been developed in which mice overexpress AMH shortly after birth. Unlike their counterpart knockout mice, *Thy1.2-AMH<sup>Tg</sup>* mice have severe fertility impairment from the outset, birthing infrequent and small litters compared to wild-type mice (Pankhurst, et al., 2018). Surprisingly, despite having the opposite genotype to AMH *null* mice, the phenotype of the *Thy1.2-AMH<sup>Tg</sup>* AMH-overexpressing mice ultimately parallels the phenotype of the knockouts, with the ovarian reserve being depleted as early as five months of age. Similar to *in vitro* data, these genetically-engineered mouse models initially suggest contradictory effects of the role of AMH in maintaining the ovarian reserve. Whether AMH is overexpressed, or not expressed at all, the eventual outcome is the same—premature exhaustion of the oocyte supply. This result stands in contrast to the AMH autoimmunity model described here, in which the ovarian supply is conserved. However, the fact that a similar phenotype of extended fertility was observed in the mouse model in which the pro-apoptotic *Bax* gene was knocked out (Perez, et al., 1999) provides indirect support for an apoptotic role of AMH.

Although it is difficult to reconcile the disparate results of all *in vitro* and *in vivo* studies, perhaps the overall lesson is that function of AMH is nuanced, and may differ based on context, i.e., the type of target cell, the timing and location, and other factors in the local microenvironment. AMH may in fact have different physiologic effects depending on the stage of development of the target follicle. In a recent study in which normal C57BL/6J mice were injected with exogenous bioactive AMH daily for 4 weeks,

the authors concluded that AMH both inhibited follicle development and also reduced the rate of atresia by an unknown mechanism (Hayes, et al., 2016). Curiously, these mice demonstrated extended conservation of the ovarian reserve, which is unexpectedly inconsistent with the phenotype of the AMH-overexpressing *Thy1.2-AMH<sup>Tg</sup>* mouse and more congruent with the results of the current study in which AMH is targeted immunologically. Nevertheless, it is conceivable that AMH may be working at both ends of the folliculogenesis process, limiting the amount of the total reserve recruited into the developing pool with each cycle, as well as influencing the rate of atresia—either by promoting it, inhibiting it, or both (Visser, et al., 2007; Seifer & Merhi, 2014). The delicate balance of the entry and exit of follicles into this cyclic pool known as the "*dynamic reserve*" is critical for the proper maintenance of fertility, and AMH clearly plays a key role (Monniaux, et al., 2014; Pankhurst, 2017). Therefore, any change in the bioavailable amount of AMH could have complex effects on follicle regulation.

Ultimately, some of the conflicting data on the role of AMH may be due in part to limitations inherent in the study techniques used. Tissue culture is by nature a reductionist approach that is devoid of the intricate network of endocrine glands and hormones that are normally in play. Knockouts and transgenic animals create an artificial system in which the expression of the target protein is absent or not regulated, and the normal developmental patterns of expression are nonexistent. Taken together, there are unavoidable artifacts generated by all of the existing models. This dilemma necessitates the development of an *in vivo* system with a normal developmental expression pattern of AMH which can be disrupted at will by the investigator. Immunization with AMH may provide exactly these tools for the study of the hormone and its properties.

## **Insights on Menopause and Aging**

Although the AMH autoimmunity model bears many similarities to other established models of human infertility, it does not share all of the features with any of them; nor does it specifically mimic any known human disorder (Table 4.1). Thus, the AMH EAO model may serve as a novel approach for studying the role of AMH in fertility, but moreover, it may represent a potentially unrecognized human condition. Regarding the unexpected superfertility observed in the inhibin- $\alpha$  EAO model, Altuntas and colleagues state that "... Human POF may possibly be biphasic with an early clinically silent and undetected period of enhanced fertility followed by a detected later period of infertility ... the early period of enhanced fertility would likely be detected only if the woman became pregnant and had multiple births" (Altuntas, et al., 2006). In a similar manner, AMH autoimmunity may remain clinically silent, as a young woman may have slightly longer than average menstrual cycles and normal fertility; and although her fertility may be preserved much later in life than average, this fact may not be evident if she is no longer attempting to conceive. In the United States, the vast majority of babies are born to women under 40. In 2017, only 3.2% of all live births were attributed to mothers aged 40 or above; births to mothers over 50 were extremely rare, representing only 0.02% of total live births (Centers for Disease Control and Prevention, 2018). Although it is difficult to estimate the relative contributions of family planning and fertility in this age group, the timing coincides with the age of menopause and perimenopause, and therefore reproductive senescence must have a major impact.

Model/Disease	T Cell Infiltrate	Antibody Titers	Estrous/Menstrual Cycle	Ovarian Reserve/Fertility	Reference
<u>Immunologic Ovarian</u>					
Neonatal thymectomy	severe	high	Normal	-	(Taguchi, et al., 1980; Murali, et al., 2020)
Ovarian homogenate	moderate	high	-	-	(Jankovic, et al., 1973)
ZP3 peptide	severe	high	Irregular	Fertility impaired	(Rhim, et al., 1992; Fu, et al., 2007)
Inhibin- $\alpha$ peptide	moderate	high	Lengthened cycle; shortened follicular, lengthened luteal	Biphasic: early superfertility, then early depletion	(Altuntas, et al., 2006)
rAMH	mild	high	Lengthened cycle; lengthened luteal	Conserved	(Johnson, 2020)
<u>Immunologic Non-Ovarian</u>					
PLP peptide (EAE)	-	-	Shortened cycle; lengthened follicular, shortened luteal	-	(Jaini, et al., 2015)
<u>Non-Immunologic Ovarian</u>					
<i>Bax</i> (-/-)	-	-	-	Conserved	(Perez, et al., 1999)
AMH (-/-)	-	-	Normal	Early depletion	(Durlinger, et al., 1999)
FSH-R (+/-)	-	-	Irregular/lengthened	Early depletion	(Danilovich & Sairam, 2002)
LHCGR Mutation	-	-	Irregular/lengthened	Early depletion	(Hai, et al., 2015)
<i>Thy1.2-AMH</i> <sup>Tg</sup>	-	-	Normal	Early depletion	(Pankhurst, et al., 2018)
rAMH-C treatment	-	-	Irregular	Conserved	(Hayes, et al., 2016)
<u>Clinical Ovarian Disease</u>					
POI	Present*	Present*	Absent	Early depletion	(Silva, et al., 2014; Kovanci & Schutt, 2015)
PCOS	Possible*	Present*	Irregular, prolonged, or absent	Fertility impaired	(Nasri, et al., 2018; Mobeen, et al., 2016; Sirmans & Pate, 2013)

**Table 4.1. Comparison of Phenotypes in Animal Models of Infertility and Human Disease.** Major findings and key references are noted. Dashes indicate data that are not applicable or unreported. \*In clinical cases with an underlying autoimmune cause.

Nevertheless, the CDC reports 840 births in 2017 to women aged from 50 all the way up to 65 (Centers for Disease Control and Prevention, 2018). It is an intriguing proposition that these remarkable birth events late in life may be attributable to a spontaneous extension in fertility, and that while beguilingly rare, at least some of these births could be the result of a silent undetected AMH autoimmunity.

One indisputable fact is that the level of AMH found in the serum of healthy women is proportional to the ovarian reserve, and AMH is widely accepted as a predictive marker of fertility as well age at menopause (Tehrani, et al., 2011; Kruszynska & Slowinska-Srzednicka, 2017). However, its precise role in the natural process of reproductive senescence is unknown. It may be merely an indicator of follicular activity, or it may actually play an active part in determining the timing of menopause. To understand how and why AMH is significant in this regard, it is necessary to understand the role of menopause itself; however, even the question of why menopause exists is fraught with debate. While reproductive senescence is common in the animal kingdom, menopause, or the complete cessation of fertility, is not—along with humans, it is shared by a handful of other animals, including rodents, dogs, non-human primates, elephants, and whales (Packer, et al., 1998). It is intriguing that humans and many of these animals share the trait of longevity. It has been suggested that menopause exists simply because humans now live considerably longer than our cave-dwelling ancestors, and that women simply outlast their natural fertile lifespan (Blurton Jones, et al., 2002). However, there are several prevailing theories (reviewed in Wu, et al., 2005) rooted in Darwinian natural selection. The "*Good Mother Hypothesis*" purports that menopause necessitates a focus on raising present children rather than having additional children, and thus exerts a

*"quality over quantity"* paradigm on motherhood (Sherman, 1998). The *"Grandmother Hypothesis"* applies the same logic to the postmenopausal stage, in which the grandmother can invest effort into helping raise her grandchildren, thus further ensuring the survival of her inherited genes (Kim, et al., 2019). In contrast, the *"Disposable Soma Theory"* states that organisms, having limited cellular resources, must trade off maintenance of somatic systems with reproductive systems. The soma must be maintained to the degree in which the animal is likely to survive in the wild, and the reproductive lifespan is independently maintained to match this extent. Inevitably, if the animal lives longer than anticipated, the investment in reproduction is expended and its consequences in soma neglect is witnessed by the effects of bodily aging (Kirkwood, 2002). Thus, this theory lends a Darwinian underpinning to the notion that menopause is the inevitable product of longevity.

While the *"Disposable Soma Theory"* may imply that reproductive lifespan is actively matched to the anticipated lifespan of the organism, the converse may be true. There is accumulating evidence to support a strong positive correlation between age at menopause and longevity. Using an epigenetic biomarker of age, Levine and colleagues found an association between early menopause and accelerated aging (Levine, et al., 2016). This finding held true whether menopause was natural or surgically induced by oophorectomy. Interestingly, women who received menopause hormonal therapy exhibited a lower epigenetic age. Taken together, the authors conclude from these results that menopause is likely the cause of the observed accelerated aging. If true, it follows that delaying the onset of menopause would extend natural lifespan. The possibility that



the fertility extension imparted by AMH immunization may increase longevity is enticing and warrants further study.

As additional evidence for the link between AMH and longevity, it has been shown that age at natural menopause (ANM) is governed in part by variants in the *AMH* and *AMHR2* genes. A number of single nucleotide polymorphisms (SNPs) have been identified that modify the ANM (Braem, et al., 2012). Intriguingly, in an unrelated study of the proteomes of dozens of mammalian species to find longevity-selected positions, the cytoplasmic kinase domain of AMHR2 stood out as the protein domain most strongly associated with longevity (Semeiks & Grishin, 2012). These studies provide molecular insights into how AMH may provide a link between reproductive lifespan and the lifespan of the organism, and suggest that the AMH/AMHR2 signaling may be ideal for targeting clinical therapies for either or both matters.

### **Novel Clinical Applications for AMH**

In a clinical setting, AMH and its receptor could be exploited in a number of novel ways for human benefit. For example, the measurement of AMH levels in serum has already proven its diagnostic value in cases of infertility; however, evaluating AMH autoantibody levels in serum to assess infertility could prove to be useful in identifying the root cause—and a possible treatment path—in idiopathic cases. In addition to its diagnostic value, AMH could be targeted immunologically in order to actively intervene in human diseases and conditions. As AMH immunization has been shown in the current study to delay reproductive senescence in a mouse model, this discovery suggests that the same method could potentially extend fertility and delay menopause in humans. This

approach could be of great benefit for women who choose to have children later in life for career or other personal reasons, as these women often run the risk of fertility problems by postponing childbearing. Additionally, by delaying the onset of menopause, these women would avoid the serious accompanying health risks such as osteoporosis and cardiovascular disease.

The concept of harnessing autoimmunity to modulate fertility has been proposed in the past; for example, Millar and colleagues suggested that immunization or women with ZP3 peptide could be employed to provide long-term contraception, and that passive transfer of ZP3 antibody could provide a reversible form of contraception (Millar, et al., 1989). The contrast between these two modes highlights one of the greatest potential pitfalls of active immunization—unlike conventional drugs, a vaccination cannot be withdrawn. Therefore, if the patient changes her mind, or if an adverse effect occurs, the path ahead may be difficult. Given the *in vitro* and mechanistic data presented in the current study, passive transfer of antibody may be effective for fertility extension. However, it may be challenging to deliver and maintain a clinically effective amount of antibody over a span lasting potentially decades. Additionally, ethical consideration must be given to the circumstances of a child born to a mother over 50, 60, or even 70. Children of mothers of extremely advanced age may have an unfair disadvantage or experience poor quality of life. Of greater concern, the health of the child may also be at risk, since health risks in pregnancies increase with the age of the mother (Coco, et al., 2014).

In addition to the general risks associated with pregnancies in older mothers, there is a chance that AMH autoantibody of the IgG isotype may cross the placenta. In the

case of a male fetus, neutralizing antibody could reduce the amount of bioavailable AMH, causing PMDS. This scenario was demonstrated experimentally in rabbits (Tran, et al., 1986) and raises the question of whether this condition occurs naturally, and whether maternal AMH antibodies account for at least some of the spontaneous cases of PMDS in humans. An analogous model in mice would likely not be feasible, as very little maternal-fetal IgG transfer in this species occurs, and only very late in gestation; however, significant amounts of IgG is transferred postnatally through lactation (Pentsuk & van der Laan, 2009). All pups in the current study were euthanized shortly after birth and no internal examinations of urogenital structures were performed; however, this will most certainly be an avenue for future study. Furthermore, the long-term effect on the fertility and ovarian reserve in female pups born and nursed by AMH-immunized mothers makes an intriguing area of further investigation.

Finally, the fact that AMH is no longer expressed in women after menopause positions the protein as an appealing target antigen for developing a preventive or therapeutic ovarian cancer vaccine. Active immunization to what has been termed "*retired self-proteins*" (Tuohy, 2014) would be expected to produce a benign immunologic memory in a woman no longer producing AMH; however, an emerging ovarian tumor aberrantly producing AMH would be immediately recognized by immune surveillance and destroyed. The active immunization approach to cancer treatment and prevention has the intrinsic benefit that it is long-lasting and self-sustaining, unlike passively transferred immunotherapeutics. For example, the humanized monoclonal antibody Avastin<sup>®</sup> (bevacizumab) effectively targets vascular endothelial growth factor A (VEGF-A) to inhibit the development of blood vessels that would nourish emerging and

growing tumors, and the drug has been approved by the FDA to treat many types of cancers including colorectal, breast, and more recently for stage III/IV ovarian cancer. However, due to the limited half-life of the antibody, the patient must receive *i.v.* infusions of the drug every 3 weeks for as many as 22 cycles. A treatment regimen may cost upwards of \$100,000 per year, and when used in combination with standard chemotherapeutic agents against well-established tumors, may only extend the life expectancy of a patient by five to six months (Fleck, 2006; Rossi, et al., 2017). The paradigm of targeting organ-specific retired self-proteins with active immunization overcomes the need for repeated and costly administration of a passive agent, and the approach has been successful in preventing or treating tumors in murine models of breast cancer (Jaini, et al., 2010) and ovarian cancer (Sakalar, et al., 2015; Mazumder, et al., 2017). In the ovarian cancer vaccine model, it has been demonstrated that vaccination of mice with extracellular domain of AMHR2 (AMHR2-ED) is highly effective in inhibiting the growth of autochthonous and transplantable epithelial ovarian carcinomas (EOCs). While the full-length protein is not completely "retired" with age akin to its ligand, the extracellular domain of AMHR2 in humans is no longer expressed at autoimmunogenic levels in any human tissues after menopause (Mazumder, et al., 2017). While the physiologic purpose of this age-related variant of the receptor is unclear, it creates an opportunity to target a domain that is no longer expressed in healthy tissues, but is expressed at high levels in >90% of human EOC. AMH may be similarly employed in a vaccine aimed at primary immunoprevention and treatment of ovarian cancer. This strategy should be reasonably safe for any postmenopausal woman, but it may not be nearly as effective as the AMHR2 approach. Ovarian tumors that secrete

AMH are almost exclusively limited to those arising from granulosa cell tumors (GCTs), and these tumors represent only 3% - 5% of ovarian neoplasms (Chang, et al., 2009). Additionally, since AMH itself has been shown to have intrinsic anti-cancer properties (Kim, et al., 2014), one must consider that immunologic targeting of AMH may have the unintended effect of alleviating any natural apoptotic pressure that AMH naturally exerts on the tumor. However, in the current study, no ovarian neoplasms were observed during necropsy at any time point, including those as long as ten months from immunization. This finding implies that even a prolonged history of anti-AMH immunity at least does not promote tumor development, and should be explored as a means of cancer prevention. Finally, while no obvious abnormalities were discovered in brain tissues or behavior of mice in the study, it is important to note that AMH expression in the brain is negligible in mice but substantial in humans (Uhlen, et al., 2015). While it remains unclear if AMH expression in the human brain is "*retired*" after menopause as it is in the ovaries, the possibility of off-target CNS effects remains a caveat for any human application of AMH autoimmunity. Nevertheless, the promise of a potential novel ovarian cancer vaccine remains appealing, and determining whether AMH vaccination is ultimately effective in preventing or treating GCTs in a mouse model will be addressed in future investigations.

In summary, the current study has for the first time generated and characterized the immune response to anti-Müllerian hormone in a murine model. Additionally, a novel phenotype of extended fertility has been identified, and this discovery may be important not only in unraveling the true nature and biologic functions of AMH, but also in better understanding and treating impairments of human fertility. In the seminal paper

describing the first successful model of EAO, the hopeful and insightful conclusion reached by the authors states: "Finally, these results suggest that autoimmune ovariopathy should be given consideration when treating problems related to fertility and sterility" (Jankovic, et al., 1973). These investigators recognized the significance of their findings—that autoimmune infertility was likely a dreadful and widespread disease hiding in plain sight. Nearly half a century later, this hypothesis has been supported by overwhelming experimental and clinical evidence. The evidence presented herein will hopefully add to the collective wealth of knowledge of human infertility and the means to address it.

## REFERENCES

- Aaltonen, J. et al., 1997. An autoimmune disease, APECED, caused by mutations in a novel gene featuring two PHD-type zinc-finger domains. *Nat Genet*, Volume 17, pp. 399-403.
- Aguilar, R., Johnson, J. M., Barrett, P. & Tuohy, V. K., 2017. Vaccination with inhibin- $\alpha$  provides effective immunotherapy against testicularstromal cell tumors. *J ImmunoTherapy Cancer*, Volume 5, p. 37.
- Altuntas, C., Johnson, J. & Tuohy, V., 2006. Autoimmune targeted disruption of the pituitary-ovarian axis causes premature ovarian failure. *J Immunol*, 177(3), pp. 1988-1996.
- Anttonen, M. et al., 2011. Anti-Mullerian hormone inhibits growth of AMH type II receptor-positive human ovarian granulosa cell tumor cells by activating apoptosis. *Lab Invest*, Volume 91, pp. 1605-1614.
- Anttonen, M. et al., 2005. High GATA-4 expression associates with aggressive behavior, whereas low anti-Müllerian hormone expression associates with growth potential of ovarian granulosa cell tumors. *J Clin Endocrinol Metab*, 90(12), pp. 6529-6535.
- Asano, M., Toda, M., Sakaguchi, N. & Sakaguchi, S., 1996. Autoimmune disease as a consequence of developmental abnormality of a T cell subpopulation. *J Exp Med*, 184(2), pp. 387-396.

- Baarends, W. M. et al., 1994. A novel member of the transmembrane serine/threonine kinase receptor family is specifically expressed in the gonads and in mesenchymal cells adjacent to the Mullerian duct. *Development*, Volume 120, pp. 189-197.
- Bakos, O., Lundqvist, O., Wide, L. & Bergh, T., 1994. Ultrasonographical and hormonal description of the normal ovulatory menstrual cycle. *Acta Obstet Gynecol Scand*, 73(10), pp. 790-796.
- Barbie, T. U. et al., 2003. Mullerian Inhibiting Substance inhibits cervical cancer cell growth via a pathway involving p130 and p107. *Proc Natl Acad Sci USA*, 100(26), pp. 15601-15606.
- Bertone-Johnson, E. R. et al., 2018. Anti-Müllerian hormone levels and incidence of early natural menopause in a prospective study. *Hum Reprod*, 33(6), pp. 1175-1182.
- Blurton Jones, N. G., Hawkes, K. & O'Connell, J. F., 2002. Antiquity of postreproductive life: are there modern impacts on hunter-gatherer postreproductive life spans?. *Am J Hum Biol*, Volume 14, pp. 184-205.
- Braem, M. G. M. et al., 2012. Interactions between genetic variants in AMH and AMHR2 may modify age at natural menopause. *PloS One*, 8(3), p. e59819.
- Broekmans, F. & Fauser, B., 2006. Diagnostic criteria for polycystic ovarian syndrome. *Endocrine*, 30(1), pp. 3-11.
- Broekmans, F. et al., 2008. Anti-Mullerian hormone and ovarian dysfunction. *Trends Endocrin Met*, 19(9), pp. 340-347.



- Broer, S. L., Broekmans, F. J., Laven, J. S. & Fauser, B. C., 2014. Anti-Mullerian hormone: ovarian reserve testing and its potential clinical applications. *Hum Reprod Update*, 20(5), pp. 688-701.
- Burnet, F. M., Freeman, M., Jackson, A. V. & Lush, D., 1941. *The production of antibodies. A review and a theoretical discussion*. Melbourne: Macmillan.
- Carp, H. J., Selmi, C. & Shoenfeld, Y., 2012. The autoimmune bases of infertility and pregnancy loss. *J Autoimmunity*, Volume 38, pp. J266-J274.
- Carre, G. & Greenfield, A., 2016. The gonadal supporting cell lineage and mammalian sex determination: The differentiation of sertoli and granulosa cells. *Results Probl Cell Differ*, Volume 58, pp. 47-66.
- Cate, R. et al., 1986. Isolation of the bovine and human genes for Mullerian inhibiting substance and expression of the human gene in animal cells. *Cell*, 45(5), pp. 685-698.
- Centers for Disease Control and Prevention, 2018. Births: Final Data for 2017. *National Vital Statistics Reports*, 67(8), pp. 1-49.
- Chang, H. L., Pahlavan, N., Halpern, E. F. & MacLaughlin, D. T., 2009. Serum Mullerian inhibiting substance/anti-Mullerian hormone levels in patients with adult granulosa cell tumors directly correlates with aggregate tumor mass as determined by pathology or radiology. *Gynecol Oncol*, 114(1), pp. 57-60.
- Clark, D. A. & Coker, R., 1998. Transforming growth factor-beta (TGF-beta). *Int J Biochem Cell Biol*, 30(3), pp. 293-298.
- Clement, F. & Monniaux, D., 2013. Multiscale modelling of ovarian follicular selection. *Prog Biophys Mol Biol*, 113(3), pp. 398-408.

- Coco, L., Giannone, T. T. & Zarbo, G., 2014. Management of high-risk pregnancy. *Minerva Ginecol*, 66(4), pp. 383-389.
- Constantinescu, C. S., Farooqi, N., O'Brien, K. & Gran, B., 2011. Experimental autoimmune encephalomyelitis (EAE) as a model for multiple sclerosis (MS): EAE as model for MS. *Brit J Pharmacol*, 164(4), pp. 1079-1106.
- Cora, M. C., Kooistra, L. & Travlos, G., 2015. Vaginal cytology of the laboratory rat and mouse: review and criteria for the staging of the estrous cycle using stained vaginal smears. *Toxicol Pathol*, Volume 43, pp. 776-793.
- Coulam, C. B., Kempers, R. D. & Randall, R. V., 1981. Premature ovarian failure: evidence for the autoimmune mechanism. *Fertil Steril*, 36(2), pp. 238-240.
- Danilovich, N. & Sairam, M. R., 2002. Haploinsufficiency of the follicle-stimulating hormone receptor accelerates oocyte loss inducing early reproductive senescence and biological aging in mice. *Biol Reprod*, 67(2), pp. 361-369.
- Deroux, A. et al., 2017. Female infertility and serum auto-antibodies: a systematic review. *Clinic Rev Allerg Immunol*, Volume 53, pp. 78-86.
- Dewailly, D. et al., 2014. The physiology and clinical utility of anti-Mullerian hormone in women. *Hum Reprod Update*, 20(3), pp. 370-385.
- di Clemente, N. et al., 2010. Processing of anti-Mullerian hormone regulates receptor activation by a mechanism distinct from TGF-beta. *Mol Endocrinol*, 24(11), pp. 2193-2206.
- Dudley, A. et al., 2003. Removal of endotoxin by reverse phase HPLC abolishes anti-endothelial cell activity of bacterially expressed plasminogen kringle 5. *BioTechniques*, 35(4), pp. 724-732.

- Durlinger, A. et al., 2001. Anti-Müllerian hormone attenuates the effects of FSH on follicle development in the mouse ovary. *Endocrinology*, 124(11), pp. 4891-4899.
- Durlinger, A. et al., 1999. Control of primordial follicle recruitment by anti-mullerian hormone in the mouse ovary. *Endocrinology*, 140(12), pp. 5789-5796.
- Ebrahimi, M. & Asbagh, F. A., 2001. Pathogenesis and causes of premature ovarian failure. *Int J Fertil Steril*, 5(2), pp. 54-65.
- El-Hayek, S. & Clarke, H. J., 2016. Control of Oocyte Growth and Development. In: R. P. Piprek, ed. *Molecular Mechanisms of Cell Differentiation in Gonad Development*. s.l.:Springer, pp. 191-224.
- Faure, E. et al., 1996. Mutant isoforms of the anti-Mullerian hormone type II receptor are not expressed at the cell membrane. *J Biol Chem*, 271(48), pp. 30571-30575.
- Fleck, L. M., 2006. The costs of caring: Who pays? Who profits? Who panders?. *Hastings Cent Rep*, 36(3), pp. 13-17.
- Fujisawa, M., Yamasaki, T., Okada, H. & Kamidono, S., 2002. The significance of anti-Mullerian hormone concentration in seminal plasma for spermatogenesis. *Hum Reprod*, 17(4), pp. 968-970.
- Fu, L., Feng, W., Li, S.-R. & Huang, B.-Y., 2007. ZP3 peptides administered orally suppress murine experimental autoimmune ovarian disease. *J Reprod Immunol*, 75(1), pp. 40-47.
- Gao, J. et al., 2017. Identification of patients with primary ovarian insufficiency caused by autoimmunity. *Reprod Biomed Online*, Volume 35, pp. 475-479.
- Gilbert, S. F. & Barresi, M. J., 2016. *Developmental Biology*. 11th ed. Sunderland(Massachusetts): Sinauer Associates.

- Gilhus, N. E., 2016. Myesthenia gravis. *N Engl J Med*, 375(26), pp. 2570-258.
- Gold, E. B., 2011. The timing of the age at which natural menopause occurs. *Obstet Gynecol Clin North Am*, 38(3), p. 425–440.
- Goodman, M. H., 2009. *Basic Medical Endocrinology*. 4th ed. New York: Elsevier.
- Hai, L. et al., 2015. Infertility in female mice with a gain-of-function mutation in the luteinizing hormone receptor is due to irregular estrous cyclicity, anovulation, hormonal alterations, and polycystic ovaries. *Biol Reprod*, 93(1), pp. 1-11.
- Hawkins, S. M. & Matzuk, M. M., 2008. Menstrual Cycle: Basic Biology. *Ann NY Acad Sci*, Volume 1135, pp. 10-18.
- Hayes, E. et al., 2016. Intra-cellular mechanism of Anti-Mullerian hormone (AMH) in regulation of follicular development. *Mol Cell Endocrinol*, Volume 433, pp. 56-65.
- Hoek, A., Shoemaker, J. & Drexhage, H. A., 1997. Premature ovarian failure and ovarian autoimmunity. *Endocr Rev*, 18(1), pp. 107-134.
- Husebye, E. S., Anderson, M. S. & Kampe, O., 2018. Autoimmune Polyendocrine Syndromes. *N Engl J Med*, 378(12), pp. 1132-1141.
- Hutson, J., Ikawa, H. & Donahoe, P. K., 1981. The ontogeny of Mullerian inhibiting substance in the gonads of the chicken. *J Pediatr Surg*, 16(6), pp. 822-827.
- Jaini, R., Altuntas, C. Z., Loya, M. G. & Tuohy, V. K., 2015. Disruption of estrous cycle homeostasis in mice with experimental autoimmune encephalomyelitis. *J Neuroimmunol*, Volume 279, pp. 71-74.
- Jaini, R. et al., 2010. An autoimmune-mediated strategy for prophylactic breast cancer vaccination. *Nat Med*, 16(7), pp. 799-803.

- Jane-wit, D. et al., 2007. Beta 1-adrenergic receptor autoantibodies mediate dilated cardiomyopathy by agonistically inducing cardiomyocyte apoptosis. *Circulation*, 116(4), pp. 399-410.
- Jankovic, B. D., Markovic, B. M., Petrovic, S. & Isakovic, K., 1973. Experimental autoimmune-oophoritis in the rat. *Eur J Immunol*, 3(6), pp. 375-377.
- Jasti, S. et al., 2012. The autoimmune regulator prevents premature reproductive senescence in female mice. *Bio Reprod*, 86(4), pp. 1-9.
- Johnson, J. et al., 2004. Germline stem cells and follicular renewal in the postnatal mammalian ovary. *Nature*, 428(11), pp. 145-150.
- Josso, N., 1991. Remembrance of Dr. Alfred Jost. *Endocrinology*, 129(5), pp. 2274-2276.
- Josso, N., Beliville, C., di Clemente, N. & Picard, J.-Y., 2005. AMH and AMH receptor defects in persistent Mullerian duct syndrome. *Hum Reprod Update*, 11(4), pp. 351-356.
- Josso, N. et al., 1993. Anti-Mullerian hormone: the Jost factor. *Rec Prog Hormone Res*, Volume 48, pp. 1-59.
- Josso, N., di Clemente, N. & Gouedard, L., 2001. Anti-Mullerian hormone and its receptors. *Mol Cell Endocrinol*, Volume 179, pp. 25-32.
- Jost, A., 1947. The age factor in the castration of male rabbit fetuses. *Proc Soc Exp Biol Med*, 66(2), pp. 302-303.
- Jost, A., 1953. Problems of fetal endocrinology: the gonadal and hypophyseal hormones. *Recent Prog Horm Res*, Volume 8, pp. 379-418.
- Kalantaridou, S. & Nelson, L., 2000. Premature ovarian failure is not premature menopause. *Ann NY Acad Sci*, Volume 900, pp. 393-402.

- Kapadia, A. & Dmytriw, A. A., 2020. Multiple sclerosis is a systemic venous vasculopathy: A single unifying mechanism. *Med Hypotheses*, Volume 140, p. 109645.
- Katsarou, A. et al., 2017. Type 1 diabetes mellitus. *Nat Rev Dis Primers*, Volume 3, p. Article 17016.
- Kawamura, K., Kawamura, N. & Hsueh, A. J., 2016. Activation of dormant follicles: a new treatment for premature ovarian failure?. *Curr Opin Obstet Gynecol*, Volume 28, pp. 217-222.
- Kawane, K. et al., 2010. Cytokine-dependent but acquired immunity-independent arthritis caused by DNA escaped from degradation. *Proc Natl Acad Sci USA*, 107(45), pp. 19432-19437.
- Kerr, J. et al., 2012. The primordial follicle reserve is not renewed after chemical or  $\gamma$ -irradiation mediated depletion. *Reproduction*, 143(4), pp. 469-476.
- Kevenaar, M. E. et al., 2006. Serum anti-Mullerian hormone levels reflect the size of the primordial follicle pool in mice. *Endocrinology*, 147(7), pp. 3228-3234.
- Kim, J. H., MacLaughlin, D. T. & Donahoe, P. K., 2014. Müllerian inhibiting substance/anti-Müllerian hormone: A novel treatment for gynecologic tumors. *Obstet Gynecol Sci*, 57(5), pp. 343-357.
- Kim, P. S., McQueen, J. S. & Hawkes, K., 2019. Why does women's fertility end in mid-life? Grandmothering and age at last birth. *J Theor Biol*, Volume 461, pp. 84-91.
- Kirkwood, T. B., 2002. Evolution of ageing. *Mech Ageing Dev*, 123(7), pp. 737-745.
- Kojima, A. & Prehn, R. T., 1981. Genetic susceptibility to post-thymectomy autoimmune diseases in mice. *Immunogenetics*, Volume 14, pp. 15-27.

- Kovanci, E. & Schutt, A., 2015. Premature ovarian failure. Clinical presentation and treatment. *Obstet Gynecol Clin N Am*, Volume 42, pp. 153-161.
- Kruszynska, A. & Slowinska-Srzednicka, J., 2017. Anti-Mullerian hormone (AMH) as a good predictor of time of menopause. *Menopause Rev*, 16(2), pp. 47-50.
- La Marca, A. et al., 2010. Primary ovarian insufficiency: autoimmune causes. *Curr Opin Obstet Gynecol*, 22(4), pp. 277-282.
- La Marca, A. et al., 2006. Serum anti-müllerian hormone levels in women with secondary amenorrhea. *Fertil Steril*, 85(5), pp. 1547-1549.
- La Marca, A. et al., 2010. Anti-Mullerian hormone (AMH) as a predictive marker in assisted reproductive technology (ART). *Hum Reprod Update*, 16(2), pp. 113-130.
- Laszczynska, M. et al., 2008. Human postmenopausal ovary--hormonally inactive fibrous connective tissue or more?. *Histol Histopathol*, 23(2), pp. 219-226.
- Levine, M. E. et al., 2016. Menopause accelerates biological aging. *Proc Natl Acad Sci USA*, 113(33), pp. 9372-9332.
- Liao, W., Lin, J.-X. & Leonard, W. J., 2011. IL-2 family cytokines: new insights into the complex roles of IL-2 as a broad regulator of T helper cell differentiation. *Curr Opin Immunol*, 23(5), pp. 598-604.
- Luborsky, J. L. et al., 2011. Autoantibodies to mesothelin in infertility. *Cancer Epidemiol Biomarkers Prev*, 20(9), pp. 1970-1978.
- Magoffin, D. A., 2005. Ovarian theca cell. *Int J Biochem Cell Biol*, 37(7), pp. 1344-1349.

- Martin, R. M., Brady, J. L. & Lew, A. M., 1998. The need for IgG2c specific antiserum when isotyping antibodies from C57BL/6 and NOD mice. *J Immunol Methods*, Volume 212, pp. 187-192.
- Matzinger, P., 1994. Tolerance, danger, and the extended family. *Annu Rev Immunol*, Volume 12, pp. 991-1045.
- Mazumder, S. et al., 2017. Primary immunoprevention of epithelial ovarian carcinoma by vaccination against the extracellular domain of anti-Mullerian hormone receptor II. *Cancer Prev Res*, 10(11), pp. 612-624.
- McLennan, I. S., Koishi, K., Batchelor, N. J. & Pankhurst, M. W., 2017. Mice with either diminished or elevated levels of anti-Mullerian hormone have decreased litter size. *Biol Reprod*, 98(1), pp. 54-62.
- McLennan, I. S. & Pankhurst, M. W., 2015. Anti-Mullerian hormone is a gonadal cytokine with two circulating forms and cryptic actions. *J Endocrinol*, 226(3), pp. R45-R57.
- Meduri, G. et al., 2007. Serum anti-Mullerian hormone expression in women with premature ovarian failure. *Hum Reprod*, 22(1), pp. 117-123.
- Meirelles, K. et al., 2012. Human ovarian cancer stem/progenitor cells are stimulated by doxorubicin but inhibited by Mullerian inhibiting substance. *Proc Natl Acad Sci USA*, 109(7), pp. 2358-2363.
- Mihm, M., Gangooly, S. & Muttukrishna, S., 2011. The normal menstrual cycle in women. *Anim Reprod Sci*, Volume 124, pp. 229-236.
- Millar, S. E. et al., 1989. Vaccination with a synthetic zona pellucida peptide produces long-term contraception in female mice. *Science*, 246(4932), pp. 935-938.



- Mishina, Y. et al., 1997. Sequence, genomic organization, and chromosomal location of the mouse Mullerian-inhibiting substance type II receptor gene. *Biochem and Biophys Res Commun*, Volume 237, pp. 741-746.
- Mitsdoerffer, M. et al., 2010. Proinflammatory T helper type 17 cells are effective B-cell helpers. *Proc Natl Acad Sci USA*, 107(32), pp. 14292-14297.
- Miyake, T. et al., 1988. Acute oocyte loss in experimental autoimmune oophoritis as a possible model of premature ovarian failure. *Am J Obstet Gynecol*, 158(1), pp. 186-192.
- Mobeen, H., Afzal, N. & Kashif, M., 2016. Polycystic ovary syndrome may be an autoimmune disorder. *Scientifica*.
- Moncayo, R. & Moncayo, H. E., 1992. Autoimmunity and the ovary. *Immunol Today*, 13(7), pp. 255-258.
- Monniaux, D. et al., 2014. The ovarian reserve of primordial follicles and the dynamic reserve of antral growing follicles: what is the link?. *Biol Reprod*, 90(4), pp. 1-11.
- Monteleone, P. et al., 2011. Female infertility related to thyroid autoimmunity: the ovarian follicle hypothesis. *Am J Reprod Immunol*, 66(2), pp. 108-114.
- Moran, L. J., Norman, R. J. & Teede, H. L., 2015. Metabolic risk in PCOS: phenotype and adiposity impact. *Trends Endocrinol Metab*, 26(3), pp. 136-143.
- Motta-Mena, N. V. & Puts, D. A., 2017. Endocrinology of human female sexuality, mating, and reproductive behavior. *Horm Behav*, Volume 91, pp. 19-35.
- Munsterberg, A. & Lovell-Badge, R., 1991. Expression of the mouse anti-müllerian hormone gene suggests a role in both male and female sexual differentiation. *Development*, Volume 113, pp. 613-624.

- Murali, P., Radhika, J. & Alwin, D., 2020. Effect of thymectomy on the female reproductive cycle in neonatal guinea pigs. *Clin Exp Reprod Med*, 47(1), pp. 12-19.
- Murata, K. & Baldwin III, W. M., 2009. Mechanisms of complement activation, C4d deposition, and their contribution to the pathogenesis of antibody-mediated rejection. *Transplant Rev*, 23(2), pp. 139-150.
- Murata, K. et al., 2007. Synergistic deposition of C4d by complement-activating and non-activating antibodies in cardiac transplants. *Am J Transplant*, 7(11), pp. 2605-2614.
- Namkung, J. et al., 2012. Mullerian inhibiting substance induces apoptosis of human endometrial stromal cells in endometriosis. *J Clin Endocrinol Metab*, 97(9), p. 3224–3230.
- Nasri, F., Doroudchi, M., Jahromi, B. N. & Gharesi-Fard, B., 2018. T helper cells profile and CD4+CD25+Foxp3+regulatory T cells in polycystic ovary syndrome. *Iran J Immunol*, 15(3), pp. 175-185.
- Novais, J. et al., 2015. Polycystic ovary syndrome and chronic autoimmune thyroiditis. *Gynecol Endocrinol*, 31(1), pp. 48-51.
- Packer, C., Tatar, M. & Collins, A., 1998. Reproductive cessation in female mammals. *Nature*, 392(6678), pp. 807-811.
- Pankhurst, M. W., 2017. A putative role for anti-Mullerian hormone (AMH) in optimizing ovarian reserve expenditure. *J Endocrinol*, 233(1), pp. R1-R13.
- Pankhurst, M. W. et al., 2018. Anti-Mullerian hormone overexpression restricts preantral ovarian follicle survival. *J Endocrinol*, Volume 237, pp. 153-163.

- Parry, R. L. et al., 1992. Recombinant human mullerian inhibiting substance inhibits human ocular melanoma cell lines in vitro and in vivo. *Cancer Res*, 52(5), pp. 1182-1186.
- Passos, G. A., Speck-Hernandez, C. A., Assis, A. F. & Mendes-da-Cruz, D. A., 2018. Update on Aire and thymic negative selection. *Immunology*, 153(1), pp. 10-20.
- Pellatt, L. et al., 2011. Anti-Müllerian hormone reduces follicle sensitivity to follicle-stimulating hormone in human granulosa cells. *Fertil Steril*, 96(5), pp. 1246-1251.
- Pentsuk, N. & van der Laan, J. W., 2009. An interspecies comparison of placental antibody transfer: new insights into developmental toxicity testing of monoclonal antibodies. *Birth Defects Res B Dev Reprod Toxicol*, 86(4), pp. 328-344.
- Pepin, D. et al., 2015. AAV9 delivering a modified human Mullerian inhibiting substance as a gene therapy in patient-derived xenografts of ovarian cancer. *Proc Natl Acad Sci USA*, 112(32), pp. E4418-44127.
- Pepinsky, R. B. et al., 1988. Proteolytic processing of Mullerian inhibiting substance produces a transforming growth factor-beta-like fragment. *J Biol Chem*, 263(35), pp. 18961-18964.
- Perez, G. I. et al., 1999. Prolongation of ovarian lifespan into advanced chronological age by Bax-deficiency. *Nat Gen*, 21(2), pp. 200-203.
- Plant, T. M., 2015. The hypothalamo-pituitary-gonadal axis. *J Endocrinol*, 226(2), pp. T41-T54.
- Punt, J., Stranford, S., Jones, P. & Owen, J., 2019. *Kuby Immunology*. 8th ed. New York: W. H. Freeman and Company.

- Qi, X., Pang, Y. & Qiao, J., 2016. The role of anti-Müllerian hormone in the pathogenesis and pathophysiological characteristics of polycystic ovary syndrome. *Eur J Obstet Gynecol Reprod Biol*, Volume 199, pp. 82-87.
- Raphael, I., Nalawade, S., Eagar, T. N. & Forsthuber, T. G., 2015. T cell subsets and their signature cytokines in autoimmune and inflammatory diseases. *Cytokine*, Volume 74, pp. 5-17.
- Rehman, Z. U. et al., 2017. Role and mechanism of AMH in the regulation of Sertoli cells in mice. *J Steroid Biochem Mol Biol*, Volume 174, pp. 133-140.
- Rekvig, O. & Van der Vlag, J., 2014. The pathogenesis and diagnosis of systemic lupus erythematosus: still not resolved. *Semin Immunopathol*, 36(3), pp. 301-311.
- Rey, R. A. et al., 1996. Antimüllerian hormone as a serum marker of granulosa cell tumors of the ovary: comparative study with alpha-inhibin and estradiol. *Am J Obstet Gynecol*, 174(3), pp. 958-965.
- Rhim, S. et al., 1992. Autoimmune disease of the ovary induced by a ZP3 peptide from the mouse zona pellucida. *J Clin Invest*, 89(1), pp. 28-35.
- Rivers, T. M. & Schwentker, F. F., 1935. encephalomyelitis accompanied by myelin destruction experimentally produced in monkeys. *J Exp Med*, 61(5), pp. 689-702.
- Roberts, L. M., Hirokawa, Y., Nachtigal, M. W. & Ingraham, H. A., 1999. Paracrine-mediated apoptosis in reproductive tract development. *Dev Biol*, Volume 208, pp. 110-122.
- Roly, Z. Y. et al., 2018. The cell biology and molecular genetics of Müllerian duct development. *WIREs Dev Biol*, 7(3), p. e310.

- Rossi, L. et al., 2017. Bevacizumab in ovarian cancer: A critical review of phase III studies. *Oncotarget*, 8(7), pp. 12389-12405.
- Sacchi, S. et al., 2016. The anti-Müllerian hormone (AMH) acts as a gatekeeper of ovarian steroidogenesis inhibiting the granulosa cell response to both FSH and LH. *Assist Reprod Genet*, 33(1), pp. 95-100.
- Sakalar, C. et al., 2015. Regulation of murine ovarian epithelial carcinoma by vaccination against the cytoplasmic domain of anti-Müllerian hormone receptor II. *J Immunol Res*, Volume 2015, p. Article ID 630287.
- Sathyapalan, T. et al., 2017. Anti-Müllerian hormone measurement for the diagnosis of polycystic ovary syndrome. *Clin Endocrinol*, 88(2), pp. 258-262.
- Schmidt, K. L. T., Kryger-Baggesen, N., Byskov, A. G. & Andersen, C. Y., 2005. Anti-Müllerian hormone initiates growth of human primordial follicles in vitro. *Mol Cell Endocrinol*, Volume 234, pp. 87-93.
- Schoenfeld, Y. et al., 2005. Accelerated atherosclerosis in autoimmune rheumatic diseases. *Circulation*, 112(21), pp. 3337-3347.
- Seifer, D. B., Baker, V. L. & Leader, B., 2011. Age-specific serum anti-Müllerian hormone values for 17,120 women presenting to fertility centers within the United States. *Fertil Steril*, 95(2), pp. 747-750.
- Seifer, D. B. & Merhi, Z., 2014. Is AMH a regulator of follicular atresia?. *J Assist Reprod Genet*, Volume 31, pp. 1403-1407.
- Semeiks, J. & Grishin, N. V., 2012. A method to find longevity-selected positions in the mammalian proteome. *PLoS One*, 7(6), p. e38595.

- Sen, A., Kushnir, V. A., Barad, D. H. & Gleicher, N., 2014. Endocrine autoimmune diseases and female infertility. *Nat Rev Endocrinol*, Volume 10, pp. 37-50.
- Sherman, P. W., 1998. The evolution of menopause. *Nature*, 392(6678), pp. 759-761.
- Shestakova, I. G., Radzinsky, V. E. & Khamoshina, M. B., 2016. Occult form of premature ovarian insufficiency. *Gynecol Endocrinol*, Volume 32, pp. 30-32.
- Shivers, C. A. & Dunbar, B. S., 1977. Autoantibodies to zona pellucida: a possible cause for infertility in women. *Science*, 197(4308), pp. 1082-1084.
- Shi, Y. & Massague, J., 2003. Mechanisms of TGF-beta signaling from cell membrane to the nucleus. *Cell*, Volume 113, pp. 685-700.
- Signorile, P. G., Petraglia, F. & Baldi, A., 2014. Anti-mullerian hormone is expressed by endometriosis tissues and induces cell cycle arrest and apoptosis in endometriosis cells. *J Exp Clin Cancer Res*, Volume 33, p. 46.
- Silva, C. A. et al., 2014. Autoimmune primary ovarian insufficiency. *Autoimmun Rev*, Volume 13, pp. 427-430.
- Sirmans, S. M. & Pate, K. A., 2013. Epidemiology, diagnosis, and management of polycystic ovary syndrome. *Clin Epidemiol*, 18(6), pp. 1-13.
- Skaznik-Wikiel, M. E., Traub, M. L. & Santoro, N., 2015. Menopause. In: J. L. Jameson & L. J. De Groot, eds. *Endocrinology: Adult and Pediatric*. 7th ed. Philadelphia: Saunders, pp. 2310-2322.
- Skiadas, C. C. et al., 2012. Ovarian reserve status in young women is associated with altered gene expression in membrana granulosa cells. *Mol Hum Reprod*, 18(7), pp. 362-371.

- Smith, D. A. & Germolec, D. R., 1999. Introduction to immunology and autoimmunity. *Environ Health Persp*, 107(S5), pp. 661-665.
- Solares, C. A., Hughes, G. B. & Tuohy, V. K., 2003. Autoimmune sensorineural hearing loss: an immunologic perspective. *J Neuroimmunol*, Volume 138, pp. 1-7.
- Taguchi, O. & Nishizuka, Y., 1980. Autoimmune oophoritis in thymectomized mice: T cell requirement in adoptive cell transfer. *Clin Exp Immunol*, Volume 42, pp. 324-331.
- Taguchi, O., Nishizuka, Y., Sakakura, T. & Kojima, A., 1980. Autoimmune oophoritis in thymectomized mice: detection of circulating antibodies against oocytes. *Clin Exp Immunol*, Volume 40, pp. 540-553.
- Takahashi, T. A. & Johnson, K. M., 2015. Menopause. *Med Clin N Am*, 99(3), pp. 521-534.
- Tehrani, F. R., Shakeri, N., Solaymai-Dodaran, M. & Azizi, F., 2011. Predicting age at menopause from serum antimullerian hormone concentration. *Menopause*, 18(7), pp. 766-770.
- Thacker, H. L. M., 2009. *The Cleveland Clinic Guide to Menopause*. New York: Kaplan Publishing.
- The Staff of The Jackson Laboratory, 1966. *Biology of the Laboratory Mouse*. 2nd ed. New York: Dover Publications.
- Tran, D. et al., 1986. Persistence of Mullerian ducts in male rabbits passively immunized against bovine anti-Mullerian hormone during fetal life. *Dev Biol*, Volume 116, pp. 160-167.

- Tuohy, V. K., 2014. Retired self-proteins as vaccine targets for primary immunoprevention of adult-onset cancers. *Expert Rev Vaccines*, 13(12), pp. 1447-1462.
- Tuohy, V. K. & Altuntas, C., 2007. Autoimmunity and premature ovarian failure. *Curr Opin Obstet Gyn*, Volume 19, pp. 366-369.
- Uhlen, M. et al., 2015. Tissue-based map of the human proteome. *Science*, 347(6220), p. 1260419.
- Vercellini, P., Vigano, P., Somigliana, E. & Fedele, L., 2014. Endometriosis: pathogenesis and treatment. *Nat Rev Endocrinol*, 10(5), pp. 261-275.
- Visser, J. A. et al., 2007. Increased oocyte degeneration and follicular atresia during the estrous cycle in anti-Müllerian hormone null mice. *Endocrinology*, 148(5), pp. 2301-2308.
- Walker, M. L. & Herndon, J. G., 2008. Menopause in nonhuman primates?. *Biol Reprod*, 79(3), pp. 398-406.
- Wang, J., Dicken, C., Lustbader, J. W. & Tortoriello, D. V., 2009. Evidence for a Müllerian-inhibiting substance autocrine/paracrine system in adult human endometrium. *Fertil Steril*, 91(4), pp. 1195-1203.
- Wang, P.-Y. et al., 2009. Mullerian inhibiting substance contributes to sex-linked biases in the brain and behavior. *Proc Natl Acad Sci USA*, 106(17), pp. 7203-7208.
- Warren, B. D. et al., 2014. Ovarian autoimmune disease: clinical concepts and animal models. *Cell Mol Immunol*, Volume 11, pp. 510-521.



- Weenen, C. et al., 2004. Anti-Mullerian hormone expression pattern in the human ovary: potential implications for initial and cyclic follicle recruitment. *Mol Hum Reprod*, 10(2), pp. 77-83.
- Welt, C. K., 2008. Primary ovarian insufficiency: a more accurate term for premature ovarian failure. *Clin Endocrinol*, 68(4), pp. 499-509.
- Wilson, C. A. et al., 1993. Mullerian inhibiting substance requires its N-terminal domain for biological activity, a novel finding within the transforming growth factor-beta superfamily. *Mol Endocrinol*, 7(2), pp. 247-257.
- Wu, J. M., Zelinski, M. B., Ingram, D. K. & Ottinger, M. A., 2005. Ovarian aging and menopause: Current theories, hypotheses, and research models. *Exp Bio Med*, 230(11), pp. 818-828.
- Xavier, F. & Allard, S., 2003. Anti-Müllerian hormone, beta-catenin and Müllerian duct regression. *Mol Cell Endocrinol*, Volume 211, pp. 115-121.
- Zhang, T. et al., 2018. Anti-Müllerian hormone inhibits proliferation and induces apoptosis in epithelial ovarian cancer cells by regulating the cell cycle and decreasing the secretion of stem cell factor. *Oncol Lett*, 166(3), pp. 3260-3266.
- Zuckerman, S., 1951. The number of oocytes in the mature ovary. *Res Prog Horm Res*, Volume 6, pp. 63-108.

## **APPENDIX**

## SUPPLEMENTARY DATA

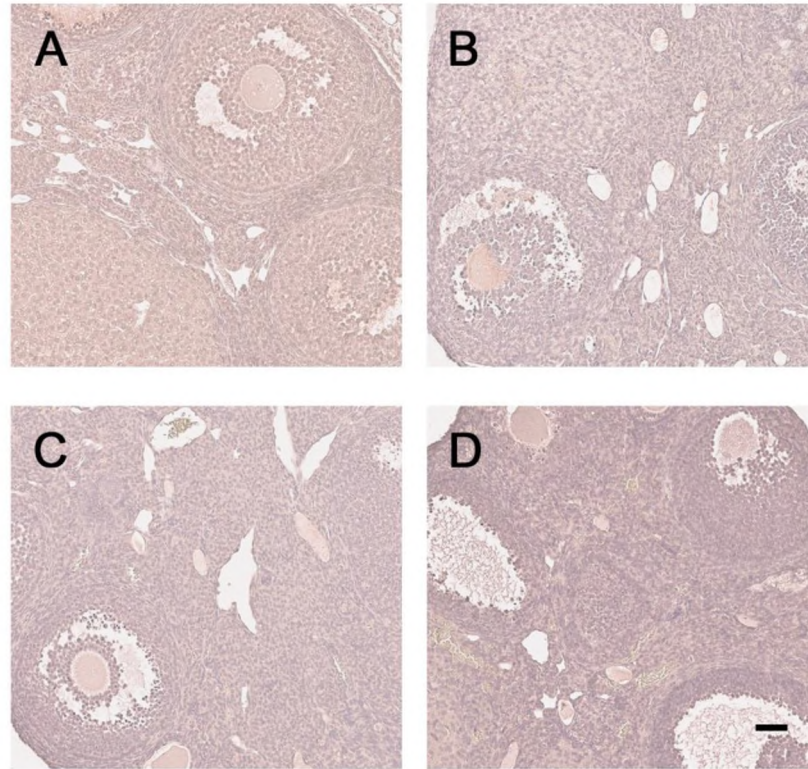


**Figure S1. Complement Activity is Absent as Evidenced by Negative C4d Staining in Ovarian Tissues.** Sections of ovaries from mice immunized with rmAMH or CFA were immunostained with C4d antibody and analyzed by light microscopy. C4d staining was absent at 4 weeks after immunization for both (A) AMH and (B) CFA mice as well as at 8 weeks after immunization for both (C) AMH and (D) CFA mice. Scale bar represents 50  $\mu$ m.

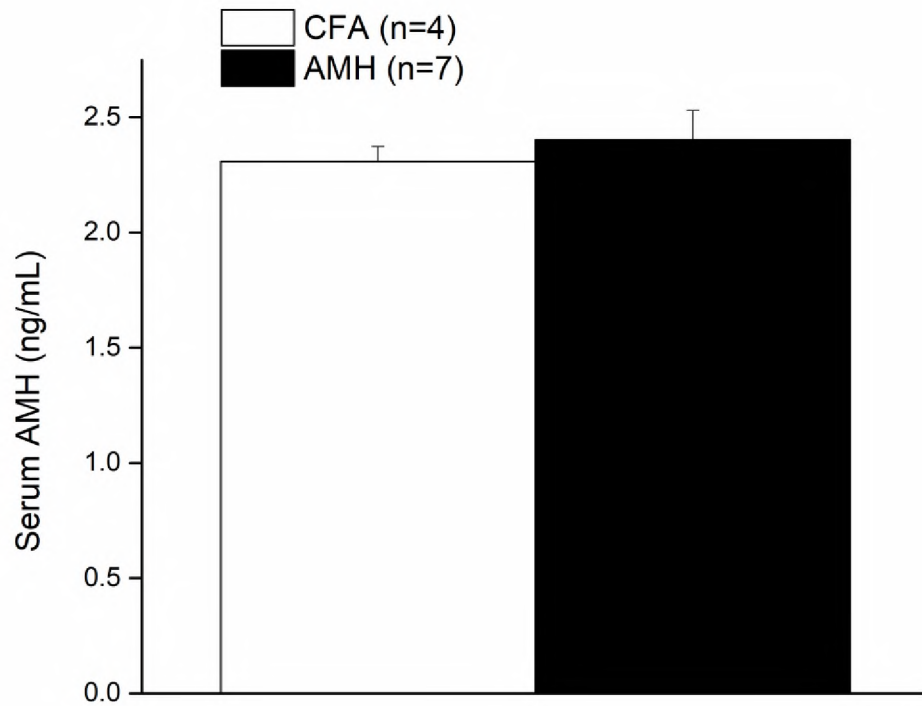


**Figure S2. Serum AMH Levels at 10 Months.** Ten months after immunization with rmAMH or CFA, mice were euthanized and serum collected via cardiac puncture. Sera were diluted 1:3 with PBS and analyzed via competitive ELISA for mouse AMH. Means for each group are plotted. No significant difference was observed between the groups. Error bars represent  $\pm$ SEM.

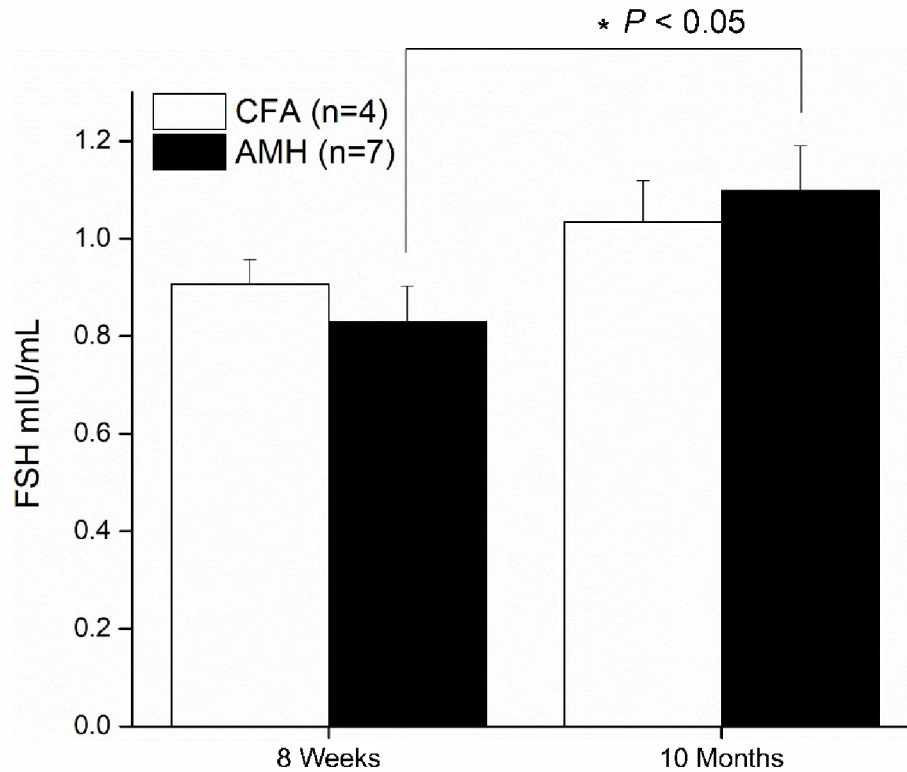


**Figure S3. Serum FSH Levels at 8 Weeks and 10 Months.** At eight weeks and ten months after immunization with rmAMH or CFA, mice were euthanized and serum collected via cardiac puncture. Sera were analyzed via sandwich ELISA for mouse FSH. Means for each group are plotted. The increase in FSH from 8 weeks to ten months was significant ( $P < 0.05$ ). However, no significant differences were observed between the groups at either time point. Error bars represent  $\pm$ SEM.

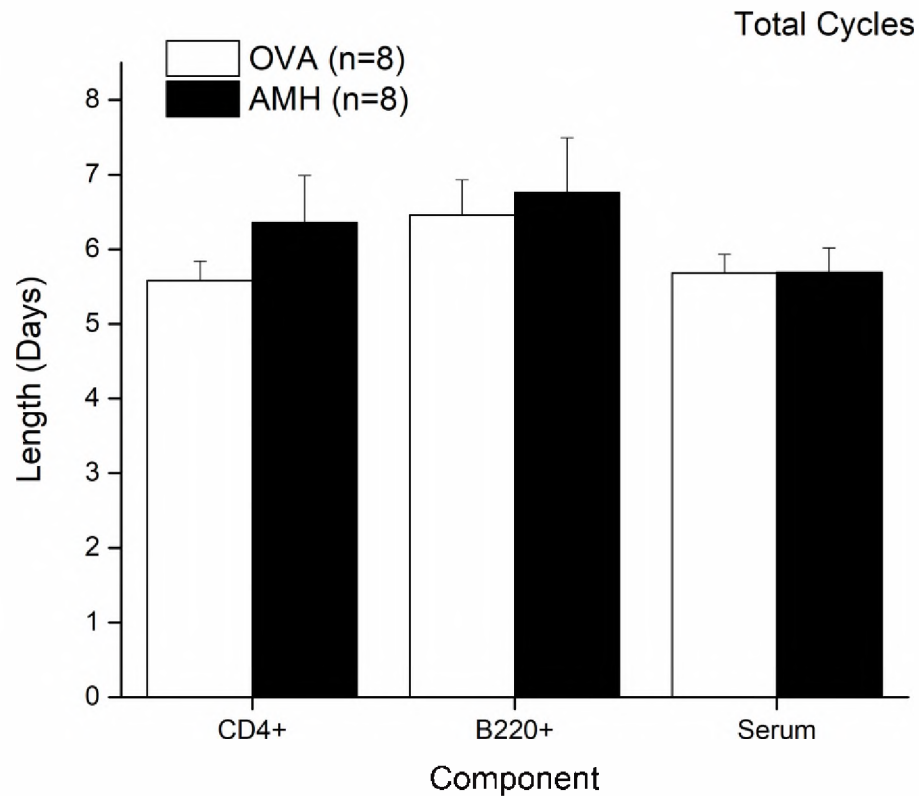


**Figure S4. Total Estrous Cycle Lengths in Passive Transfer to Naive Hosts.** Four weeks after immunization with rmAMH or OVA control, splenocytes and serum were harvested from mice. Purified CD4<sup>+</sup> T cell and B220<sup>+</sup> B cell populations were produced from whole splenocytes by MACS positive selection. Naive mice received a single *i.p.* injection of  $2 \times 10^7$  activated T cells or B cells, or four *i.v.* injections of 200  $\mu$ L of serum every third day. After one week, estrous cycles were evaluated as previously described. The mean total cycle lengths are plotted for each group. No significant differences were observed. Error bars represent  $\pm$ SEM.

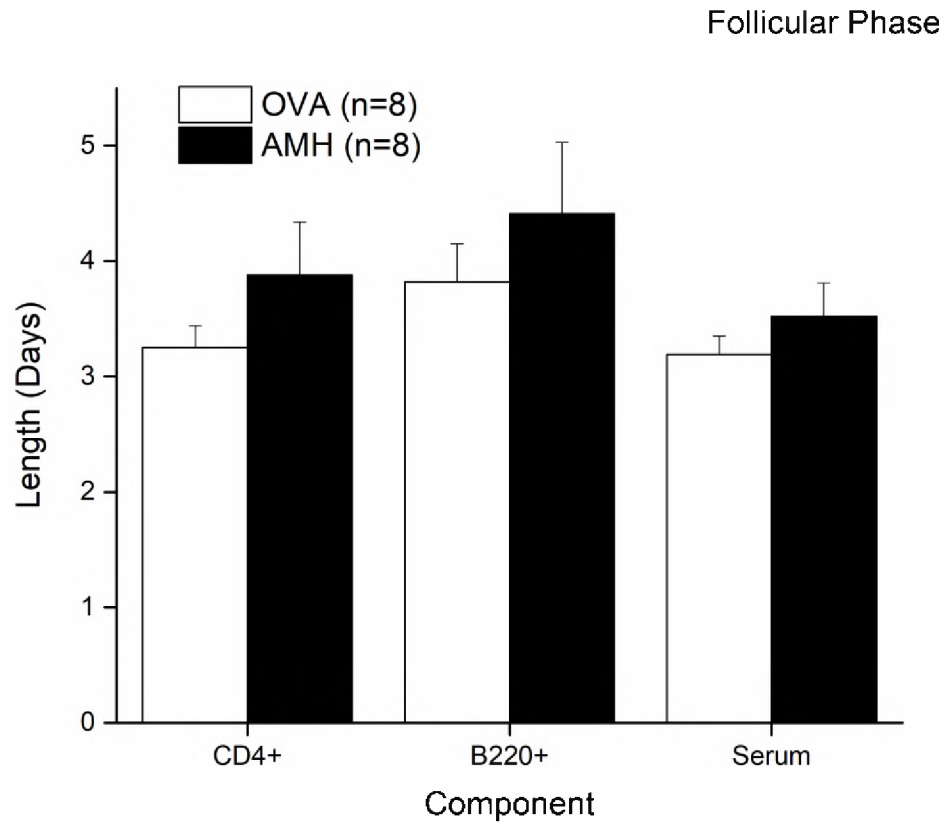


**Figure S5. Follicular Phase Lengths in Passive Transfer to Naive Hosts.** Four weeks after immunization with rmAMH or OVA control, splenocytes and serum were harvested from mice. Purified CD4<sup>+</sup> T cell and B220<sup>+</sup> B cell populations were produced from whole splenocytes by MACS positive selection. Naive mice received a single *i.p.* injection of  $2 \times 10^7$  activated T cells or B cells, or four *i.v.* injections of 200  $\mu$ L of serum every third day. After one week, estrous cycles were evaluated as previously described. The mean follicular phase lengths are plotted for each group. No significant differences were observed. Error bars represent  $\pm$ SEM.

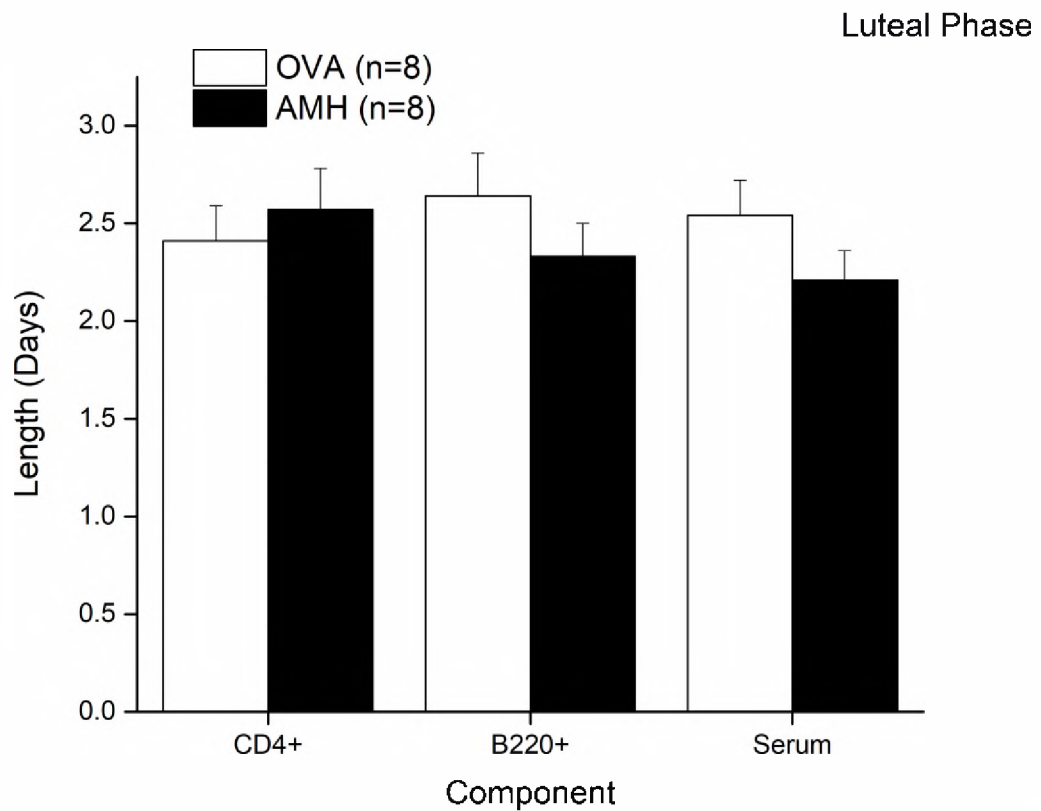


**Figure S6. Luteal Phase Lengths in Passive Transfer to Naive Hosts.** Four weeks after immunization with rmAMH or OVA control, splenocytes and serum were harvested from mice. Purified CD4+ T cell and B220+ B cell populations were produced from whole splenocytes by MACS positive selection. Naive mice received a single *i.p.* injection of  $2 \times 10^7$  activated T cells or B cells, or four *i.v.* injections of 200  $\mu$ L of serum every third day. After one week, estrous cycles were evaluated as previously described. The mean luteal phase lengths are plotted for each group. No significant differences were observed. Error bars represent  $\pm$ SEM.